République Algérienne Démocratique et Populaire

Ministère de l'Enseignement Superieur et de la Recherche Scientifique

Ecole Nationale Polytechnique

Département d'Electronique

THESIS

Radar detection in interfering target environment

Algorithm design and real-time implementation

by

Boualem MAGAZ

A dissertation submitted in partial fulfillment of the requirements for the degree of Doctor in Electronics at Ecole Nationale Polytechnique

March 11, 2012

Examining Committee

President :	Mohamed TRABELSI	Full Professor	ENP, Algiers
Members :	Faouzi SOLTANI	Full Professor	University of Constantine
	Karim ABED-MERAIM	Associate Professor	TélécomParisTech, France
	Youcef REMRAM	Associate Professor	USTHB, Algiers
Supervisors :	Adel BELOUCHRANI	Full Professor	ENP, Algiers
	Mhamed HAMADOUCHE	Associate Professor	University of Boumerdès

"This page is intentionally left blank"

THESIS

Radar detection in interfering target environment

Algorithm design and real-time implementation

by

Boualem Magaz

A dissertation submitted in partial fulfillment of the requirements for the degree of Doctor in Electronics Engineering at Ecole Nationale Polytechnique

Ecole Nationale Polytechnique

Algiers, Algeria

2012

(Defended March 11, 2012)

"This page is intentionally left blank"

"This page is intentionally left blank"

Authorization

I herby declare that I am the sole author of the thesis.

I authorize the "Ecole Nationale Polytechnique" to lend this thesis to other institutions or individuals for the purpose of scholarly research.

I further authorize the "Ecole Nationale Polytechnique" to reproduce the thesis by photocopying or by other means, in total or in part, at the request of other institutions or individuals for the purpose of scholarly research.

_____

Boualem MAGAZ

March 2012

"This page is intentionally left blank"

Radar detection in interfering target environment Algorithm design and real-time implementation

by

Boualem MAGAZ

This is to certify that I have examined the above thesis and have found that it is complete and satisfactory in all respects, and that any and all revisions required by the thesis examination committee have been made.

_____

Prof. Adel Belouchrani, Thesis Supervisor

_____

Prof. Mohamed Trabelsi, Thesis Examination Committee Chairman

_____

Dr. Hichem Bousbia-Salah, Acting Head of the Department

Department of Electronics

March 2012

"This page is intentionally left blank"

to my parents

to my wife and children Ikram, Douâa and Taha

to my brothers and sisters

"This page is intentionally left blank"

ACKNOWLEDGEMENTS

First of all, I would like to thank my advisor, Professor Adel BELOUCHRANI, who has shaped my way of conducting research via consistent help and quidance all through my thesis, allowing ma enough freedom to move forward in my own way under his supervision.

I would like to express my gratitude to my second advisor Dr M'hamed HAMADOUCHE for his many suggestions and constant support during the early times of this research.

I am deeply indebted to the examining committee members : Professor Mohamed TRABELSI, Professor Faouzi SOLTANI, Dr Karim ABED-MERAIM and Dr Youcef REMRAM for accepting to assess this work.

I also want to thank Professor Yide Wang from the IREENA institute, Ecole Polytechnique de Nantes, France, for sharing with me his great experience in MIMO radar techniques during my stay in his laboratory.

I am also very grateful to the FDAT headquarters for their constant encouragement and helpful guidelines.

My thanks extend also to my colleagues researchers whom gave me a great deal of help and encouragement throughout the hard periods of this thesis.

Special thanks to my parents, my wife and children for their forbearance and unconditional support during the trouble times of this thesis.

"This page is intentionally left blank"

TABLE OF CONTENTS

DEDICATION ix

ACKNOWLEDGEMENTS xi

LIST OF FIGURES xvii

LIST OF APPENDICES xxiii

LIST OF ABBREVIATIONS xxv

ABSTRACT xxvii

CHAPTER

I. Introduction 1

1.1 Context 1
1.2 Motivation 2
1.3 Contribution 5
1.4 Thesis organization 7
1.5 Publications 7

II. Generalities 11

2.1 Introduction 11
2.2 Radar principle 12
2.3 Useful definitions 15
2.3.1 Pulse Repetition Frequency (PRF) 15
2.3.2 Dwelling time and integrated sweeps 15
2.3.3 Target fluctuation models 17
2.4 Detection theory 18
2.4.1 Bayes criterion 20
2.4.2 Neyman-pearson criterion 22
2.5 Constant false alarm basic concepts 23

2.6 Review of some CFAR detectors 26
2.7 The OS-CFAR procedure 28
2.7.1 The OS-CFAR rank order parameter selection . . . 29
2.7.2 Final comment 35
2.8 Signal model 35
2.9 Application of digital signal processors in radar systems . . . 36
2.10 Some requirements of radar signal processor 37
2.10.1 Dynamic range 37
2.10.2 Instruction cycle and clock frequency 38
2.10.3 Fixed point versus floating point arithmetic 38
2.11 Conclusion 39

III. Application of the information theoretic criteria in radar detection 41

3.1 Introduction 41
3.2 Radar detection in presence of interfering targets 42
3.3 The proposed detector architecture 45
3.4 Estimation of the number of interfering targets 48
3.5 Simulation and performance analysis 50
3.5.1 Detection thresholds 51
3.5.2 Probability of detection 52
3.5.3 False alarm regulation 56
3.6 Conclusion 58

IV. Adaptive Linear Combined CFAR detection 61

4.1 Introduction 61
4.2 Environment effect on the detection 62
4.3 The proposed ALC-CFAR detector 65
4.3.1 The ALC-CFAR principle 65
4.3.2 The adaptive weighting factor 66
4.3.3 Analysis of the weighting factor behavior 68
4.3.4 The threshold multiplier 70
4.4 Performance assessment 70
4.4.1 Probability of detection 71
4.4.2 False alarm regulation of the ALC-CFAR detector . 77
4.4.3 Gain of the ALC-CFAR detector 77
4.5 Performance comparison ALC-CFAR vs FAOSOSD 79
4.5.1 Homogeneous environment 79
4.5.2 Non-homogeneous environment 81
4.6 Conclusion 83

V. Implementation 85

5.1 Introduction 85
5.2 Architecture of the proposed radar signal processor 86
5.2.1 The proposed radar signal processor scheme 86
5.3 Real time constraints 88
5.4 Digitalization effect on the detection performance 90
5.4.1 Number of the Analog to Digital conversion bits . . 90
5.4.2 Presence of an offset 94
5.4.3 Sampling frequency 96
5.5 Implementation of the proposed detectors 98
5.5.1 Introduction 98
5.5.2 Radar signal acquisition and data rearrangement . . 99
5.5.3 Radar signal processing 100
5.6 Validation with real-life data 112
5.6.1 Data description 113
5.6.2 Experimental results 115
5.7 Conclusion 118

APPENDICES 125

BIBLIOGRAPHY 153

"This page is intentionally left blank"

LIST OF FIGURES

Figure

2.1 A simplified bloc diagram of a modern mono-static radar. 13

2.2 Decision regions 19

2.3 Effect of the noise power increase on the probability of false alarm for a fixed threshold. Design $P_{fa} = 10^{-8}$ 24

2.4 Adaptive threshold detection 24

2.5 A block diagram of the CFAR processor 25

2.6 The ADT as a function of the rank order index k, $N = 16$ and $P_{fa} = 10^{-5}$ 31

2.7 The ADT as a function of the rank order index k, $N = 32$ and $P_{fa} = 10^{-5}$ 32

2.8 The ADT as a function of the rank order index k, $N = 16$ and $P_{fa} = 10^{-6}$ 32

2.9 The ADT as a function of the rank order index k, $N = 32$ and $P_{fa} = 10^{-6}$ 33

2.10 Principal impact of the rank order parameter k on the clutter power estimation in OS-CFAR. For $k > \frac{N}{2}$, the clutter areas appears extended. 34

2.11 Principal impact of the rank order parameter k on the clutter power estimation in OS-CFAR. For $k < \frac{N}{2}$, the clutter areas appears shrunk. 34

3.1 The bloc diagram of the OS-CFAR algorithm. 43

3.2 The OS-CFAR detector limitation in severe multi-targets situation. 44

3.3 The bloc diagram of the OR-CFAR and AND-CFAR detectors. . . . 45

3.4 The bloc diagram of the FAOSOSD detector. 46

3.5 Interference samples number estimation in presence of five interfering targets with $INR = 15dB$. 49

3.6 Interference samples number estimation in presence of eight interfering targets with $INR = 7dB$. 50

3.7 CFAR thresholds in presence of three separated targets, $Pfa = 10^{-5}$, $N = 16$ and $K = 12$. 51

3.8 CFAR thresholds in presence of two separated targets and a group of four interfering targets, $Pfa = 10^{-5}$, $N = 16$ and $K = 12$ 52

3.9 CFAR thresholds in presence of a group of eight interfering targets, and five interfering signals, $Pfa = 10^{-5}$, $N = 16$ and $K = 12$. 53

3.10 Detection probabilities for $N = 16$, $K = 12$ and $Pfa = 10^{-4}$. 54

3.11 Detection probabilities for $N = 16$, $K = 12$ and $Pfa = 10^{-5}$. 55

3.12 Detection probabilities for $N = 16$, $K = 12$ and $Pfa = 10^{-6}$. 55

3.13 Detection probabilities for $Pfa = 10^{-5}$, $K = \frac{3N}{4}$ (a)- N=24. (b)- N=32. 57

3.14 Effect of the INR on the effective P_{fa} of the FAOSOSD detector in presence of $(N - K + 1)$ interfering targets : - Desired $P_{fa} = 10^{-5}$. - $N = 16, 24, 32, 48$ and 64. 58

4.1 The OS-CFAR and CA-CFAR detection thresholds in an homogeneous environment, $P_{fa} = 10^{-5}$, $N = 16$ and $K = 12$. 63

4.2 The OS-CFAR detection loss versus the CA-CFAR detector in an homogeneous environment, $P_{fa} = 10^{-5}$, $N = 16$ and $K = 12$. 63

4.3 The OS-CFAR and CA-CFAR thresholds in presence of interfering targets, $P_{fa} = 10^{-5}$, $N = 16$ and $K = 12$. 64

4.4 The proposed Adaptive Linear Combined CFAR detector. 65

4.5 Illustration of step 1 for the adaptive weighting factor estimation. . 67

4.6 The threshold multiplier of the ALC-CFAR detector versus P_{fa} for different N. 71

4.7 Detection probabilities of the ALC-CFAR, OS-CFAR and CA-CFAR detectors in homogenous environment, $P_{fa} = 10^{-4}$ and $N = 16$. . . . 72

4.8 Detection probabilities of the ALC-CFAR, OS-CFAR and CA-CFAR detectors in homogenous environment, $P_{fa} = 10^{-5}$ and $N = 16$. . . . 72

4.9 Detection probabilities of the ALC-CFAR, OS-CFAR and CA-CFAR detectors in homogenous environment, $P_{fa} = 10^{-6}$ and $N = 16$. . . . 73

4.10 Detection probabilities of the ALC-CFAR, the OS-CFAR and the CA-CFAR detectors in homogenous environment, $P_{fa} = 10^{-5}$ and $N = 4$. 73

4.11 Detection probabilities of the ALC-CFAR, the OS-CFAR and the CA-CFAR detectors in homogenous environment, $P_{fa} = 10^{-5}$ and $N = 32$. 74

4.12 Detection probabilities of the ALC-CFAR, the OS-CFAR and the CA-CFAR detectors in presence of one interfering target. 75

4.13 Detection probabilities of the ALC-CFAR, OS-CFAR and CA-CFAR detectors in presence of five interfering targets. 76

4.14 Detection thresholds for the ALC-CFAR, the CA-CFAR and the OS-CFAR detectors for $N = 16$ and $P_{fa} = 10^{-5}$. 77

4.15 The false alarm regulation performance for different N. The desired $P_{fa} = 10^{-4}$. 78

4.16 Probability of detection of the ALC-CFAR and the FAOSOSD for $P_{fa} = 10^{-5}$ and $N = 8$ in homogeneous environment. 79

4.17 Probability of detection of the ALC-CFAR and the FAOSOSD for $P_{fa} = 10^{-5}$ and $N = 16$ in homogeneous environment. 80

4.18 Probability of detection of the ALC-CFAR and the FAOSOSD for $P_{fa} = 10^{-5}$ and $N = 24$ in homogeneous environment. 80

4.19 Probability of detection of the ALC-CFAR and FAOSOSD for $P_{fa} = 10^{-5}$ and $N = 16$ in presence of one interfering targets. 81

4.20 Probability of detection of the ALC-CFAR and the FAOSOSD for $P_{fa} = 10^{-5}$ and $N = 16$ in presence of three interfering targets. . . . 82

4.21 Probability of detection of the ALC-CFAR and the FAOSOSD for $P_{fa} = 10^{-5}$ and $N = 16$ in presence of five interfering targets. 82

4.22 ALC-CFAR and FAOSOSD thresholds for $P_{fa} = 10^{-6}$ and $N = 16$. 83

5.1 The proposed radar signal processor architecture. 87

5.2 The development platform architecture. 88

5.3 Real time constraints. 89

5.4 Effect of the number of A/D conversion bits on the number of integrated sweeps using the 16bits 'C24x fixed point processor. 91

5.5 Effect of the number of the A/D conversion bits on the CA-CFAR threshold level for $N = 16$ and $Pfa = 10^{-5}$. 93

5.6 Effect of the number of the A/D conversion bits on the FAOSOSD threshold level for $N = 16$ and $Pfa = 10^{-5}$. 93

5.7 Effect of the number of the A/D conversion bits on the ALC-CFAR threshold level for $N = 16$ and $Pfa = 10^{-5}$. 94

5.8 The FAOSOSD and the ALC-CFAR thresholds, Offset=0V. 95

5.9 The FAOSOSD and the ALC-CFAR thresholds, Offset=0.25V. . . . 96

5.10 The FAOSOSD and the ALC-CFAR thresholds, Offset=1.25V. . . . 96

5.11 The FAOSOSD and the ALC-CFAR thresholds, Offset=5V. 97

5.12 Buffer memory and data rearrangement. 99

5.13 The double buffering technique principle. 100

5.14 The homogeneous range and the reference window size limitation. . 101

5.15 The execution time for the CA-CFAR detector DSP implementation for different reference window sizes. 102

5.16 The GASW technique principle. 103

5.17 The GASW technique effect on the processing time. 104

5.18 Implementation results of the CA-CFAR detector, (a) : The input radar signal, (b) : The CA-CFAR threshold, (c) : The decision. . . . 105

5.19 Direct implementation of the OS-CFAR processor architecture. . . . 106

5.20 Block diagram of the OS-CFAR processor DSP optimized implementation 107

5.21 Implementation results of the OS-CFAR detector, (a) : The input radar signal, (b) : The OS-CFAR threshold, (c) : The decision. . . . 108

5.22 Implementation results of the FAOSOSD, (a) : The input radar signal, (b) : The FAOSOSD threshold, (c) : The decision. 110

5.23 Implementation results of the ALC-CFAR, (a) : The input radar signal, (b) : The ALC-CFAR threshold, (c) : The decision. 113

5.24 Radar signal intensity of the datafile1 114

5.25 Datafile1 histogram compared to the exponential PDF. 114

5.26 Datafile1 histogram compared to the log-normal PDF. 115

5.27 Radar signal intensity of the recorded datafile2. 116

5.28 Datafile2 histogram compared to the exponential PDF. 116

5.29 Datafile2 histogram compared to the log-normal PDF. 117

5.30 Results of the FAOSOSD (Datafile1). 117

5.31 Results of the FAOSOSD (Datafile2). 118

5.32 Results of the ALC-CFAR (Datafile1). 119

5.33 Results of the ALC-CFAR (Datafile2). 119

B.1 Schéma bloc du détecteur FAOSOSD. 132

B.2 Estimation du nombre de cibles interférentes présentes dans la fenêtre de référence, $INR = 15dB$. 135

B.3 Seuils CFAR en présence d'un groupe de huit cibles interférentes, et cinq signaux d'interférence, $Pfa = 10^{-5}$, $N = 16$ et $K = 12$. 136

B.4 Probabilités de détection pour $N = 16$, $K = 12$ et $Pfa = 10^{-5}$. . . . 137

B.5 Effet du INR sur la P_{fa} effecftive du détecteur FAOSOSD en présence de $(N - K + 1)$ cibles interférentes, P_{fa} désirée $P_{fa} = 10^{-5}$, $N = 16, 24, 32, 48$ et 64. 139

B.6 Architecture du détecteur ALC-CFAR. 140

B.7 Probabilités de détection des détecteurs ALC-CFAR, OS-CFAR et CA-CFAR en présence de cinq cibles interférentes. 143

B.8 Seuils de détection des détecteurs ALC-CFAR, CA-CFAR et OS-CFAR pour $N = 16$ et $P_{fa} = 10^{-5}$. 144

B.9 Régulation de la probabilité de fausses alarmes pour différentes valeurs de N. $P_{fa} = 10^{-4}$. 145

B.10 Résultats d'implémentation du détecteur FAOSOSD avec des données expérimentales.) 149

B.11 Résultats d'implémentation du détecteur ALC-CFAR avec des données expérimentales. 151

LIST OF APPENDICES

Appendix

A. The ASR-12 Radar specifications 127

B. Résumé 129

"This page is intentionally left blank"

LIST OF ABBREVIATIONS

ADT	Average Decision Threshold
AIC	Akaike Criterion
$ALC-CFAR$	Adaptive Linear Combined CFAR
ASR	Air Surveillance Radar
$CA-CFAR$	Cell-Averaging CFAR
$CFAR$	Constant False Alarm Rate
$CMLD$	Censored Mean Level Detector
$GO-CFAR$	Greatest Of CFAR
$GCMLD$	Generalized CMLD
CNR	Clutter to Noise Ratio
INR	Interference to Noise Ratio
$OS-CFAR$	Ordered-Statistics CFAR
PDF	Probability Density Function
PRF	Pulse Repetition Frequency
SNR	Signal to Noise Ratio
$SO-CFAR$	Smallest Of CFAR
$TM-CFAR$	Trimmed-Mean CFAR
$OSGO-CFAR$	Ordered Statistics Greatest Of CFAR
$OSSO-CFAR$	Ordered Statistics Smallest Of CFAR
$MIPS$	Million of Instructions Per Second
ITC	Information Theoretic Criteria
MDL	Minimum Description Length
INR	Interference to Noise Ratio
$MFLOPS$	Trimmed-Mean CFAR
$FAOSOSD$	Forward Automatic Order Selection Ordered Statistics Detector
$GASW$	Generalized Automatic Sliding Window
MTD	Moving Target Detector
PRT	Pulse repetition Time
RCS	Radar Cross Section
$WCA-CFAR$	Weighted CA-CFAR

"This page is intentionally left blank"

ABSTRACT

Radar detection in interfering target environment :
Algorithm design and real-time implementation

by

Boualem MAGAZ

Supervisors : Adel BELOUCHRANI and M'hamed HAMADOUCHE

In radar, the performance improvement of the detection system under complex situations deals not only with the upgrade of the radar technology, but especially the enhancement of the signal processing techniques using dedicated processors.

The contribution of this thesis considers this development trend and involves two parts. ***The first part*** concerns the design of two novel algorithms for radar target detection in heterogeneous environments, referred to as, FAOSOSD, Forward Automatic Order Selection Ordered Statistics Detector, based on the minimization of the information theoretic criteria, and ALC-CFAR, Adaptive Linear Combined CFAR, based on an adaptive linear combination of the well known CA-CFAR and OS-CFAR detectors thresholds.

The proposed algorithms present the ability to sense automatically the environment changes, especially in presence of interfering targets, and then adapt their thresholds to ensure better performance compared to classical detectors.

The second part of this thesis deals with the development of new and efficient

architectures for real time implementation of the proposed detectors using a DSP development platform based on the Texas Instruments TMS320C6711 processor. The real time processing constraints and the radar signal digitalization effect on the detection quality have been evaluated and discussed, considering the satisfaction of the Air Surveillance Radar, ASR-12, technical specifications.

The proposed architectures for the FAOSOSD and the ALC-CFAR detectors implementation have been tested with synthetic data and validated using real-life data.

The obtained results show that, for practical application in radar detection, it is very interesting to note that the proposed detectors are particularly suitable for low resolution radars which use low number of reference cells to ensure the minimum homogeneity range.

As a conclusion, we would like to highlight that our work has shed new light on the applied radar research, and there are still lots of interesting methodologies to be discovered.

CHAPTER I

Introduction

In this chapter, we introduce the context and the motivation behind this thesis and we present briefly the key contributions of this work. Finally, we present the organization of the manuscript.

1.1 Context

The word radar, formed from the capitalized letters in Radio Detection And Ranging, means the exploitation of radio waves for detecting and locating material objects. It transmits electromagnetic signal and then receives echoes from target objects to get their location and other information [1].

Generally speaking, target detection would be an easy task if the echoing objects were located in front of an otherwise clear background. In such a case the echo signal can simply be compared with a fixed threshold, and targets are detected whenever the signal exceeds this threshold [1,2,3,4,5].

In real radar application, the target appears before a background filled (mostly in a complicated manner) with point, area, or extended clutter. Frequently, the location of this background clutter is additionally subject to variations in time and position. This fact calls for adaptive signal processing techniques operating with a variable detection threshold to be determined in accordance to the local clutter situation. In

order to obtain the needed local clutter information, a certain environment defined by a window around the radar test cell must be analyzed.

Usually the background reflections, undesired as they are from the standpoint of detection and tracking, are denoted by the term "clutter", and in the design of the signal processing circuits the assumption is made that this clutter is uniformly distributed over the entire environment. Signal processing is designed so that, whenever possible, target reports are received from useful targets only, rather than from background reflections [3,7].

In practice, however, clutter phenomena may be caused by a number of different sources. Improvements in target detection and clutter suppression over the present state of the art can be effected only by removing the simplifying assumptions step by step and introducing a more differentiating way of argumentation. Ultimately, it may become necessary to identify clutter regions of different types and describe their properties such as type, size and borders, power, and spectral features rather than trying to suppress and ignore them at an early stage of signal processing. Thus for discriminating targets from clutter, it might be useful to build up a clutter situation encountered in the overall observation space [3].

The application of digital signal processing in radar systems began from signal detection in video frequency and is now developing into signal processing in intermediate frequency. It seems possible to process the RF signal directly owing to the development of high performance devices. The percentage of digitized parts in radar system becomes larger, since it is a cost-effective way to improve the performance of the hole radar system.

1.2 Motivation

The assumption of a uniform clutter situation within the reference window is no longer maintained. Instead, provisions are made to handle transitions in clutter

characteristics, clutter areas of small extensions, and interfering target echo occurring within the reference window of the radar test cell. The idea is to modify the common constant false alarm rate, CFAR, techniques by replacing the usual clutter power estimation [8,9,10,11,15,16].

In existing CFAR systems, target decision is commonly performed using the sliding window technique. The data available in the reference window enter into an algorithm for the calculation of the decision threshold.

These procedures are nearly the same in all CFAR systems. The first step is to measure the mean clutter power level. The second step is to multiply this estimation Z by a scaling factor depending on the applied estimation method and the required false alarm rate. The resulting product is directly used as the threshold value. This threshold is set on a cell by cell basis according to the estimated noise/clutter power, which is determined by processing a group of reference cells surrounding the cell under investigation.

For example, the cell-averaging "CA"-CFAR detector [18] adaptively sets the threshold by estimating the mean level in a reference window of N range cells. The detection performance of the CA-CFAR detector is optimum in an homogeneous environment when the reference cells contain independent and identically distributed (i.i.d) observations governed by an exponential distribution [20].

In practice, the environment is usually non-homogeneous due to the presence of multiple targets and/or clutter edges in the reference window. However, there is a significant decrease in performance of the CA-CFAR detector when the assumption of homogeneous environment is not met [21].

Modifications of the CA-CFAR schemes have been proposed to improve the original CA-CFAR performance in regions with either clutter transitions or multi-target situation [19-38].

The order statistics, OS, detectors have been known to yield a good performance as

long as the non-homogeneous background and outlying returns are properly discarded [20].

The OS-CFAR scheme is suitable to alleviate these problems above to some level. Its performance in a multiple target environment is clearly superior compared to the CA-CFAR detector [20].

Nevertheless, the OS-CFAR detector exhibits some additional loss of detection in homogenous background compared to the CA-CFAR detector. For complex environment such as anti-collision radars, where the environment changes abruptly, these conventional detectors cannot detect targets properly.

However, most of the work in the literature consider some types of censoring based on a priori knowledge and some approaches based on automatic censoring of unwanted cells [29,43]. When the assumed number of interferences exceeds the actual one, these detectors present a serious performance degradation.

Other detection architectures based on a fusion criteria of the CA-CFAR and the OS-CFAR detectors, namely the AND-CFAR and the OR-CFAR detectors have been also proposed [52,53,54]. These detectors remain limited by the CA-CFAR and the OS-CFAR detectors disadvantages in different environments.

On the other hand, for the hardware realizations of radar detection systems, only few attempts considering the implementation of CFAR processors have been reported in the literature. In particular, a configurable hardware architecture for adaptive processing of noisy signals for target detection based on CFAR algorithms has been presented in [67]. The architecture has been designed to deal with parallel/pipeline processing and to be configured for three versions of CA-CFAR algorithms. In [69,70,75], hardware implementations of a CA-CFAR processor using conventional discrete components has been reported.

It should be noticed that, in our knowledge, no enough digital signal processor, DSP, application dealing with real-time hardware implementation for ordered statis-

tics based radar detection algorithms has been published.

Currently, DSP have emerged as an attractive and ideal environment for hardware realizations for high speed algorithms and intensive computation applications for real time radar signal processing [10].

1.3 Contribution

In this thesis, the main contribution involves two fundamental parts.

The first part concerns *the design of two novel algorithms for radar target detection*, in presence of interfering targets, referred to as, FAOSOSD, Forward Automatic Order Selection Ordered Statistics Detector, based on the minimization of the information theoretic criteria, and ALC-CFAR, Adaptive Linear Combined CFAR, based on an adaptive linear combination of the well known CA-CFAR and the OS-CFAR detector thresholds.

The proposed algorithms present the ability to sense automatically the environment changes, especially in presence of interfering targets, and adapt their thresholds to ensure better performance compared to ordinary detectors.

The FAOSOSD detector offers the ability to determine the number of interfering targets in the reference window by minimizing the information theoretic criteria and the adjustment of the OS-CFAR threshold sample order accordingly.

For the ALC-CFAR detector, the threshold is adapted automatically according to the environment changes thanks to an adaptive weighting factor which measures the homogeneity level of the reference window samples. Its performance is closer to the CA-CFAR detector in homogeneous environment, with less CFAR losses compared to the OS-CFAR and performs like the OS-CFAR in presence of interfering targets.

The second part of this thesis deals with *the development of new and efficient architectures for real-time implementation* of the designed detection algorithms, the FAOSOSD and the ALC-CFAR, using a DSP development platform based on the

Texas Instruments TMS320C6711 processor. The real time processing constraints are managed so as to satisfy the Air Surveillance Radar, ASR-12, technical requirements.

We consider, also, the radar signal digitalization effect on the detection quality in the implementation architectures parameters.

It should be noticed the important improvement of the computing burden by developing optimized implementation architectures for adaptive radar detection algorithms.

The first one concerns the CA-CFAR threshold estimation referred to as the Generalized Automated Sliding Window, GASW, technique which efficiently re-uses data to reduce the memory accesses and reutilizes pre-computed values to compute the new thresholds for adjacent cells. This technique reduces the computing to four operations only (two additions and two subtractions) whatever the reference window size is, and the number of guard cells, which makes the computing time for the CA-CFAR threshold estimation almost constant and independent of the number of reference and guard cells [68,75].

The second one deals with the direct selection of the OS-CFAR detector order. The proposed method is based on a new structure for direct determination of the K^{th} ordered sample in the CFAR reference window which reduces significantly the computational burden of ordered statistics based detection algorithms.

The FAOSOSD and the ALC-CFAR detectors have been implemented using the above optimized techniques applied to the CA-CFAR and the OS-CFAR thresholds estimation. We notice that the implementation architectures of the FAOSOSD and the ALC-CFAR detectors have been tested with synthetic data and validated using real-life data.

We point out that the proposed implementation architectures are fully parameterizable in terms of the sampling frequency, the reference window size, the number of guard cells and the false alarm probability. This feature offers the ability to apply

easily these architectures to other kind of radars by the readjustment of the corresponding parameters.

1.4 Thesis organization

The rest of this thesis is organized as follows. In chapter 2, we present some generalities on the radar principle, a review of some CFAR detectors and we provide some useful definitions and significant DSP applications in radar systems. In chapter 3, we introduce an original idea based on the determination of the number of interfering targets in the reference window using the information theoretic criteria. Chapter 4 deals with the target detection performance improvement using the ALC-CFAR detector in homogenous and non-homogeneous environments compared to the classical CA-CFAR and OS-CFAR detectors. In chapter 5, we present the complexity related to the real-time implementation of the proposed detectors to satisfy the requirements of the ASR-12 radar specifications. The experimental results, using real-life data, on TMS320C6711 processor based development platform are also presented and discussed. Finally, the conclusions highlighting the key contributions of this research and the area of potential future work are presented.

1.5 Publications

Journals

1. **B. Magaz**, A. Belouchrani and M. Hamadouche, Automatic Threshold Selection in OS-CFAR Radar Detection Using Information Theoretic Criteria, Progress in Electromagnetics Research B, Vol.30, 157-175, 2011.
2. **B. Magaz**, A. Belouchrani and M. Hamadouche, A New Adaptive Linear Combined CFAR Detection in Presence of Interfering Targets, Progress in Electromagnetics Research B, Vol. 34, 367-387, 2011.

3. **B. Magaz**, A. Abbadi, T. Mabed, M. Hamadouche and A. Belouchrani, Design and Implementation of a Real Time FPGA Based CFAR Processor for Radar Target Detection Using ML403 FPGA Development Board, International Journal on Programmable Devices, Circuits and Systems, PDCS, Volume 9, Issue I, P29-34, October 2009.
4. **B. Magaz**, A. Abbadi, T. Mabed, M. Hamadouche and A. Belouchrani, Using D.S.P in Radar Domain Application : Optimal Implementation of CFAR Detection Algorithms on TMS320C6711 DSP, International Journal on Programmable Devices, Circuits and Systems, PDCS, Volume 9, Issue I, P47-51, October 2009.

Conferences

1. **B. Magaz**, M.L. Bencheikh, M. Hamadouche, A. Belouchrani, Design and Real-Time Implementation of a Novel Combined CA-CFAR/SLB System on TMS320C67X processor, International Radar Symposium, IRS 2006, May 2006, Krakow, Poland.
2. **B. Magaz**, M.L. Bencheikh, M. Hamadouche and A. Belouchrani, Optimized Implementation of a Parallel DSP Architecture for Real-Time Stacked Beam Radar Signal Processing, IET Conference on Radar systems, Oct. 2007, Edinburgh, UK.
3. **B. Magaz**, A. Belouchrani et M. Hamadouche, Automatic Order Selection for OS-CFAR Detection Improvement Under Severe Interference Situations Using Information Theoretic Criteria, International Conference on Radar Systems, RADAR 2009, October, 2009, Bordeaux, France.
4. **B. Magaz**, M. Hamadouche and A. Belouchrani, Design and DSP Implementation of an Adaptive Linear Combined CFAR Processor, International Radar Symposium, IRS'2009, September 2009, Hamburg, Allemagne.

5. **B. Magaz**, M.L. Bencheikh, Y. Wang and A. Belouchrani, Numerical Analysis of MIMO Radar Detection Performance Under Weibull-Distributed Clutter, International Radar Symposium, IRS'2010, Juin 2010, Vilinus, Lithuania.

6. **B. Magaz**, B. Ferrah, S. Atta, M. Hamadouche and A. Belouchrani, Conception et Implémentation d'une Nouvelle Architecture de Détection Radar, DAT'2011, Février 2011, Algiers.

"This page is intentionally left blank"

CHAPTER II

Generalities

In this chapter, we introduce the radar principle, the constant false alarm rate detection basics with the review of some important CFAR detectors. In addition, we provide some useful definitions and DSP applications in modern radar systems.

2.1 Introduction

The basic concept of radar is relatively simple even though in many instances its practical implementation is not. A radar operates by radiating electromagnetic energy and detecting the echo returned from reflecting objects (targets). The nature of the echo signal provides information about the target. The range, or distance, to the target is found from the time it takes for the radiated energy to travel to the target and back. The angular location of the target is found with a directive antenna (one with a narrow beamwidth) to sense the angle of arrival of the echo signal. If the target is moving, a radar can derive its track, or trajectory, and predict the future location. The shift in frequency of the received echo signal due to the Doppler effect caused by a moving target allows a radar to separate desired moving targets (such as aircraft) from undesired stationary targets (such as land and sea clutter) even though the stationary echo signal may be many orders of magnitude greater than the moving target. With sufficiently high resolution, a radar can discern something about the

nature of a target's size and shape. Radar resolution may be obtained in range or angle, or both. Range resolution requires large bandwidth. Angle resolution requires (electrically) large antennas. Resolution in the cross-range dimension is usually not as good as the resolution that can be obtained in range.

2.2 Radar principle

The principle of radar has been applied for frequencies ranging from few megahertz (HF, or high-frequency region of the electromagnetic spectrum) to well beyond the optical region (laser radar). The techniques for implementing a radar differ greatly over this range of frequencies, but the basic principles remain the same.

Radar was originally developed to satisfy the needs of the military for surveillance and weapon control. Military applications have funded much of the development of its technology. However, radar has seen significant civil applications for the safe travel of aircraft, ships, and spacecraft, the remote sensing of the environment, especially the weather and many other applications.

The radar signal, usually a repetitive train of short pulses, is generated by the transmitter and radiated into space by the antenna. The duplexer permits a single antenna to be time-shared for both transmission and reception. Reflecting objects (targets) intercept and reradiate a portion of the radar signal, a small amount of which is returned in the direction of the radar. The returned echo signal is collected by the radar antenna and amplified by the receiver. If the output of the radar receiver is sufficiently large, detection of a target is said to occur. A radar generally determines the location of a target in range and angle, but the echo signal also can provide information about the nature of the target. The output of the receiver may be presented on a display to an operator who makes the decision as to whether or not a target is present, or the receiver output can be processed by electronic means to automatically recognize the presence of a target and establish a track of the target from detections

made over a period of time. With automatic detection and track the operator usually is presented with the processed target track rather than the raw radar detections. In some applications, the processed radar output might be used to directly control a system (such as a guided missile) without any operator intervention.

The basic parts of a radar system are illustrated in the simple block diagram of Fig. 2.1.

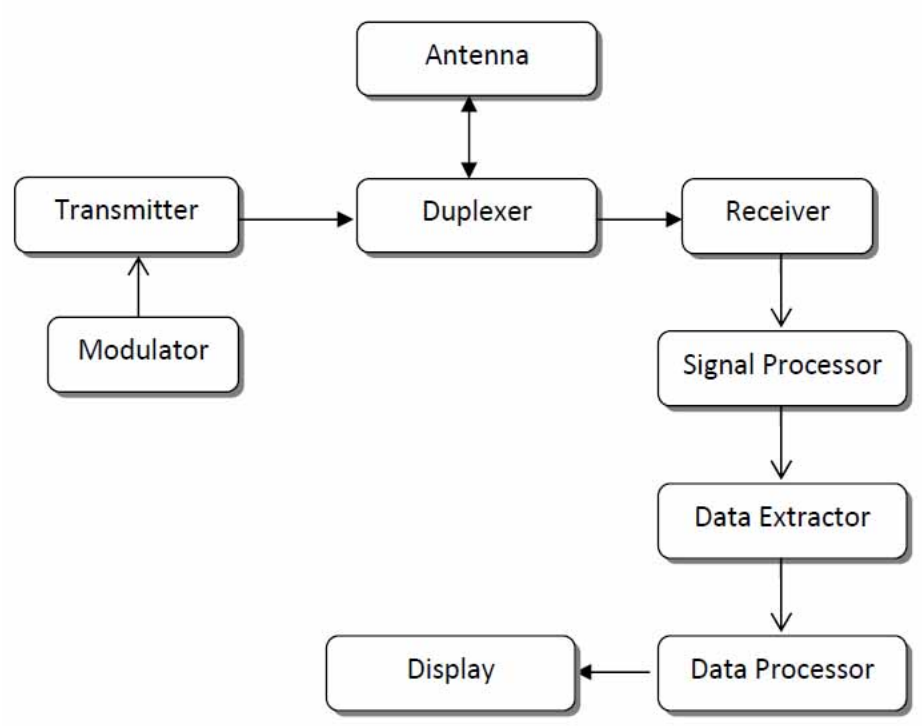

FIGURE 2.1: A simplified bloc diagram of a modern mono-static radar.

The major blocks of a radar are the modulator, the receiver, the signal processor, the data extractor, the data processor and the display. Their functions are briefly described below.

Modulator : Upon reception of each timing pulse, the modulator produces a high power pulse direct current and supplies it to the transmitter.

Transmitter : The transmitter is a high-power oscillator, generally a magnetron. It generates a high peak power coherent train of pulses to illuminate the target.

Receiver : Typically, the receiver is of a type called superheterodyne. It provides

frequency conversion (to lower frequency called intermediate frequency), interference rejection and low-noise amplification. The noise reduction is an important issue in radar receiver design and it is accomplished by a matched filter which maximizes the signal-to-noise power ratio (SNR) at the output.

Signal processor : This device processes the target echoes and interfering signals to increase the signal to interference ratio. The signal processor is implemented in real time special purpose hardware. Basic operations are routinely exploited as results of the advances in digital technology include [10], Pulse Compression, Doppler range clutter suppression techniques and Constant False Alarm Rate (CFAR) circuit.

Pulse compression (PC) provides the resolution benefits of short pulse in the reception phase and the energy of long duration pulse at the transmission phase.

Doppler-range clutter suppression techniques remove the clutter caused by ground, sea, or moving clouds of rain clutter by appropriate filtering. Such techniques include Moving Target Indicator (MTI), Pulse Doppler Processing (PDP) and Moving Target Detector (MTD).

Constant False Alarm Rate (CFAR)- circuit keeps the rate of occurrence of false decisions (alarms) due to background noise and clutter at a constant rate, thus preventing saturation of the system. It estimates the noise and clutter level from a number of range, Doppler, and/or azimuth cells to allow the threshold to be set correctly.

Data extractor : It provides the target measurements in range, angles (azimuth, elevation), radial velocity and possibly provides the target signature.

Data processor : This is a general-purpose computer that controls and performs routine computations for the radar units.

Display : The output is generally converted to a display to visualize the information contained in the target echo signal in a form suitable for operator action and interpretation. The Plan Position Indicator (PPI) is the usual display employed in radar receiver. It indicates the range and the azimuth of the detected target.

2.3 Useful definitions

2.3.1 Pulse Repetition Frequency (PRF)

The Pulse Repetition Frequency (PRF) of a radar system is the number of pulses that are transmitted per second. Radar systems radiate each pulse at the carrier frequency during transmit time (or Pulse Width, PW), wait for returning echoes during listening or rest time, and then radiate the next pulse. The time between the beginning of one pulse and the start of the next pulse is called pulse repetition time (PRT) and is equal to the reciprocal of the PRF as follows :

$$PRT = \frac{1}{PRF} \tag{2.1}$$

The radar system pulse repetition frequency determines its ability to unambiguously measure target range and range rate in a single coherent processing interval as well as determining the inherent clutter rejection capabilities of the radar system. In order to obtain an unambiguous measurement of target range, the interval between radar pulses must be greater than the time required for a single pulse to propagate to a target at a given range and back. The maximum unambiguous range is then given by :

$$R_{unamb} = \frac{c_0}{2PRF} = \frac{c_0 PRT}{2} \tag{2.2}$$

where c_0 is the velocity of electromagnetic propagation.

2.3.2 Dwelling time and integrated sweeps

Most processes in pulse radar are time-dependent. So, there are some terms established to describe this time dependence.

Dwelling Time

The time that an antenna beam spends on a target is called dwell time T_d. The dwelling time of a 2D-search radar depends predominantly on :

- the antenna horizontally beam width θ_{AZ} expressed in degrees ;
- the turn speed n of the antenna (rotations per minute).

The dwelling time (in seconds) can be calculated using the following equation :

$$T_d = \frac{60\theta_{AZ}}{360^{\circ}.n} \tag{2.3}$$

Integrated sweeps

The number of integrated sweeps m is usually determined by the scanning speed, n, of the antenna beam in conjunction with the antenna beamwidth, θ_{AZ}, in the plane of the scanning.

The dwell time T_d and the pulse repetition time PRT determine the maximum number of integrated sweeps.

$$m = \frac{T_d}{PRT} = \frac{60\theta_{AZ}}{360^{\circ}.n.PRT} \tag{2.4}$$

Some modern radars are capable of scanning the covered area by electronic means, i.e., without mechanical motion of the antenna step scanning. In this scanning technique, the antenna beam is pointed in a fixed direction while a programmed number of pulses is radiated in that direction. Then the beam is shifted to a new direction, and the process is repeated. The number of pulses integrated in this scanning method is thus determined by the programming and not by the beam-width. Also, the integrated pulses are then all of the same amplitude (except for the effect of target fluctuation), and so there is no pattern loss. There is, however, a statistical loss if the target direction and the antenna beam maximum do not always coincide when the pulses are radiated.

2.3.3 Target fluctuation models

Basically all radar target objects produce echo signals that vary in amplitudes either in power or cross-sectional terms. These amplitudes can vary from scan to scan or between echo and echo due to aspect changes relative to the radar. This variation is often referred to as target scintillation [78].

Target cross-section fluctuations are complex to quantify by a simple mathematical expression. Swerling postulated models that describe slowly and fast varying targets. The slowly fluctuations target model is assumed to have complete correlation, or dependence, between echo signals during a radar scan. The fast fluctuating target model is assumed to have partial correlation from echo to echo instead of scan to scan. The virtue of these models lies in the fact that they are a reasonable approximation of a variety of targets. The models are briefly described as follows.

Swerling I Target describes a target whose magnitude of the backscattered signal is relatively constant during the dwell time. It varies according to a Chi-square probability density function with two degrees of freedom. The radar cross-section is constant from pulse-to-pulse, but varies independently from scan to scan. The density of probability of the RCS is given by the exponential-function :

$$P(\sigma) = \frac{1}{\sigma_{average}}.exp(\frac{-\sigma}{\sigma_{average}}), \sigma \geq 0. \tag{2.5}$$

Where σ is the RCS variable, and $\sigma_{average}$ is the arithmetic mean of all values of RCS of the reflecting object.

Swerling II Target is similar to Swerling I, using the same equation, except the RCS values change faster and vary from pulse to pulse additionally.

Swerling III Target is described like Swerling I, but with four degrees of freedom.

The scan-to-scan fluctuation follows the density of probability given by :

$$P(\sigma) = \frac{4\sigma}{\sigma_{average}}^{2} .exp(\frac{-2\sigma}{\sigma_{average}}), \sigma \geq 0. \tag{2.6}$$

Swerling IV is similar to Swerling III, but the RCS varies from pulse to pulse rather than from scan to scan and follows the Eq. 2.6.

Swerling V also known as Swerling 0, it describes an idealized target without any fluctuation.

The Swerling cases I and II are applied to a target that is made up of many independent scatterers of roughly equal areas like airplanes. Cases III and IV approximate an object with one large scattering surface with several other small scattering surfaces.

2.4 Detection theory

Detection is the process of deciding whether or not a target is present. It is accomplished by comparing the signal plus noise, after all processing has occurred, to a threshold. If the signal plus noise or noise alone crosses the threshold, detection is declared. If not, no detection occurs.

Since, one is facing the problem of two possible outputs, the detection of a radar signal can be modeled as a binary hypothesis detection problem. A statistical hypothesis is an assertion concerning the distribution of one or more random variables.

In this case, one has two possible hypotheses : The null hypothesis H_0 that represents the absence of a target, and the alternate hypothesis H_1 that corresponds to the presence of a target. Each hypothesis maps into a point in the observation space, Z, in accordance to the known conditional probability densities $f_{Q/H_0}(q/H_1)$ and $f_{Q/H_1}(q/H_0)$ as illustrated in Fig. 2.2.

The observation space is partitioned into two disjoint regions Z_0 and Z_1 by some decision rules. If the received signal, q, falls within Z_0 one decides in favor of H_0, but

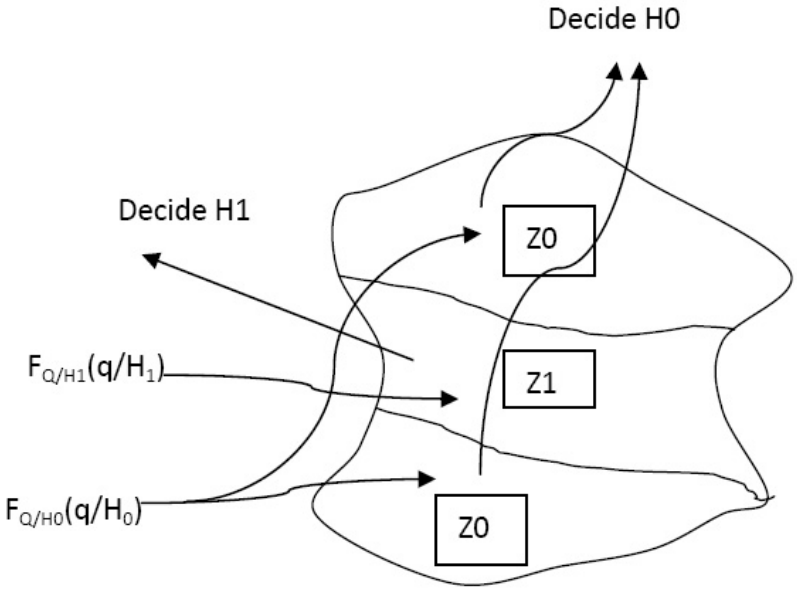

FIGURE 2.2: Decision regions

if it falls within Z_1 one decides in favor of H_1. Thus, each time the test is conducted, one of the four possible cases can occur :

1. Decide H_1 when H_1 is true (target present when a target is present) ;
2. Decide H_0 when H_1 is true (target not present when a target is present) ;
3. Decide H_1 when H_0 is true (target present when a target is not present) ;
4. Decide H_0 when H_0 is true (target not present when a target is not present).

In radar terminology, the first event is called a target detection, the probability associated with this event is called the probability of detection P_d, event (2) always occurs whenever event (1) does not occur, therefore its probability is given by $(1-P_d)$ and it is known as the probability of miss, P_m. Event (3) is called a false alarm since a target is declared present even though it is not actually present ; its probability is denoted P_{fa}. Using the same reasoning used with event (1) and (2), the probability of event (4) must be the complement of event (3) or $(1-P_{fa})$. Since the decision process is binary, only two probabilities are needed to fully specify the detection radar statistical performance, namely, P_d and P_{fa}. The decision rule is most often designed based on

a decision criterion, the most known one are Bayes and Neyman-Pearson [4,17].

2.4.1 Bayes criterion

When using Bayes criterion, two assumptions are made. First, the probability of occurrence of the two source outputs is known. They are the a priori probabilities $P(H_0) = P_0$ and $P(H_1) = P_1$. The second assumption is the cost assignment to each possible decision. If we let D_i, i=0,1, denote the decision associated to H_0 and H_1, we can define $C_{ij}, i, j = 0, 1$, as the cost associated with the decision D_i ; given that the true hypothesis is H_i. The goal in the Bayes criterion is to determine the decision rule so that the average cost $E(C)$, also known as risk $\Re$, is minimized. We assume that the cost of making a wrong decision is greater than the cost of a correct decision. That is,

$$C_{01} > C_{11}, C_{10} > C_{00} \tag{2.7}$$

Given $P(D_i, H_j)$, the joint probability that we decide D_i and that hypothesis H_i is true, the average cost is

$$\Re = E(C) = \sum_{ij} P(D_i, H_j) \tag{2.8}$$

From Bayes rule, we have

$$P(D_i, H_j) = P(D_i/H_j)P(H_j) \tag{2.9}$$

The conditional densities $P(D_i/H_j); i, j = 0, 1$, in terms of the observation regions are

$$P(D_i/H_j) = P\{decideH_i/H_jtrue\} = \int_{Z_1} f_{Q/H_j}(q/H_{j)}dq; i, j = 0, 1. \tag{2.10}$$

The probabilities $P(D_0/H_1)$, $P(D_1/H_0)$ and $P(D_1/H_1)$ represent the probability of miss P_m, the probability of false alarm, P_{fa}, and the probability of detection P_d, respectively. We also observe that

$$P_m = 1 - P_d \tag{2.11}$$

and

$$P(D_0, H_0) = 1 - P_{fa} \tag{2.12}$$

The average cost becomes

$$\Re = E(C) = C_{00}(1 - P_{fa})P_0 + C_{01}(1 - P_d)P_1 + C_{10}P_{fa}P_0 + C_{11}P_dP_1 \tag{2.13}$$

In terms of the decision regions, the average cost is [5]

$$\Re = E(C) = p_0C_{10} + p_1C_{11} + \int_{Z_0} \{p_1(C_{01} - C_{11})f_{Q/H_1} - p_0(C_{10} - C_{00})f_{Q/H_0}\}dq \tag{2.14}$$

The quantity $P_0C_{10} + P_1C_{11}$ is constant and from Eq. 2.22 the terms $P_1(C_{01} - C_{11})f_{Q/H_1}(q/H_1)$ and $P_0(C_{10} - C_{00})f_{Q/H0}(q/H_0)$ are positive, consequently the risk is minimum if we select the point in the region Z_0 for which

$$P_1(C_{01} - C_{11})f_{Q/H_1}(q/H_1) < P_0(C_{10} - C_{00})f_{Q/H_0}(q/H_0) \tag{2.15}$$

Hence, the decision rule resulting from Bayes criterion is

$$\bigwedge(q) = \frac{f_{Q/H_1}(q/H_1)}{f_{Q/H0}(q/H_0)} \underset{<H_0}{\overset{>H_1}{}} \frac{P_0(C_{10} - C_{00}}{P_1(C_{01} - C_{11}} = \eta \tag{2.16}$$

where $\bigwedge(q)$ is the likelihood ratio test. Therefore, if we have a vector of samples

$q = [q_1, q_2, ..., q_K]^T$, then the decision rule is performed simply by processing the vector q to yield the likelihood ratio $\bigwedge(q)$ and comparing it with the threshold η.

2.4.2 Neyman-pearson criterion

In the previous section, the knowledge of the a priori probabilities and the cost assignments for each possible decision is required.

However, in many physical situations, such as radar detection, it is difficult to assign realistic costs and a priori probabilities [9]. To overcome this difficulty, we use the conditional probabilities of false alarm, P_{fa}, and detection, P_d. In the Neyman-Pearson test, P_{fa} is constrained to a desired value α while P_d is maximized [17]. Since $P_m = (1 - P_d)$, maximizing P_d is equivalent to minimizing P_m.

In order to solve this, we form the objective function $J(\lambda)$

$$J(\lambda) = P_m + \lambda(P_{fa} - \alpha) \tag{2.17}$$

where λ ($\lambda \geq 0$) is the Lagrange multiplier. In terms of the decision, the objective function can be written as

$$J(\lambda) = \int_{Z_0} f_{Q/H_1}(q/H_1)dq + \lambda[\int_{Z_1} f_{Q/H_0}(q/H_0)dq - \alpha] \tag{2.18}$$

Since $Z = Z_{01}$, Eq. 2.18 reduces to

$$J(\lambda) = \lambda(1 - \alpha) + \int_{Z_0} f_{Q/H_1}(q/H_1)dq - \lambda f_{Q/H_0}(q/H_0)dq \tag{2.19}$$

Hence, minimizing $J(\lambda)$ results to the following decision rule

$$\bigwedge(q) = \frac{f_{Q/H_1}(q/H_1)}{f_{Q/H0}(q/H_0)} \underset{<H_0}{\overset{>H_1}{}} \lambda \tag{2.20}$$

λ is the detection threshold from the constraint $P_{fa} = \alpha$, that is

$$P_{fa} = \int_{\lambda}^{\infty} f_{\bigwedge/H_0} dq \tag{2.21}$$

where $f_{\bigwedge/H_0}$ is the conditional density of that H_0 is true. The solution of Eq. 2.21 yields a threshold, which is a function of the noise variance.

2.5 Constant false alarm basic concepts

The detection of a radar target embedded in noise and clutter background is of considerable practical applications. The radar surveillance volume is divided into small regions called range cells (in terms of distance from the radar), and the problem is to determine whether a target is present in a given range cell (test cell) while maintaining a constant probability of false alarm. When the noise and clutter background is stationary and its probability distribution along with its parameters is completely known, the classical detection technique using a matched filter receiver and a fixed threshold can be employed and a constant probability of false alarm (P_{fa}) is maintained [3].

Since the clutter environments yield unknown and time-varying average values of back-scattering energy (statistically non-stationary returns), conventional receiver configuration and a fixed threshold is not applicable.

In fact, a small increase in the total noise power results in a corresponding increase of several orders of magnitude in the probability of false alarm. As shown in Fig. 2.3, for a design probability of false alarm, $P_{fa} = 10^{-8}$, a $3dB$ increase in the total noise power yields a 10.000 folds increase in the false alarm probability. This undesirable increase in the number of false alarm would significantly exceed the radar data handling.

Fig. 2.4 shows clearly a situation in which the setting of the threshold is crucial.

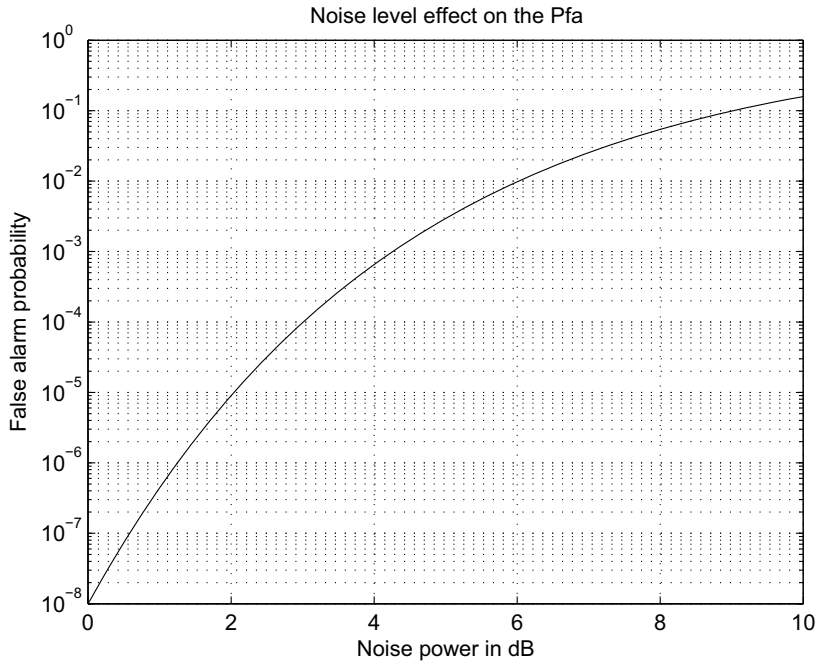

FIGURE 2.3: Effect of the noise power increase on the probability of false alarm for a fixed threshold. Design $P_{fa} = 10^{-8}$

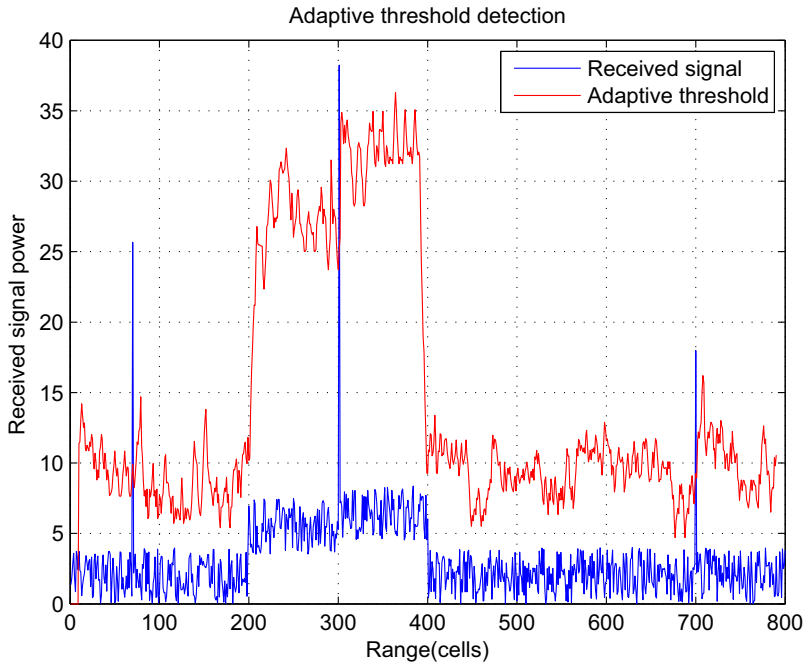

FIGURE 2.4: Adaptive threshold detection

If the threshold is too high, some targets may go undetectable. If it is too low, too many false alarms will occur.

Therefore, adaptive threshold techniques are needed to maintain a Constant False Alarm Rate (CFAR). The adaptive threshold is based on the estimate of the noise power obtained from the cells (range and/or doppler) surrounding the test cell.

A block diagram of the CFAR processor is shown in Fig. 2.5 [3].

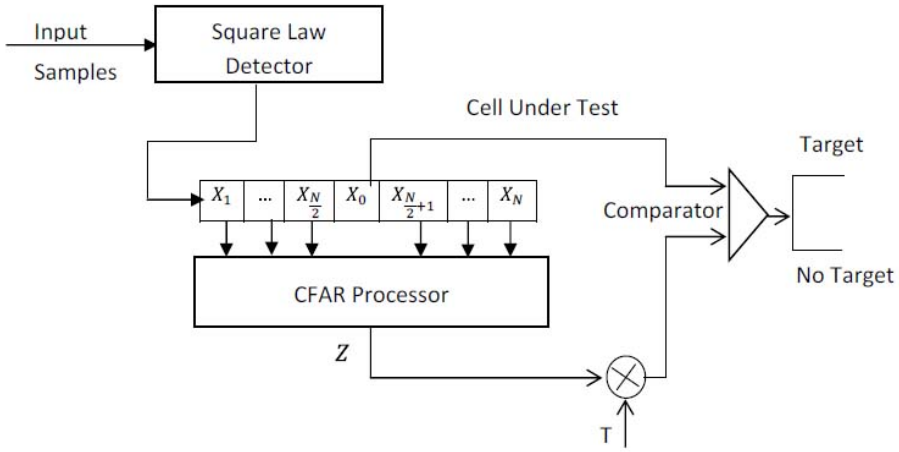

FIGURE 2.5: A block diagram of the CFAR processor

The square-law detected samples are sent serially into a shift register of length $(N+1)$. The leading N/2 samples and the lagging $N/2$ samples surrounding the test cell form the reference window. The statistic Z is multiplied by a scale factor or threshold multiplier T so as to maintain the probability of false alarm at a desired level. The product TZ is the resulting adaptive threshold. The test cell sample, X_0, from the center tap is then compared with this adaptive threshold to make the decision.

A relatively simple CFAR processor is the Cell Averaging Constant False Alarm Rate (CA-CFAR) detector proposed by Finn and Johnson [18]. In this CFAR processor, the noise level estimate in the cell under test (the statistic Z) is equal to the arithmetic mean of the reference cells. The CA-CFAR processor performs well in an homogenous background when the reference cells contain independent and identically distributed (i.i.d.) observations. As the size of the reference window increases, the

detection probability approaches that of the (ideal) Neyman-Pearson detector and the additional signal to clutter ratio or CFAR loss is minimized. However, with the number of cells increasing, the occurrence of non-homogeneities in the reference window is more likely, thereby, the optimal performance of the CA-CFAR detector will not be maintained.

2.6 Review of some CFAR detectors

The conventional CA-CFAR detector performs well in a homogenous environment. In a non-homogeneous environment, its performance degrades significantly. Two commonly observed situations that give rise to non-homogeneity in the reference window are the clutter edge and the multiple targets. Clutter edges refer to abrupt noise power level transition within the reference window. In this situation, two cases may be encountered depending whether the cell under test is in the clear or in the clutter region. If the cell under test is in the clear region but a group of the reference cells are immersed in the clutter, a masking effect results. That is, the threshold is raised unnecessarily and therefore the probability of detection along with the false alarm probability are significantly lowered. On the other hand, if the test cell is in the clutter but a group of reference cells are in the clear, the probability of false alarm may increase intolerably. When there are one or more targets (other than the primary target) within the reference window, the threshold is raised and the detection probability may be seriously degraded. This is known as the capture effect. To alleviate these problems, a number of modified CFAR detectors have been proposed [19-38].

The problem of increase in the false alarm probability due to step discontinuity (clutter edge) has been treated by Hansen and Sawyers [19]. They proposed the greatest-of (GO) CFAR detector in which the leading and the lagging samples are separately summed and the larger of the two is used to set the threshold. A detailed analysis of the false alarm regulation capabilities of the GO-CFAR detector has

been proposed by Moore and Lawrence [34]. In [35], Weiss has shown that if one or more interfering targets are present, the detection of the GO-CFAR detector is very poor. He suggested the use of the smallest-of (SO) CFAR detector. In the SO-CFAR detector, the estimate of the noise level is the minimum of the sums of the outputs of the leading and the lagging range cells. The SO-CFAR detector was first proposed by Trunk [36] in order to improve the resolution of closely spaced targets.

The SO-CFAR detector performs well when the interfering targets returns appear in either the leading or the lagging window. If the interfering targets are located in both leading and lagging window, the performance of the SO-CFAR detector degrades significantly and the processor fails to maintain a constant false alarm rate.

Furthermore, Barkat and Varsheny [37] proposed the weighted cell-averaging CFAR, WCA-CFAR detector by assigning optimum weights to the leading and the lagging windows such that the CFAR property is maintained.

To overcome the problem of interfering targets, some algorithms based on ordered statistics have been proposed. Rohling [20] introduced the ordered statistics (OS) CFAR detector in which the k^{th} ordered sample is used to estimate the background noise. The OS-CFAR detector exhibits a significant performance gain and a high false alarm rate regulation in the presence of interfering targets compared to the CA-CFAR detector at the expense of a small detection loss in homogeneous background. Kim et al. [23] extended the OS-CFAR detector analysis to multiple pulses using non-coherent integration. To reduce the processing time of the OS-CFAR detector in ordering magnitudes of the cells in a reference window, two versions of modified OS-CFAR detectors have been proposed, the order statistics greatest of (OSGO) CFAR and order statistics smallest of (OSSO) CFAR which have been analyzed for the case of multiple pulses using non-coherent integration [24]. In clutter power transition, the OS-CFAR detector is unable to prevent an excessive false alarm rate and presents a greater loss in detection performance. Rickard and Dillard [21] suggested the Censored

Mean Level Detector (CMLD), in which the estimate of the noise level is obtained by the sum of the lower k ordered samples in the reference window. Ghandi and Kassam [26] proposed the Trimmed Mean (TM) CFAR detector, which implements trimmed averaging after ordering.

A major problem with the aforementioned censoring algorithms is that they require some a priori knowledge about the background environment to set the censoring point(s). Otherwise, they may suffer a masking effect and degradation in false alarm probability as in the case of the CA-CFAR detector. To alleviate this problem, some more robust algorithms have been proposed by Himonas and Barkat [27,28] ; namely, the Generalized (G)CMLD and the Generalized Two Level (GTL)CMLD. Hammoudi and Soltani suggested a distributed CA-CFAR and OS-CFAR detection architecture using fuzzy fusion rules in order to improve the radar detection quality [51] and proposed in [58] a variability index based distributed detection system in non-homogeneous environments.

Other detection architectures based on a fusion criteria of the CA-CFAR and the OS-CFAR detectors, namely the AND-CFAR and OR-CFAR detectors have been proposed [53,54]. These detectors remain limited by the CA-CFAR and the OS-CFAR disadvantages in different environments.

2.7 The OS-CFAR procedure

The adaptive threshold of the OS-CFAR detector is formally defined by selecting the K^{th} largest sample in the reference window, $X(K)$, as shown in Eq. 2.22.

$$X(1) \leq X(2) \leq \cdots \leq X(K) \leq \cdots \leq X(N) \tag{2.22}$$

The indices in brackets indicate the rank order number. $X(1)$ denotes the minimum and $X(N)$ the maximum value.

The threshold level is computed according to Eq. 2.23.

$$T_{OS}Z_{OS} = T_{OS}X(K); K \in \{1, 2, 3, ..., N\} \tag{2.23}$$

where T_{OS} is a scale factor chosen according to the desired P_{fa} and N, $X(K)$ is the K^{th} ordered sample in the reference window. T_{OS} can be derived from the above Eq. 2.24 [20].

$$P_{fa} = K\binom{K}{N}\frac{(K-1)!(T_{OS}+N-K)!}{(T_{OS}+N)!} \tag{2.24}$$

The estimate Z_{OS} is then multiplied by T_{OS} to get the threshold level. The result is compared with the sample level in the cell under test, X_0. After comparison, if the cell under test is greater than the threshold level, hypothesis H_1 (presence of target in the cell under test) is declared true ; else the alternative hypothesis H_0 (absence of target) is declared true.

The detection probability is given by [20] :

$$P_d = K\binom{K}{N}\frac{(\frac{T_{OS}}{1+S}+N-K)!(K-1)!}{(\frac{T_{OS}}{1+S}+N)!} \tag{2.25}$$

where S is the signal to noise ratio.

2.7.1 The OS-CFAR rank order parameter selection

At this point of analysis, the probability of detection would normally have to be considered. Here we use instead the single-valued measure adaptive detection threshold (ADT) [20].

A formal definition of the ADT measure is

$$ADT = E(TZ)/\mu \tag{2.26}$$

where the random variable Z is the result of the estimation method used in the CFAR system, T is the scaling factor for threshold adjustment adapted to the estimation method and the required P_{fa}, and μ is the mean clutter power level. E stands for the expectation.

The use of the ordered statistic in the context of CFAR processing does not define a single CFAR method but rather a series of several different CFAR methods.

For any given random variable $X(k)$ a distinct CFAR procedure is established. For practical application, however, only a few of the N possible values k are of interest.

Deviating from the methods usually described in the radar literature, we use for the comparison of various CFAR procedures the normalized average decision threshold, ADT. This provides the advantage that the difference existing between various CFAR systems are then expressed by a single-valued-measure. These differences between two CFAR systems in a homogeneous clutter situation can be expressed by the ratio of the two ADT's measured in dB :

$$\Delta[dB] = 10log\frac{E(T_1Z_1)}{E(T_2Z_2)} \tag{2.27}$$

This measure reflects the separation between two P_d curves valid for a homogeneous clutter situation.

The average decision threshold, ADT, on which the comparison of different CFAR systems is given for the CA-CFAR by

$$ADT_{CA} = E(T_{CA}Z_{CA}/\mu) = T_{CA}E(Z_{CA})/\mu = T_{CA} \tag{2.28}$$

For the exponentially distributed random variables X_1,..., X_N, the mean values $E(X(k))$ of the random variables $X(k)$ are given by [20]

$$E(X_k) = \mu\Sigma_{j=1}^{k}1/(N-k-1) \tag{2.29}$$

Fig. 2.6 and Fig. 2.7 display the average decision threshold (ADT) as a function of the rank order index, k. The parameters used for this representation are the reference window length $N = 16, 32$ respectively and the false alarm probability $P_{fa} = 10^{-5}$.

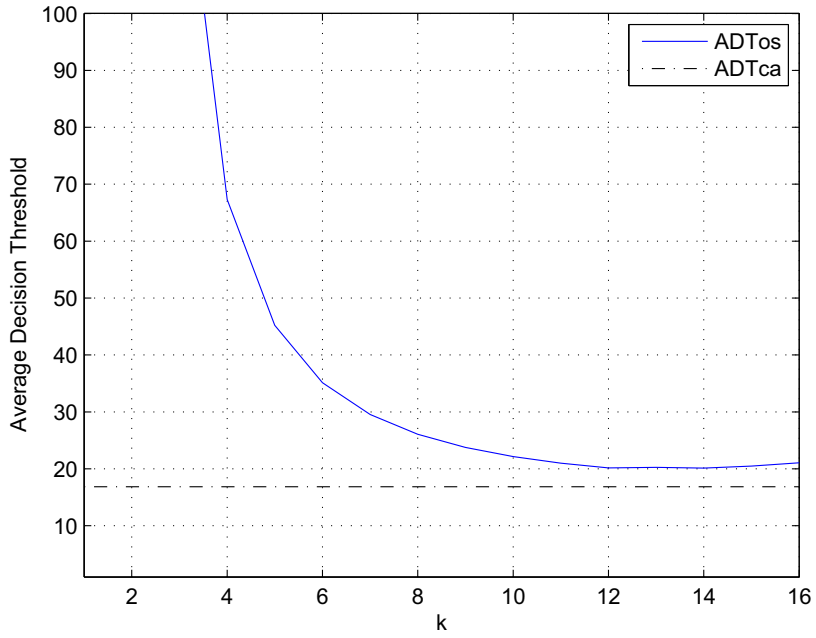

FIGURE 2.6: The ADT as a function of the rank order index k, $N = 16$ and $P_{fa} = 10^{-5}$

Fig. 2.8 and Fig. 2.9 display the average decision threshold (ADT) as a function of the rank order index, k, $N = 16, 32$ respectively and the false alarm probability $P_{fa} = 10^{-6}$.

The function $ADT(k)$ exhibits a broad minimum, the absolute minimum lying at $k = 12$ for $N = 16$ and $k = 24$ for $N = 32$ for different P_{fa} values which corresponds to $(\frac{3N}{4})$.

For example, it approaches the reference value of ADT=16.8564 (dashed line) valid for the CA-CFAR procedure with identical window length $N = 16$ and $P_{fa} = 10^{-5}$, and approaches ADT=21.942 for $P_{fa} = 10^{-6}$ for the same reference window length.

The quotient of the respective ADT values of the OS and the CA-CFAR procedures corresponds directly to the CFAR loss to be suffered if the CA-CFAR procedure is

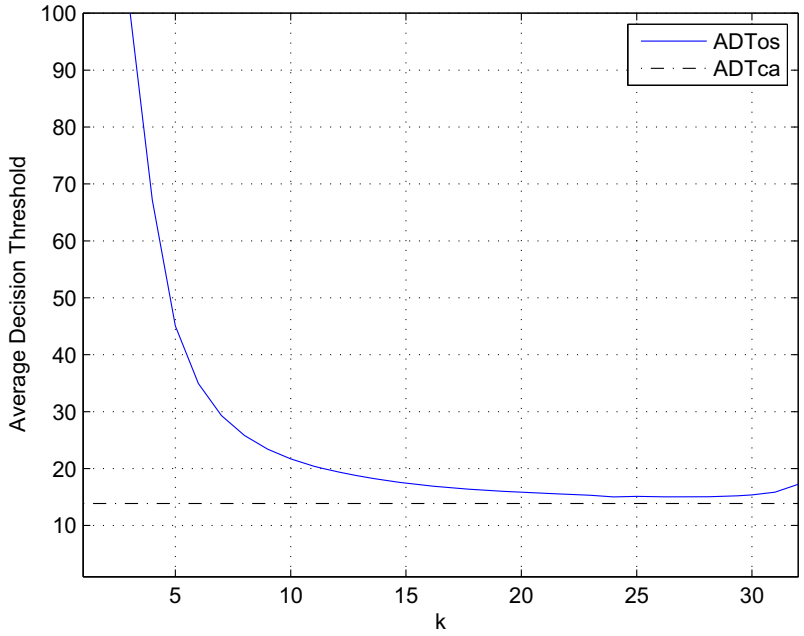

FIGURE 2.7: The ADT as a function of the rank order index k, $N = 32$ and $P_{fa} = 10^{-5}$

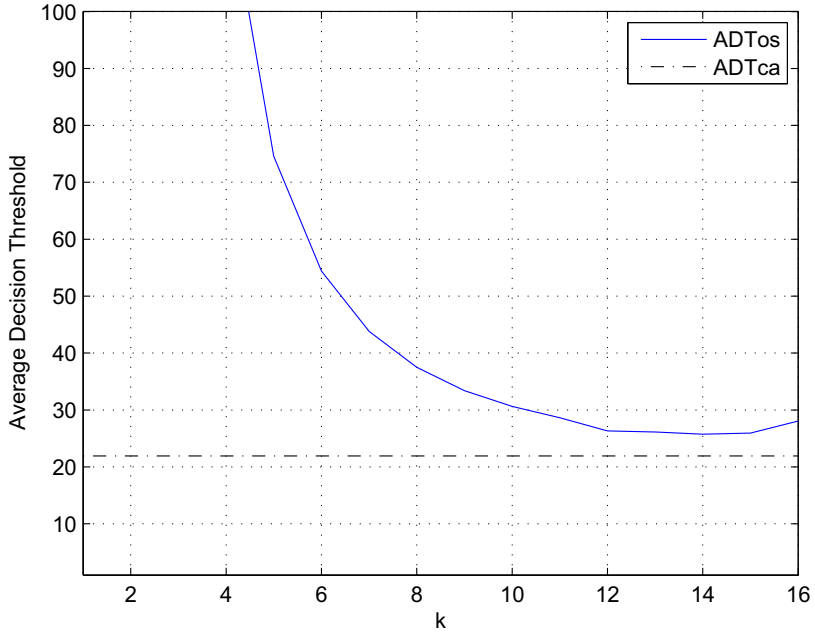

FIGURE 2.8: The ADT as a function of the rank order index k, $N = 16$ and $P_{fa} = 10^{-6}$

replaced by an OS-CFAR one.

Herein, for specifying the OS-CFAR procedure, the parameter $k = \frac{3N}{4}$ is chosen.

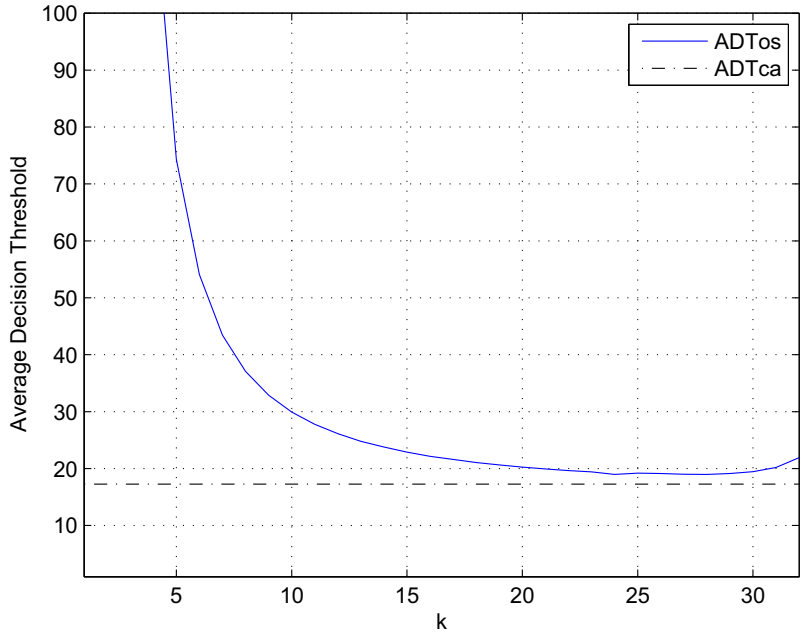

FIGURE 2.9: The ADT as a function of the rank order index k, $N = 32$ and $P_{fa} = 10^{-6}$

This choice is motivated by the fact that it results in a negligible additional loss in ADT versus rank order index k. A value of k about $k = \frac{3N}{4}$ is well suited for practical application.

In presence of clutter edges, the response of the OS-CFAR depends strongly on the clutter area length, L, the reference window size, N, and the rank-order k.

Fig. 2.10 and Fig. 2.11 show the behavior of the OS-CFAR detector for different combinations of the considered parameters, N, L and k. The conducted experiences are performed for $L > (N - k)$ in two cases, $k < \frac{N}{2}$ and $k > \frac{N}{2}$.

Fig. 2.10 shows the behavior of the OS-CFAR to expected clutter area. The threshold (red line) follows the clutter amplitudes with sufficient distance to avoid undesired clutter detections.

There remains a kind of safety zone depending on the relation $\frac{N}{k}$. With k greater than $\frac{N}{2}$, clutter areas are expanded, with k less than $\frac{N}{2}$, they are shrunk. These relations are illustrated in Fig. 2.10 and Fig. 2.11 for $k < \frac{N}{2}$ and $k > \frac{N}{2}$, respectively.

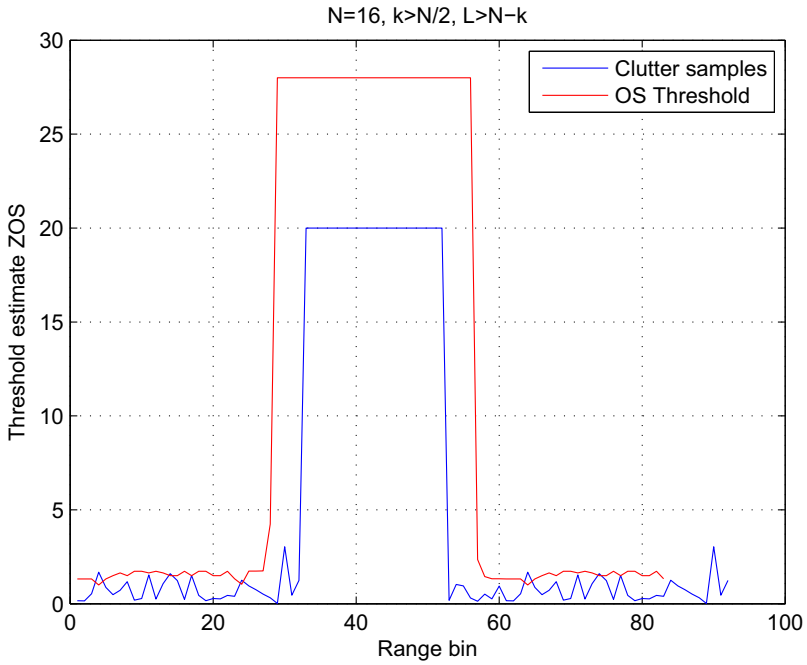

FIGURE 2.10: Principal impact of the rank order parameter k on the clutter power estimation in OS-CFAR. For $k > \frac{N}{2}$, the clutter areas appears extended.

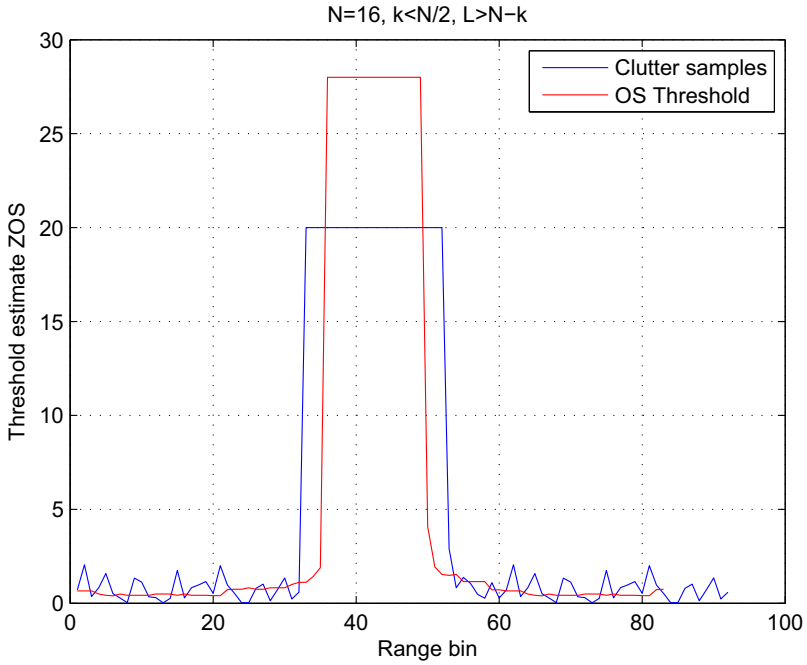

FIGURE 2.11: Principal impact of the rank order parameter k on the clutter power estimation in OS-CFAR. For $k < \frac{N}{2}$, the clutter areas appears shrunk.

It is obvious that for CFAR applications, a value of k greater than $\frac{N}{2}$ should be used in order to avoid clutter detections at clutter edges.

Independently of the clutter length, L, clutter detections are sufficiently suppressed even if a reference window size N distinctly larger than L is used.

2.7.2 Final comment

The rank order parameter, k, of the OS-CFAR detector should be greater than $\frac{N}{2}$ which results in selecting a value greater than the median from the ordered sequence and has the effect of expanding the clutter areas. On the other hand, the difference $(N-k)$ should not be less than the double the target length in order to avoid two targets from being mutually blanked. This leaves a certain range for defining the parameter k within which the clutter level estimation performance of the OS CFAR procedure is only slightly changed ; see the broad minimum in Fig. 2.6, Fig. 2.7, Fig. 2.8 and Fig. 2.9. The rank-order parameter k can therefore be deliberately determined within this range according to geometric considerations on reference window size N, minimum suppressible clutter size L, and maximum target width. k should be chosen between $\frac{N}{2}$ and $\frac{3N}{2}$.

2.8 Signal model

Real radar environment cannot be described by a single model, yet consideration of a larger number of different situations might be confusing. For this reasons, it is assumed that the random variables of the reference window at the output of the square law detector are independent and identically distributed (i.i.d.) and are governed by an exponential distribution with probability density function (pdf) :

$$f(x) = \frac{1}{\lambda} e^{-\frac{x}{\lambda}}, x \geq 0 \tag{2.30}$$

and the distribution function (df) :

$$F(x) = 1 - e^{-\frac{x}{\lambda}}, x \geq 0 \tag{2.31}$$

Under the null hypothesis H_0 of no target in the cell under test, λ is the total background noise power, which is denoted by μ. Under hypothesis H_1 in presence of a target, λ is $\lambda = \mu(1 + S)$, where S is the average signal to noise ratio (SNR).

The assumption of an exponential distribution is justified for the square law detector in the case of normally distributed noise in the video range.

2.9 Application of digital signal processors in radar systems

Digital techniques have been used in radar systems for a long time. The radar timing unit and ranging unit were the first digitized units in radar systems. The radar display, servo-system and monitor system were digitized later.
The application of digital signal processing techniques in radar systems can be summarized as follows.

Radar transmitter :

- Adaptive frequency agility [10] ;
- Adaptive waveform generation [10].

Antenna system :

- Synthetic aperture [72] ;
- Inverse synthetic aperture [72] ;
- Doppler beam shaping [9] ;
- Digital beamforming [10] ;
- Adaptive sidelobe cancelation [72].

Radar receiver :

- Matched filters [72] ;

– Clutter cancelation [7].

Detector :

– CFAR detector in time domain [75] ;

– Non coherent signal integration [72] ;

– Coherent signal integration (Doppler filter bank) [10] ;

– CFAR detector in frequency domain [10].

2.10 Some requirements of radar signal processor

The fundamental requirements of radar signal processor can be summarized as follows.

2.10.1 Dynamic range

The required dynamic range of a digital signal processor depends on the system performance specifications. For example, the dynamic range of a digital MTI is determined by the specification of the improvement factor [1]. However, the improvement factor of DMTI is different from the improvement factor of the whole radar system. The later not only depends on the dynamic range but also on the instability of the system, antenna scanning modulation, and spectral spread of the clutter. Once the improvement factor of the system has been determined, the dynamic range of all the parts, from receiver front end to digital signal processor, should not limit this improvement factor specification.

The dynamic range of a radar signal processor is determined by the number of bits of the processor. In general, it is equal to 6dB/bit. Since the number of bits of a digital processor itself is large enough, such as 16 bits, the dynamic range of a digital

1. The MTI improvement factor is a measure of MTI performance, defined as the signal to clutter ratio of the output of the clutter filter divided by the signal to clutter ratio at the input of the clutter filter, averaged uniformly over all target radial velocities of interest.

processor is mainly determined by the number of bits of the A/D converter. The A/D converter is the "bottle-neck" of a radar signal processor [10].

2.10.2 Instruction cycle and clock frequency

The requirement on the instruction cycle depends on the algorithm, the number of data points, and sampling rate of data. In a general purpose computer, it is measured in "Million of Instructions Per Second" (MIPS).
In the signal processor, the instruction cycle is replaced by "throughput rate".
Since with most signal processors, including radar signal processors, the data are complex numbers, so the throughput rate is measured in "Million Complex Operations Per Second" (MCOPS).

The instruction cycle of a practical signal processor is defined by the devices and architecture. For example, if DSP chips are used in a radar signal processor, the instruction cycle of the DSP chip is $100ns$. If the required instruction cycle is $10ns$, then 10 DSP chips can operate in parallel. This is because most radar signal processors can be combined in parallel sub-processors. Each processor processes equal amounts of range bin data, since the algorithm is the same for all data.

The clock frequency is related to the instruction cycle but is different from it. In most microprocessors, performing one instruction requires several clock periods. However, in signal processors with Harvard architecture, more than two instructions can be performed within one clock period. The main clock of the radar signal processor is synchronized with the sampling rate of the A/D converter.

2.10.3 Fixed point versus floating point arithmetic

Most radar signal processors employ fixed-point arithmetic for simplicity. In fixed-point arithmetic, addition, assuming no overflow occurs, is an exact operation, but multiplication is inherently non-exact. The reason for this is that the product of two

n bit numbers is $2n$ bit number, and if the register length is to be kept constant to n bit, the product should be reduced to n bits. The approximation can be affected by truncation or rounding. This problem is more serious in FFT operation. To avoid overflow in FFT operation, block floating point is often used. It seems that 16 bit fixed-point arithmetic is sufficient for most radar signal processors. Floating-point processors can be used in high performance processors.

2.11 Conclusion

In this chapter, we have provided some generalities on radar systems, the detection basics and a review of some important CFAR detectors. We have also pointed out some significant DSP applications in radar system.

In the next chapter, we propose a new CFAR detector using the information theoretic criteria for target detection under severe interference situation in order to overcome the classical OS-CFAR detector limitation when the number of interfering targets exceeds the tolerable one.

"This page is intentionally left blank"

CHAPTER III

Application of the information theoretic criteria in radar detection

In this chapter, we propose a new approach for determining efficiently the unwanted interfering samples in the reference window, for the ordered statistics constant false alarm rate detector. This approach is based on the application of the information theoretic criteria principle.

3.1 Introduction

The signal returns from radar targets are usually buried in thermal noise and clutter. Target detection is commonly performed by comparing radar returns to an adaptive threshold such that a constant false alarm rate (CFAR) is maintained [1].

For complex environment such as anti-collision radars, where the environment changes abruptly, the conventional detectors cannot detect targets properly. However, most of the works in the literature consider some types of censoring based on a priori knowledge and some approaches based on an automatic censoring of unwanted cells have been proposed in the literature [29,43].

Herein, we consider the problem of automatic determination of the unknown number of interfering targets in the reference window, by minimizing the information

theoretic criteria. The main motivation behind the development of such automatic detection of the number of interfering targets is the degradation of the OS-CFAR performance when the number of interfering targets exceeds a known integer threshold. This is to reduce the CFAR loss and improve the detection probability of the OS-CFAR processor. The proposed processor is referred to as Forward Automatic Order Selection Ordered Statistics Detector (FAOSOSD) and does not require any prior information about the number of interfering targets.

3.2 Radar detection in presence of interfering targets

In a radar system, it is needed to determine the power threshold from which any return can be considered as a target. In most radar detectors, the threshold is set in order to maintain a required probability of false alarm rate. In actual environment, unwanted clutter and interference sources change spatially and temporally. In this situation, an adaptive threshold should be employed, where the threshold level is changed to maintain a constant probability of false alarm.

Many CFAR algorithms are developed to meet different situations namely in a transition in the clutter power distribution and the presence of interfering targets which refer to targets present in the reference window cells. When the number of interfering targets exceeds the assumed number, these detectors exhibit a serious performance degradation.

The most commonly used detector in radar in presence of interfering target is the OS-CFAR processor. The bloc diagram of the OS-CFAR detector is presented in Fig. 3.1.

The adaptive threshold of OS-CFAR processors is formally defined in terms of ranked samples of reference cells. To reduce the CFAR loss and improve the detection probability of OS-CFAR processors, the largest sample of ranked cells, involved in the computation of detection threshold, can be properly selected when the exact number

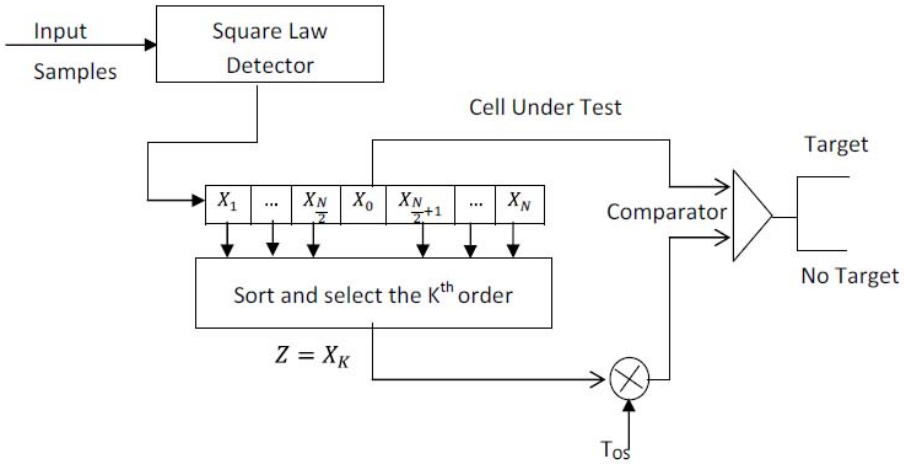

FIGURE 3.1: The bloc diagram of the OS-CFAR algorithm.

of interfering targets is accurately determined.

In Fig. 3.2, we consider radar signal detection using the classical OS-CFAR detector with a sliding reference window size, $N = 16$, a threshold sample order, $K = \frac{3N}{4} = 12$ which is known to be the optimum value (see section 2.7.1) and a probability of false alarm, $P_{fa} = 10^{-5}$, in presence of two clusters. The first cluster contains three targets (cells 14, 15 and 16), while the second one contains nine targets (from cell 45 to 52) with different signal to noise ratios. The application of the OS-CFAR detector permits the detection of all the targets of the first cluster, while all the targets of the second cluster are missed. We observe also that the target at cell 41 is masked by the power of the second cluster targets. This situation presents a limitation for the OS-CFAR detection when the number of interfering targets forming the group exceeds the assumed number [62,65].

The performance degradation of the OS-CFAR detector in this kind of situation is due to the fact that if the number of interfering targets exceeds a known integer threshold which is defined to be $(N - K)$ [20] ; the threshold estimate considers the sample corresponding to an interfering target which has an important power compared to that of the noise. The detection threshold will be higher and invokes a masking effect of the target in the cell under test.

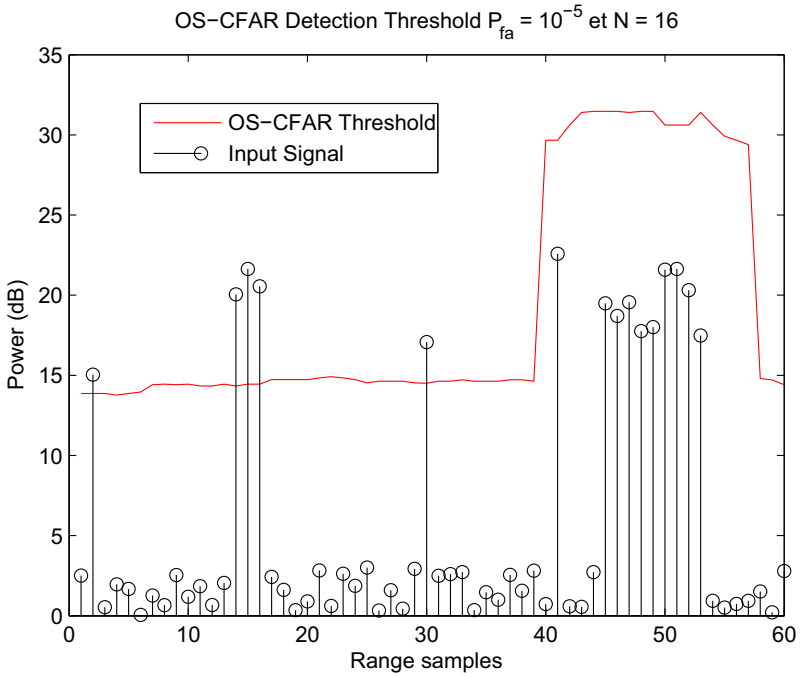

FIGURE 3.2: The OS-CFAR detector limitation in severe multi-targets situation.

Therefore, the proposed method has an attractive feature by adding to the available OS-CFAR detector the potential to determine efficiently the unwanted interfering samples in the reference window, which may cause a poor probability of detection.

Some combinations of the CA-CFAR and the OS-CFAR detectors are proposed in the literature [53,54]. We consider as example the AND-CFAR and the OR-CFAR detectors. The corresponding bloc diagram is shown in Fig. 3.3. T_1, T_2 represent the scale factors to maintain a given constant false alarm rate, and Z_1, Z_2 represent the threshold estimates for the CA-CFAR and the OS-CFAR detectors, respectively. The final decision is made according to the binary rule "OR" or "AND" established in the fusion center (see Fig. 3.3).

It is shown that these detectors have better detection probabilities than OS-CFAR in special situations under different false alarm probabilities [54].

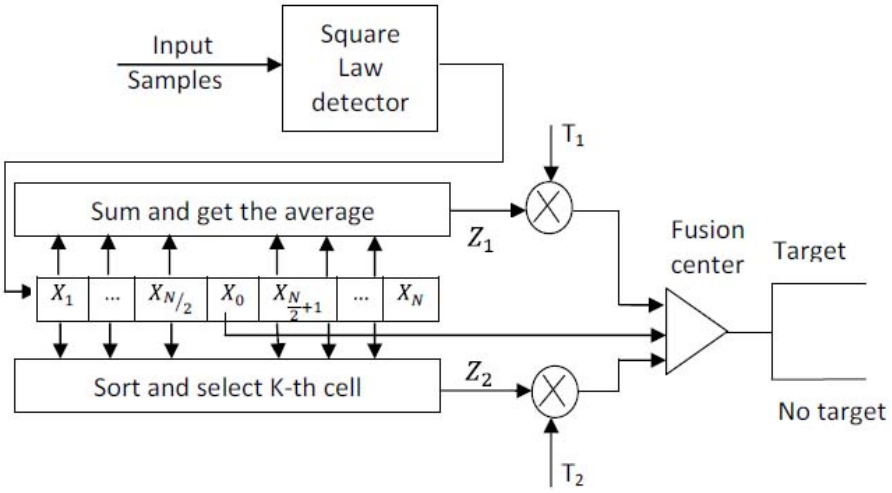

FIGURE 3.3: The bloc diagram of the OR-CFAR and AND-CFAR detectors.

3.3 The proposed detector architecture

The bloc diagram of the proposed detector is depicted in Fig. 3.4. The radar echo is received and the square law detected range samples are sent to a window register of length $(N+1)$, the statistic Z is obtained from the noise power formed by processing the contents of N reference cells surrounding the cell under test (CUT).

The radar outputs $X_i : i = 0, 1, ..., X_N$ are stored in a tapped delay line. The cell with the subscript 0 is the cell under test, where it contains the signal which should be detected as a target or not. The last N surrounding cells are the auxiliary cells used to construct the CFAR threshold.

The proposed detector referred to as Forward Automatic Order Selection Ordered Statistics Detector (FAOSOSD), consists of five fundamental steps. These steps are performed dynamically by using a suitable set of ranked cells to estimate the unknown background level and set the adaptive threshold accordingly. This detector does not require any prior information about the clutter parameters nor the number of interfering targets.

The procedure, first ranks the outputs of all reference range cells in ascending order according to their magnitudes as follows :

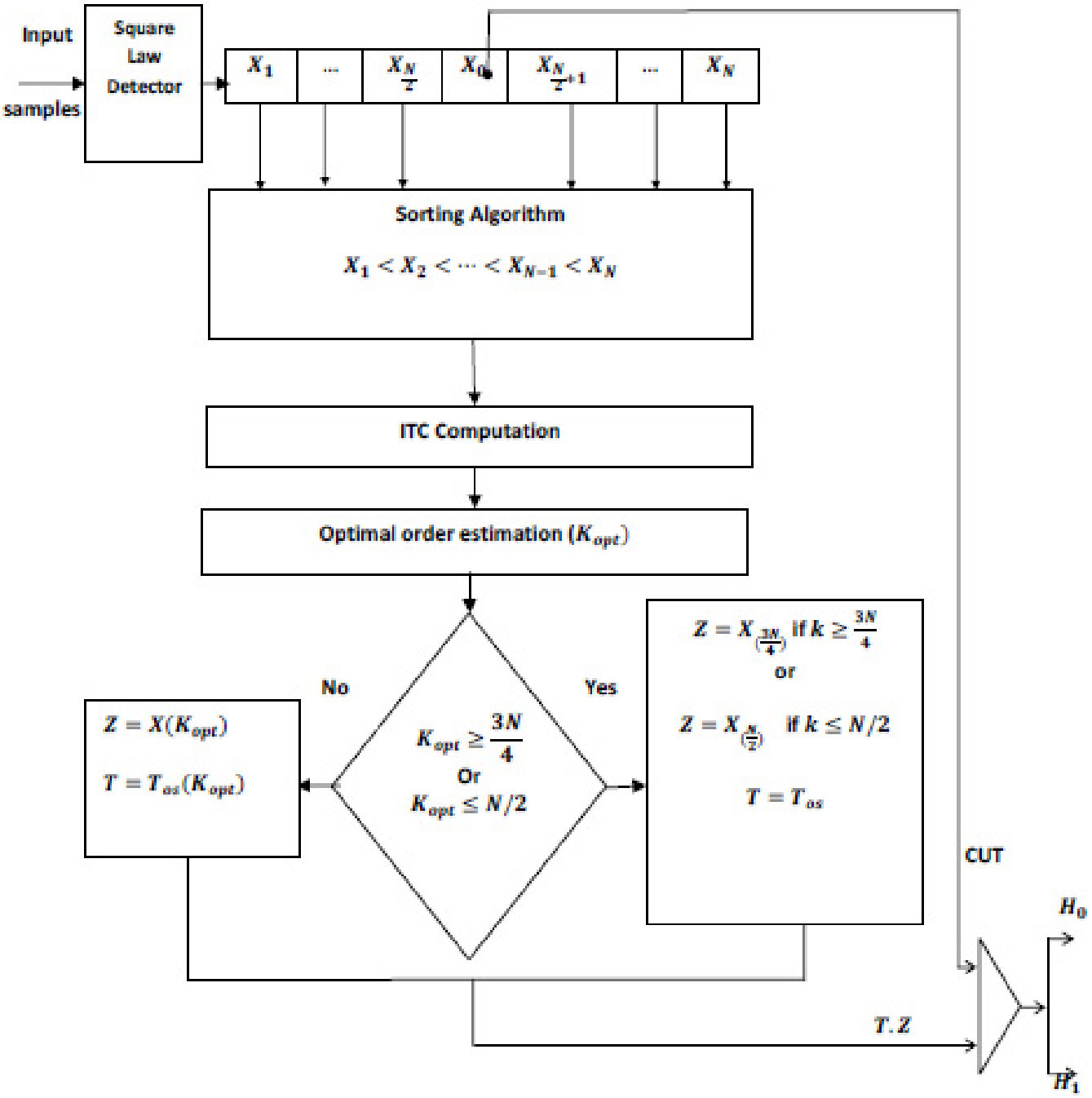

FIGURE 3.4: The bloc diagram of the FAOSOSD detector.

Step1 : Sorting the samples of the reference window ;

$$X(1) \leq X(2) \leq \cdots \leq X(k) \leq \cdots \leq X(N) \tag{3.1}$$

Step2 : Computing the corresponding information theoretic criteria for the sorted window ;

Step3 : Estimating the optimal order for the OS-CFAR detector, K_{opt} ;

Step4 : Selecting the corresponding scale factor and computing the threshold level ;

$$TZ = TX(K_{opt}) \tag{3.2}$$

Step5 : The cell under test is compared with the derived threshold and a decision is made according to the tests :

$$H_1 : X_0 \geq TX(K_{opt}) \tag{3.3}$$

$$H_0 : X_0 < TX(K_{opt}) \tag{3.4}$$

Hypothesis H_1 denotes the presence of target in the test cell, while H_0 denotes there is no target. In the FAOSOSD detector, the threshold multiplier T is defined according to the estimated number of interfering targets. Note that when the estimated rank exceeds $\frac{3N}{4}$ or less than $\frac{N}{2}$, we keep the classical OS-CFAR threshold for $k = \frac{3N}{4}$ or $k = \frac{N}{2}$, respectively.

The proposed detector requires the estimation of the interfering targets number to set the corresponding threshold. The scale factor is selected with respect to the estimated interfering target number from a pre-organized lookup table. The proposed algorithm consists of detecting the corrupted reference cells and adjusting the OS-CFAR detector parameters to minimize the CFAR loss.

Both steps are performed dynamically by using a suitable set of ranked cells to estimate the unknown background level and set the adaptive thresholds accordingly.

3.4 Estimation of the number of interfering targets

The proposed approach proceeds as follows. First, we sort the reference window samples in increasing order. Then, we apply the information theoretic criteria, $ITC(k)$, for each sample. We determine the minimum of the ITC and the corresponding sample order. The obtained order represents the estimated rank of interfering targets.

The ITC is defined as [6,61] :

$$AIC(k) = -2(N-k)N\ln(\frac{G(\lambda_{k+1},\cdots,\lambda_N)}{A(\lambda_{k+1},\cdots,\lambda_N)}) + 2k(2N-k) \tag{3.5}$$

for Akaike, AIC, criteria, and

$$MDL(k) = -(N-k)N\ln(\frac{G(\lambda_{k+1},\cdots,\lambda_N)}{A(\lambda_{k+1},\cdots,\lambda_N)}) + \frac{1}{2}k(2N-k)\ln(N) \tag{3.6}$$

for the minimum description length, MDL, criterion.
where N the number of samples, $\lambda_1, \lambda_2 \cdots, \lambda_N$ denote, in our case, the samples of the reference window [1], G and A denote respectively, the geometric and the arithmetic means of their arguments.

The k order of the OS-CFAR detector is taken to be the value of $k \in \{0, 1, ..., N-1\}$ for which either $AIC(k)$ or $MDL(k)$ is minimized.

In the sequel, we are interested in the MDL criterion. This approach allows to perform an automatic detection of the interfering target groups.

We present the simulation results that illustrate the performance of the proposed method applied to the OS-CFAR detector in multi-target situations.

Several scenarios are conducted to show the effectiveness of the proposed method, we present herein two significant examples.

1. Note that these samples are positive values since they come from the square law detector.

In the first one, illustrated in Fig. 3.5, we consider a reference window of 32 cells with the presence of five interfering targets at cells number 17, 18, 19, 20 and 24 with equal Interference to Noise Ratio, $INR = 15dB$ as shown in Fig. 3.5 (a). Observing the gradual decrease of the ordered samples in Fig. 3.5 (b) it is clear that the separation of the five largest samples from the smallest ones is an easy task. In Fig. 3.5 (c), we present the information theoretic criteria variation.

We observe a minimum at cell number 27 which separates the two regions of noise and interfering targets. The number of interfering targets is determined as the value for which the ITC criteria is minimized. The position of this minimum, K_{int}, indicates the first interfering target rank in the ordered reference window. The above $(N-K_{int})$ cells correspond to interfering targets.

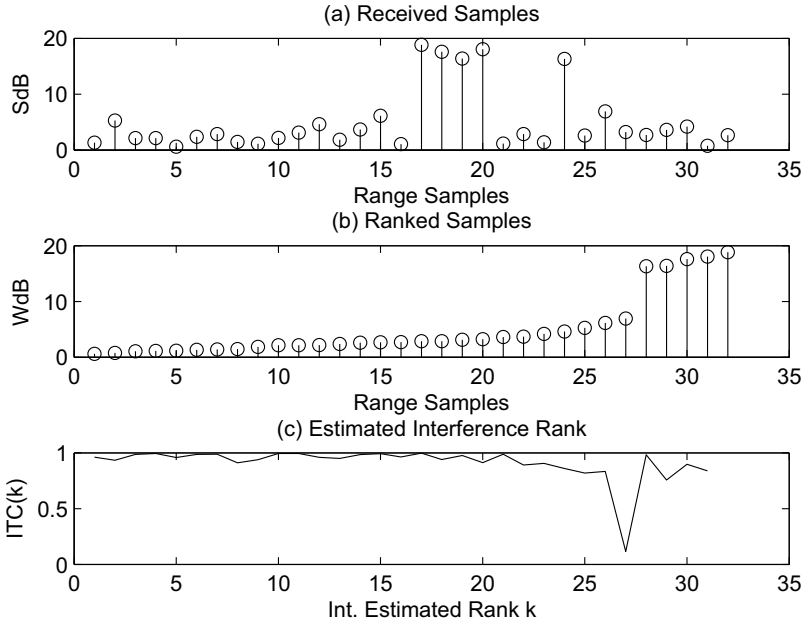

FIGURE 3.5: Interference samples number estimation in presence of five interfering targets with $INR = 15dB$.

In the second example, shown in Fig. 3.6, we consider the same reference window size, and the number of interfering targets is increased to eight, and we decrease the

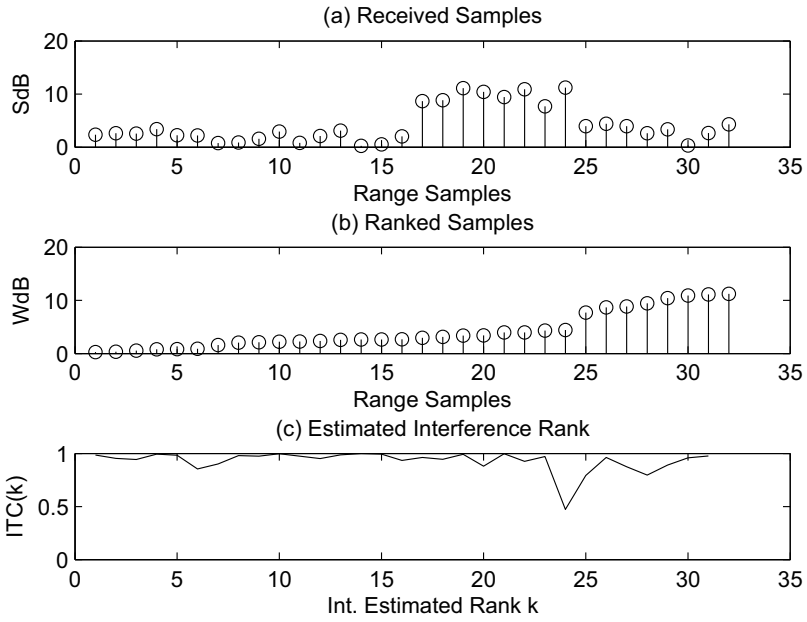

FIGURE 3.6: Interference samples number estimation in presence of eight interfering targets with $INR = 7dB$.

INR to $7dB$ to have a small gap between the noise and target samples. We observe in Fig. 3.6, that the ITC estimates eight as the number of interfering targets.

For the FAOSOSD order selection, we use the K_{opt} ordered sample which corresponds to (K_{int}) to prevent the use of an interfering target sample to compute the threshold. This technique reduces the effect of target masking when the number of interfering targets exceeds the supposed limit.

3.5 Simulation and performance analysis

In this section, we evaluate the performance of the proposed algorithm in different interfering target situations.

3.5.1 Detection thresholds

The simulated data are generated according to exponential $i.i.d$ random variables for the reference window samples. For targets, the corresponding data consider the signal to noise ratio, SNR, for the cell under test and the corresponding interference to noise ratio, INR, for the interfering target samples.

We consider the detection thresholds of the classical OS-CFAR detector for $K = 12$ and the FAOSOSD for $Pfa = 10^{-5}$ and $N = 16$.

We present three interfering target situations. In Fig. 3.7, we consider three separated targets at range cells 2, 14 and 41. Both the OS-CFAR and the FAOSOSD detect the three targets and the corresponding threshold levels are close to each other.

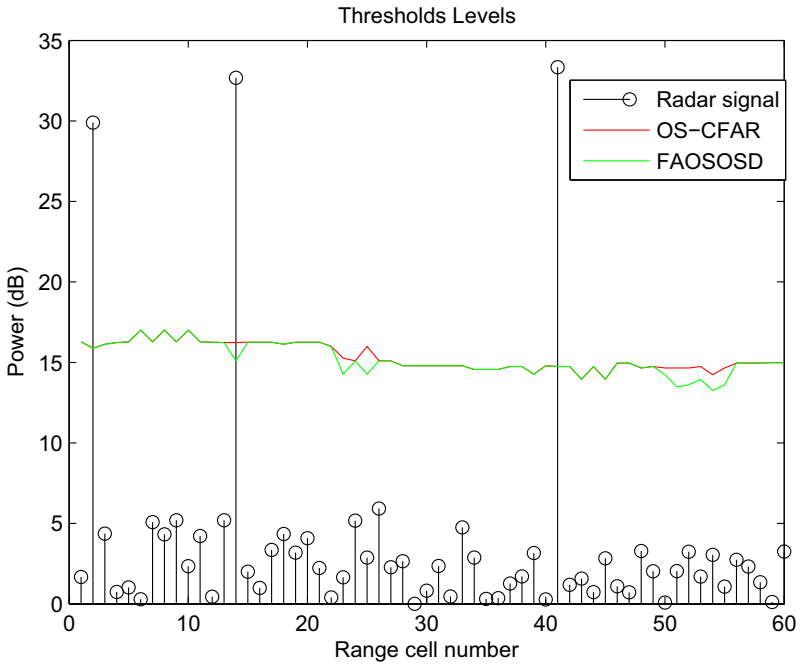

FIGURE 3.7: CFAR thresholds in presence of three separated targets, $Pfa = 10^{-5}$, $N = 16$ and $K = 12$.

In Fig. 3.8, we present a radar signal in presence of two separated targets and a group of four targets (less than or equals to $(N - K)$). The separated targets present at cells 2 and 14 and the group of targets centered at cell 50 are easily detected by

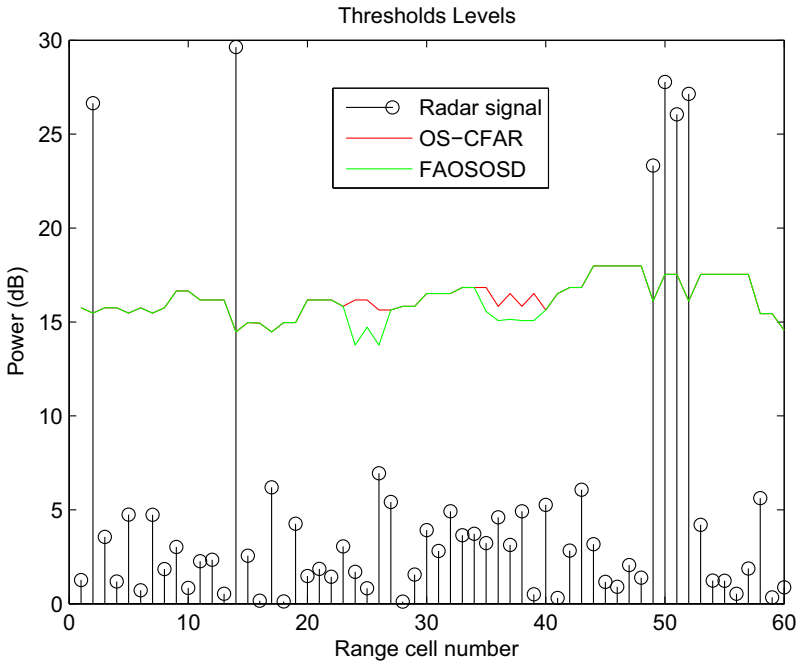

FIGURE 3.8: CFAR thresholds in presence of two separated targets and a group of four interfering targets, $Pfa = 10^{-5}$, $N = 16$ and $K = 12$

the two detectors.

In Fig. 3.9, we observe that the group of targets are not detected by the classical OS-CFAR detector because the number of interfering targets exceeds four, for $K = 12$ and $N = 16$, while the FAOSOSD detects the eight targets present in the group by reducing the threshold sample order accordingly to the obtained estimated interfering target number. Similarly, the FAOSOSD detects all the five targets present between cell range 10 and 20, while the OS-CFAR misses the target with the lower SNR present at cell range 11. The missed target is masked by the interfering signals present in the reference window.

3.5.2 Probability of detection

A total number of 10^4 independent trials were used to obtain the estimates of the detection probability. Note that the Interference to Noise Ratio, INR, is taken equal to signal to noise ratio, SNR, in all simulations.

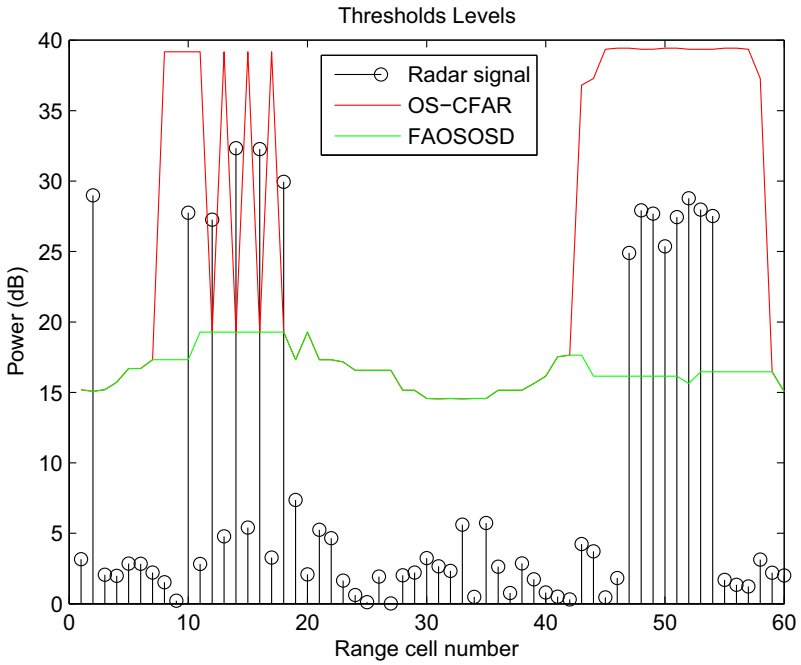

FIGURE 3.9: CFAR thresholds in presence of a group of eight interfering targets, and five interfering signals, $Pfa = 10^{-5}$, $N = 16$ and $K = 12$.

The obtained results show that the FAOSOSD has a much better performance than the classical OS-CFAR, in terms of detecting groups of close targets or targets masked by interfering signals.

As the number of interfering targets present in the reference window increases, the detection performance of the OS-CFAR processor decreases, while the detection probability of the FAOSOSD is relatively maintained, as shown in Fig. 3.11.

The probabilities of detection of the OS-CFAR detector, $K = 3N/4$, and the FAOSOSD, $K = K_{opt}$, are obtained by Monte Carlo simulations in presence of eight interfering targets.

We notice the performance degradation of the OS-CFAR because the number of interfering targets exceeds the supposed one (four for $N = 16$). For example, to achieve a probability of detection of 0.6, the OS-CFAR detector requires additional signal to noise ratio of about 12dB more than the FAOSOSD detector.

The performances of the FAOSOSD in severe interference situations are compared

also to the AND-CFAR and OR-CFAR detectors.

The corresponding detection probabilities are plotted in Fig. 3.11. It can be seen that the FAOSOSD yields the best detection of all the three detectors. The AND-CFAR detection performance is the worst among the three CFAR detectors. This is due to the performance degradation of the OS-CFAR detector because the number of the interfering targets exceeds the upper limit which is four in this case, and on the other hand the CA-CFAR detector presents the worst performance in presence of interfering targets. The OR-CFAR detector remains subject to the performances of the CA-CFAR and the OS-CFAR detectors separately.

In order to generalize the obtained results, other simulations have been conducted for different values of the false alarm probability, P_{fa}, and the size of the reference window, N.

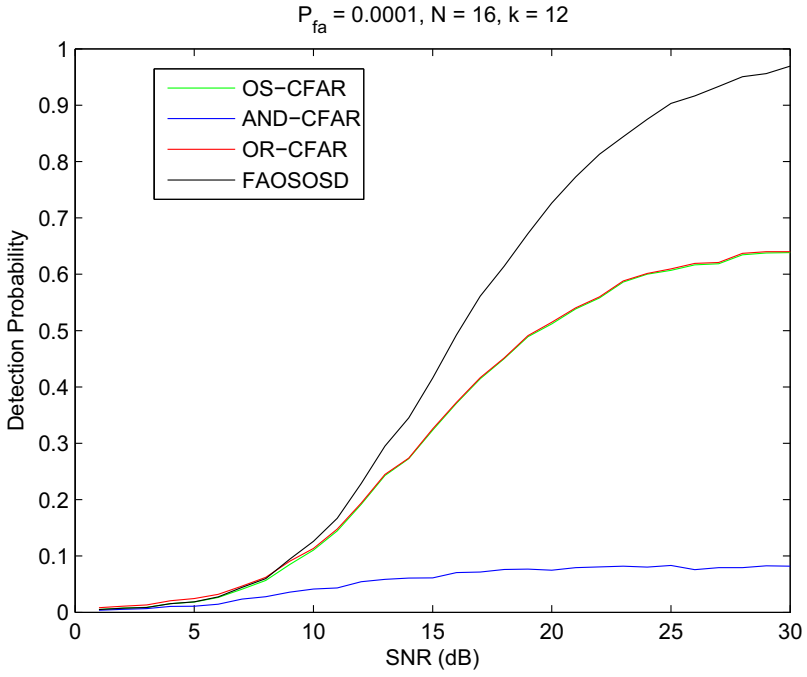

FIGURE 3.10: Detection probabilities for $N = 16$, $K = 12$ and $Pfa = 10^{-4}$.

Fig. 3.10, 3.11 and 3.12 show the detection probabilities of the FAOSOSD, the OS-CFAR, the AND-CFAR and the OR-CFAR detectors for different values of the

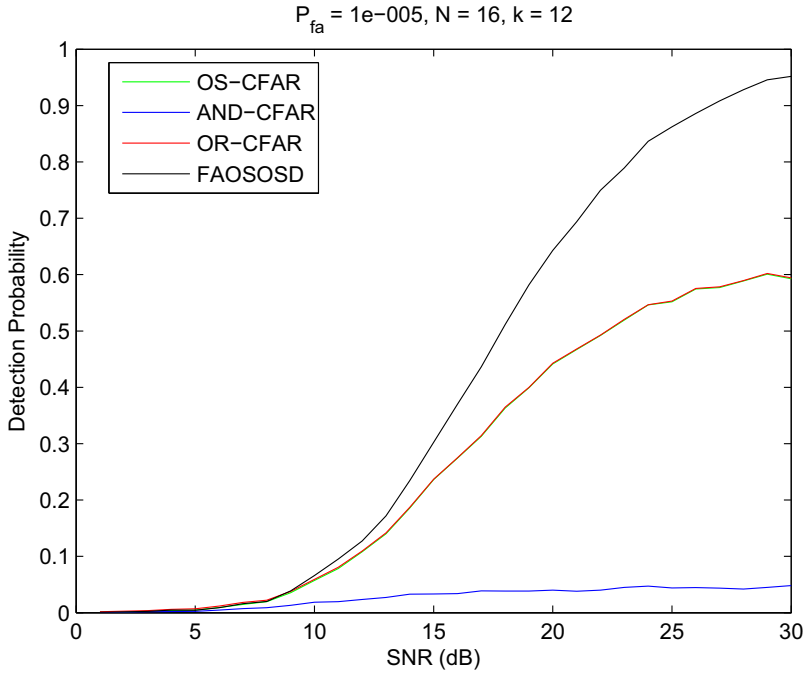

FIGURE 3.11: Detection probabilities for $N = 16$, $K = 12$ and $Pfa = 10^{-5}$.

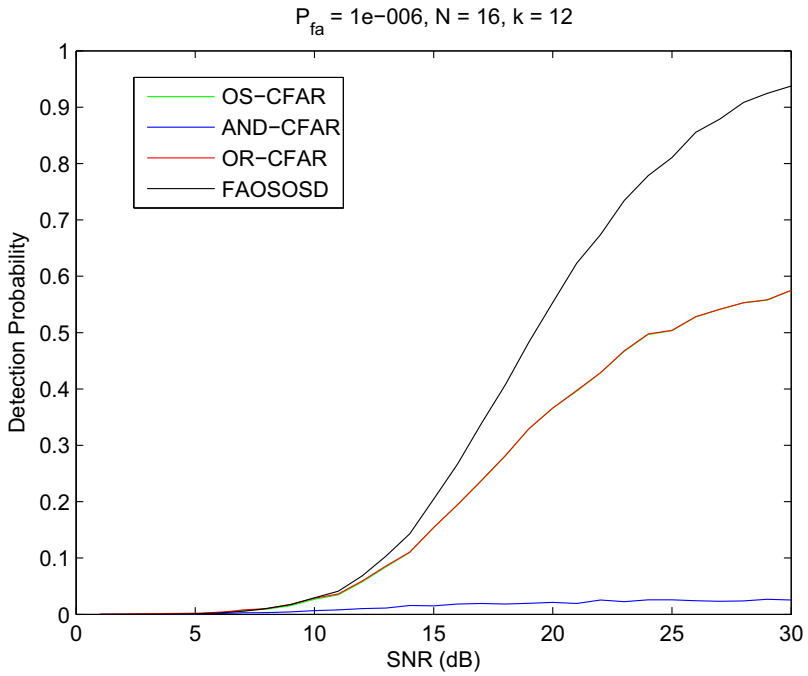

FIGURE 3.12: Detection probabilities for $N = 16$, $K = 12$ and $Pfa = 10^{-6}$.

false alarm rate, $Pfa = 10^{-4}$, $Pfa = 10^{-5}$ and $Pfa = 10^{-6}$, respectively, in presence of five interfering targets, for $N = 16$ and $K = 12$. It can be seen that when the false

alarm probability increases the detection probability increases and the FAOSOSD detector is again the best among all CFAR schemes.

Notice that the OS-CFAR and the OR-CFAR detectors have the same performance because of the significant detection loss of the CA-CFAR detector in severe interference situations, hence the OR-CFAR selects the OS-CFAR in such environment conditions.

Fig. 3.13 shows the detection probabilities of the FAOSOSD, the OS-CFAR, the AND-CFAR and the OR-CFAR detectors for $Pfa = 10^{-5}$ and $K = \frac{3N}{4}$ for different values of N, $N = 24$ (3.13 (a)) and $N = 32$ (3.13 (b)), in presence of eight interfering targets. It is noted that higher values of N yield better detection probabilities and the FAOSOSD detector has always the better performance.

3.5.3 False alarm regulation

In this subsection, we present the effect of the presence of interfering targets in the reference window on the false alarm control of the FAOSOSD processor. The number of interfering targets in these simulations, N_i, is chosen to be equal to $(N - K + 1)$.

The results are obtained by Monte Carlo experiments using a total of 10^6 independent trials for the false alarm performance assessment for different reference window sizes. In each case we consider a desired $P_{fa} = 10^{-5}$ and N_i=$(N - K + 1)$.

Fig. 3.14 shows the effective false alarm performance of the proposed detector in presence of $(N - K + 1)$ interfering targets for different INR values. It can be seen that the effective P_{fa} exhibits a slight fluctuations relatively to the desired one for high values of N and low INRs. So, according to these results, we can conclude that the effective false alarm rate of the proposed detector is relatively maintained close to the desired one for large reference window size.

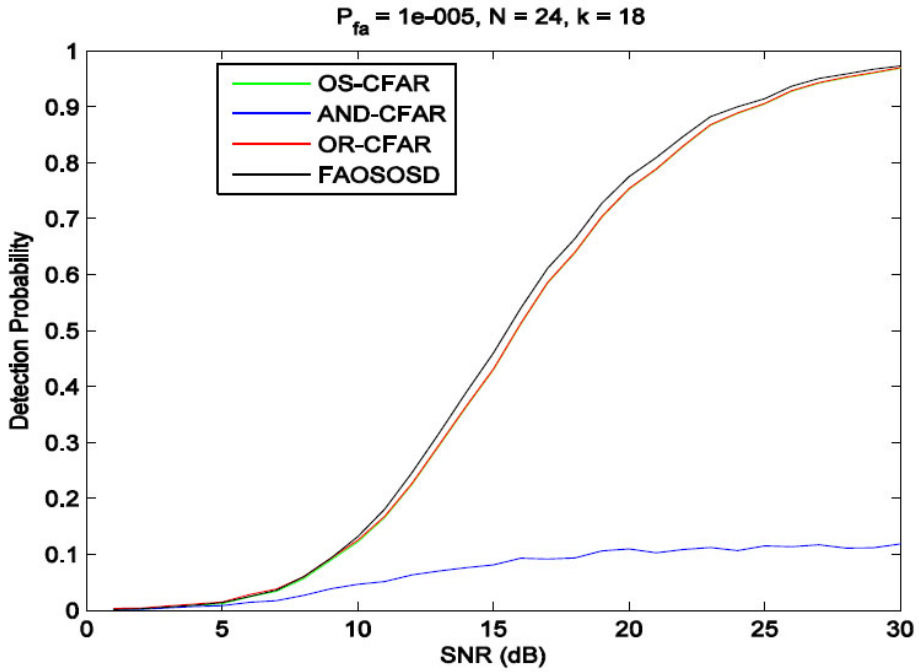

(a)

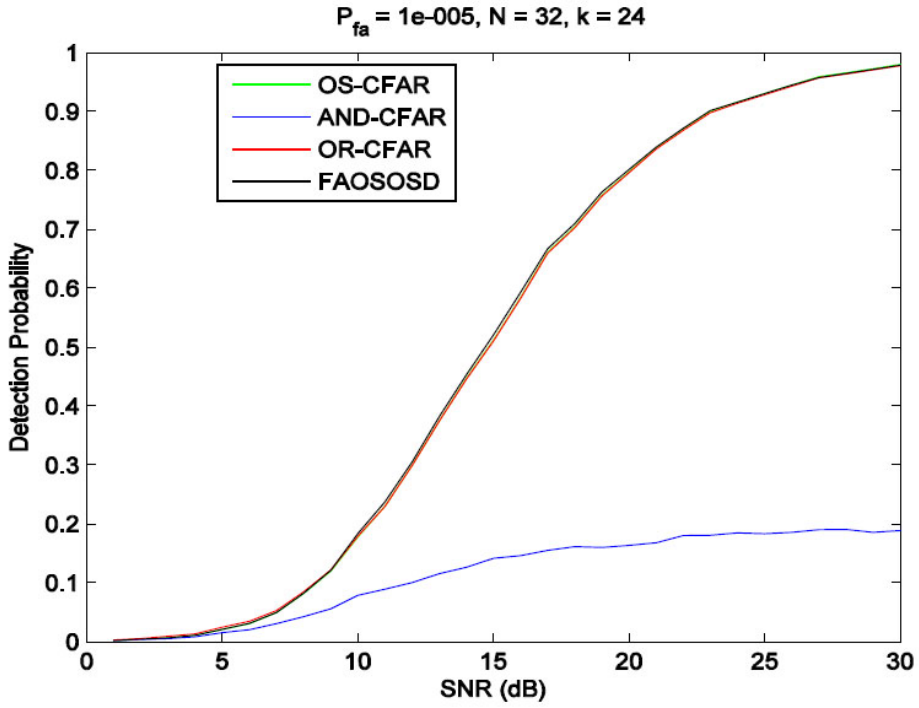

(b)

FIGURE 3.13: Detection probabilities for $Pfa = 10^{-5}$, $K = \frac{3N}{4}$ (a)- N=24. (b)- N=32.

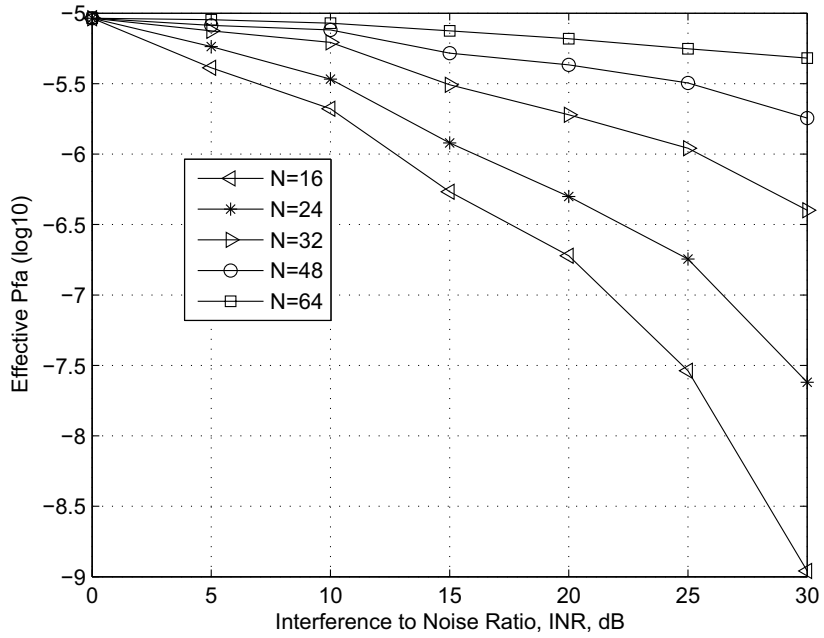

FIGURE 3.14: Effect of the INR on the effective P_{fa} of the FAOSOSD detector in presence of $(N-K+1)$ interfering targets : - Desired $P_{fa} = 10^{-5}$. - $N = 16, 24, 32, 48$ and 64.

3.6 Conclusion

In this chapter, a new approach to the detection of the number of interfering target samples in the CFAR reference window has been presented. The approach is based on the application of the information theoretic criteria principle to improve radar detection under severe interference situations.

Unlike the conventional detection hypothesis test based approach, the proposed detector does not require any prior information about the number of interfering targets. The number of interfering samples is determined merely by minimizing the ITC. The obtained rank is exploited to determine the optimal sample order to establish accordingly the detection threshold level.

It should be pointed out that the obtained simulation results based on synthetic data show that the FAOSOSD processor has a much better performance than the

classical OS-CFAR, the AND-CFAR and the OR-CFAR detectors in severe interference radar situations. Moreover, the performance of the FAOSOSD detector has been validated with real-life data (see Chapter 5).

In the next chapter, we introduce a new CFAR detector based on an adaptive combination of the classical CA-CFAR and OS-CFAR detectors to reduce the additional CFAR losses of ordered statistics based detectors in an homogenous environment, and prevent target masking in presence of interfering targets for the CA-CFAR detector.

"This page is intentionally left blank"

CHAPTER IV

Adaptive Linear Combined CFAR detection

As mentioned in chapters II and III, the CA-CFAR detector suffers from serious detection issues in presence of interfering targets and the OS-CFAR detector presents some additional detectability loss in an homogeneous environment. In this chapter, we propose a new CFAR detector which employs an adaptive composite approach based on the CA-CFAR and the OS-CFAR detectors. The proposed detector provides low CFAR loss in an homogeneous environment and performs robustly, like the OS-CFAR, in presence of interfering targets [33].

4.1 Introduction

In practice, the environment is usually non-homogeneous due to the presence of multiple targets and/or clutter edges in the CFAR reference window. However, there is a significant decrease in performance when the assumption of homogeneous environment is not met.

Herein, we propose a new CFAR detector referred to as Adaptive Linear Combined CFAR detector, ALC-CFAR. The main motivation behind the development of such detector is the degradation of the CA-CFAR performance in presence of interfering targets and the additional losses involved in the OS-CFAR detector in an homogeneous background. Data in the reference window is used to compute an adaptive

weighting factor employed in the fusion scheme. Based on this factor, the ALC-CFAR tailors the background estimation algorithm to reduce the CFAR detection loss and improve the detection probability in heterogenous environment.

4.2 Environment effect on the detection

In order to analyze the detection performance in different kinds of environments, we consider the signal model presented in chapter II. The performance of the CA-CFAR and the OS-CFAR detectors have been examined by means of computer simulations under an homogeneous and non-homogeneous (presence of interfering targets) environments using synthetic data.

For performance assessment, we consider two environments.

(a) An homogeneous environment :

We consider the detection of four separate targets using the conventional CA-CFAR and OS-CFAR detectors.

In Fig. 4.1, we show the detection thresholds for the CA-CFAR and the OS-CFAR detectors for $P_{fa} = 10^{-5}$, $N = 16$ and $K = 12$. Both detectors distinguish easily the four targets present at range cells 10, 40, 60 and 80.

Nevertheless, the OS-CFAR processor exhibits some additional losses in detection power under an homogenous background compared with the CA-CFAR detector. We observe clearly in Fig. 4.2 that the detection curve of the OS-CFAR detector differs from that of the CA-CFAR detector with some detection loss and we note that the detection performance of the OS-CFAR detector depends on the order parameter K as discussed in section 2.7.1.

The corresponding curves have been obtained by Monte Carlo experiments. A trial of 10000 experiments is used.

(b) Non-homogeneous environment :

In Fig. 4.3, we consider radar signal detection in a non-homogeneous environment,

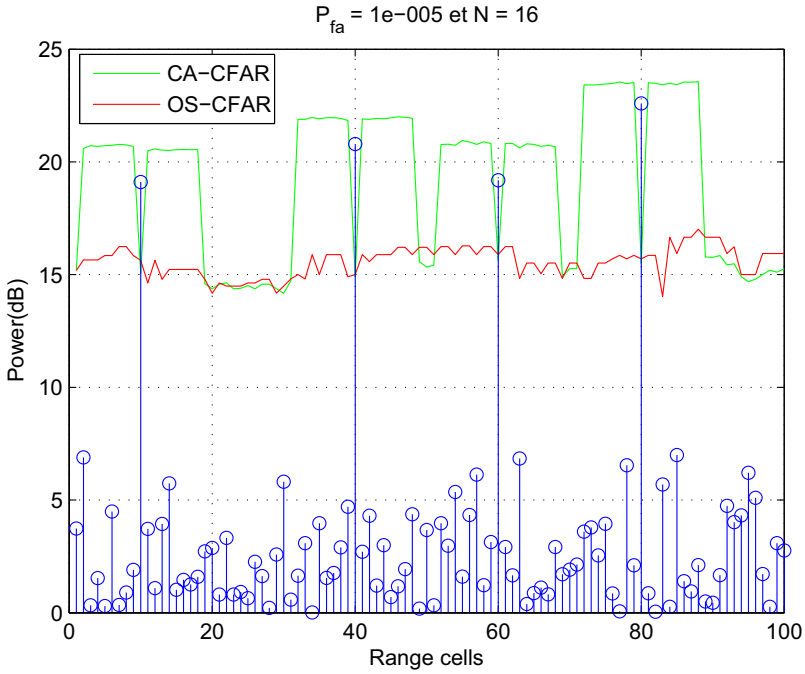

FIGURE 4.1: The OS-CFAR and CA-CFAR detection thresholds in an homogeneous environment, $P_{fa} = 10^{-5}$, $N = 16$ and $K = 12$.

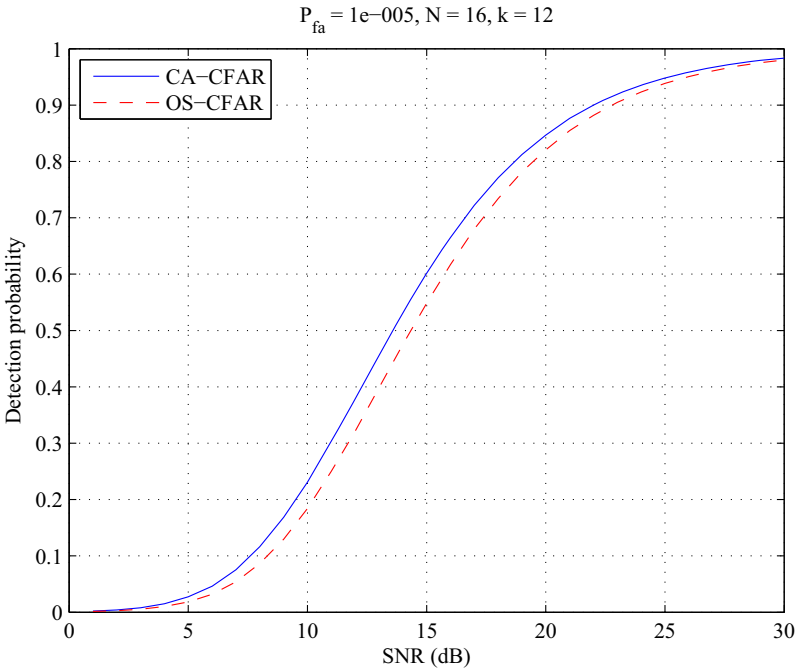

FIGURE 4.2: The OS-CFAR detection loss versus the CA-CFAR detector in an homogeneous environment, $P_{fa} = 10^{-5}$, $N = 16$ and $K = 12$.

presence of interfering targets, using the CA-CFAR and the OS-CFAR detectors for $N = 16$, $K = \frac{3N}{4} = 12$ and $Pfa = 10^{-5}$, in presence of two groups of targets and a separate target present at range cell 80. The first one contains two targets (cells 15

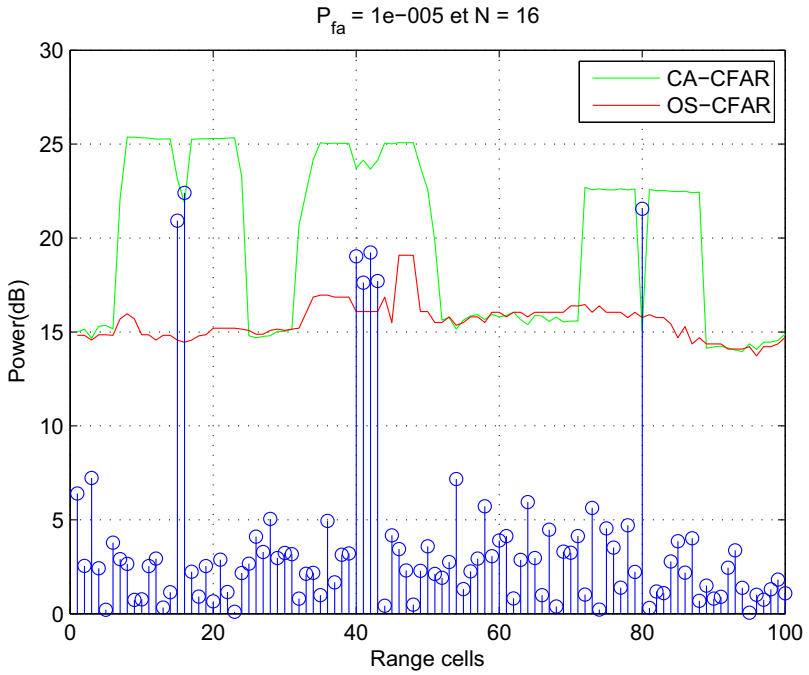

FIGURE 4.3: The OS-CFAR and CA-CFAR thresholds in presence of interfering targets, $P_{fa} = 10^{-5}$, $N = 16$ and $K = 12$.

and 16), while the second one contains four targets (from cell 40 to 43) with different signal to noise ratios.

The application of the CA-CFAR detector allows the detection of the separate target and only the target with higher SNR of the first group, while all the targets of the second group are missed. The OS-CFAR detector detects all the targets of the two groups.

In order to apply different CFAR techniques in a non-homogenous and an homogeneous environment simultaneously, setting a fusion criterion is necessary in order to discriminate the local homogenous character from the non-homogeneous one. Therefore, the ALC-CFAR detector has an attractive feature by adding to the available

conventional detectors the potential to perform the detection procedure with a better detection quality in heterogenous radar environment.

4.3 The proposed ALC-CFAR detector

In section 4.2, we have presented some limitations of the CFAR detection especially for the conventional CA-CFAR and OS-CFAR detectors by comparison of their performances in different radar situations. In this section, we introduce a new CFAR detector which has the capability to present detection performance close to the CA-CFAR detector with less detection losses than the OS-CFAR detector in homogenous environment, and very close to the OS-CFAR in presence of interfering targets to overcome the CA-CFAR detector performance degradation in this kind of situation.

4.3.1 The ALC-CFAR principle

The proposed detector referred to as ALC-CFAR (Adaptive Linear Combined CFAR), is depicted in Fig. 4.4.

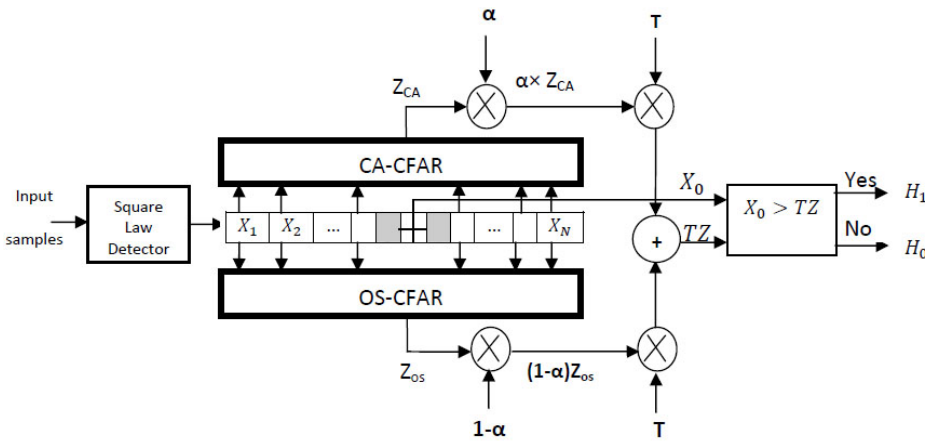

FIGURE 4.4: The proposed Adaptive Linear Combined CFAR detector.

The ALC-CFAR detector is an adaptive linear combination of the CA-CFAR and the OS-CFAR threshold estimates using an adaptive weighting factor according to

the environment changes.

The ALC-CFAR detector estimates the noise level, Z, in the CFAR reference window according to Eq. 4.1.

$$Z = \alpha Z_{CA} + (1 - \alpha) Z_{OS} \tag{4.1}$$

where Z_{CA} and Z_{OS} are the noise level estimates for the CA-CFAR and the OS-CFAR detectors respectively and α is a measure of homogeneity of the reference window samples and belongs to the interval]0,1].

The estimate Z is then multiplied by the scale factor T to form the threshold. The result is compared with the sample level in the cell under test, X_0. After comparison, if the cell under test is greater than the threshold level, hypothesis H_1 (presence of target in the cell under test) is declared true ; else the alternative hypothesis H_0 (absence of target) is declared true.

4.3.2 The adaptive weighting factor

The parameter α, is computed according to the following steps :

Step1 : The CFAR reference window samples are sorted to form a new window W which will be subdivided in two sub-windows W_0 and W_1 according to the rule :

$$k \underset{\leq W_0}{\overset{> W_1}{}} \beta \tag{4.2}$$

where β is an integer threshold. The reference cell $Z_k \in W$, $k = 1, 2, ..., N$, is in the sub-window W_1 if $k > \beta$ and in the sub-window W_0 if $k \leq \beta$.

The principle of this selection is illustrated in Fig. 4.5.

Step2 : The two sub-windows W_0 and W_1 are used to compute α according to

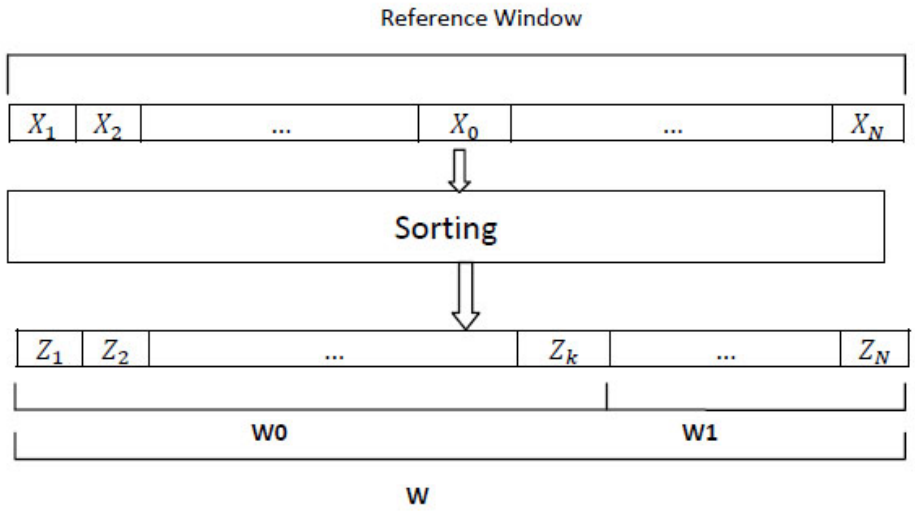

FIGURE 4.5: Illustration of step 1 for the adaptive weighting factor estimation.

expression 4.3.

$$\alpha = \frac{1}{\beta Z_N} \sum_{k=1}^{\beta} Z_k \tag{4.3}$$

Where Z_N is the largest sample in the CFAR reference window, so in the sub-window W_1, and Z_k is the k^{th} largest sample in the sub-window W_0.

We agree that Z_{CA} defined in Eq. 4.1 is the arithmetic mean of the reference window samples. The use of the mean instead of the sum is to make Z_{CA} and Z_{OS} similar.

The expressions of Z_{CA} and Z_{OS} are given by Eq. 4.4 and Eq. 4.5 respectively :

$$Z_{CA} = \frac{1}{N} \sum_{i=1}^{N} Z_k \tag{4.4}$$

$$Z_{OS} = Z_{K_{OS}} \tag{4.5}$$

In what follows, we consider $K_{OS} = \frac{3}{4}N$, which is known to be the optimum value, to protect against interfering targets. The integer threshold β defined in Eq. 4.2 also equals to K_{OS}.

The objective of this preference is to have only the noise samples in W_0 with as great number of cells as possible. The advantage of this choice is developed below.

From Eq. 4.3, one can observe that α is the arithmetic mean of W_0 divided by the largest sample in the reference window.

According to the value of the parameter α, the ALC-CFAR uses either the CA-CFAR threshold (for $\alpha = 1$) or the OS-CFAR threshold (for $\alpha = 0$).

To show that Z is adapted to the environment changes, several experimental situations are conducted.

In an homogeneous environment, no interfering targets, if the reference window samples have close magnitudes, the CA-CFAR estimate is favorable in the threshold level estimation.

In presence of one interfering target, α becomes lower than that in the previous case, because the largest sample in the reference window corresponds, probably, to the interfering target sample. In this case, the OS-CFAR detector which is adapted to this kind of situation has a greater weighting factor than that of the CA-CFAR detector.

In multiple target situations, α remains closer to zero and practically only the OS-CFAR estimate, Z_{OS}, is used in the ALC-CFAR threshold estimation. So, the ALC-CFAR uses, in limit cases, either the CA-CFAR or the OS-CFAR detectors according to the environment homogeneity level.

4.3.3 Analysis of the weighting factor behavior

In this sub-section, we study the effect of α on the estimation of the noise level, Z, in the reference window given by Eq. 4.1, and the influence of the environment changes on the value of α.

We consider two environments : An homogeneous environment, presence of noise only, and an heterogenous environment, presence of interfering targets.

In the first case, the reference cells contain noise only, the parameter α becomes a random variable because it is formed by a combination of random variables, so, we can compute its expectation.

The computation of the expectation of α is done by Monte Carlo experiments. The number of experiments is taken equal to 10^4. The obtained results are presented in Table 4.1, where $E(\alpha)$ is the expectation of α.

TABLE 4.1: The expectation of the parameter α, in an homogeneous environment for different N.

N	4	8	16	24	32
$E(\alpha)$	0.351	0.244	0.185	0.160	0.147

Table 4.1 presents the expectation of the adaptive weighting factor versus N. It shows that α is not very close to one in an homogeneous environment, the observed value of $E(\alpha)$ for $N = 4$ is 0.351. It can be seen also that when the number of reference cells increases, the expectation of α decreases. As a consequence, in presence of noise only, the weighting factor of the CA-CFAR is around 0.351, while the OS-CFAR achieves 0.649 for $N = 4$.

In the second case, presence of interfering targets, the expectation of α is depicted in Table 4.2.

TABLE 4.2: The expectation of the parameter α, in nonhomogeneous environment for different, N, in presence of one interfering target with $SNR = 15dB$.

N	4	8	16	24	32
$E(\alpha)$	0.078	0.066	0.054	0.049	0.047

Table 4.2 shows that $E(\alpha)$ falls to 0.079 for $N = 4$ in presence of one interfering target with $SNR = 15dB$. The value of $E(\alpha)$ decreases if the SNR of the interfering target increases more. In these conditions, the weighting factor of the CA-CFAR

detector is about 20 percent and the OS-CFAR detector is about 80 percent. The ALC-CFAR detector is effectively close to the OS-CFAR detector in presence of one interfering target.

Table 4.2 shows also that when N increases the ALC-CFAR performance tends to that of the OS-CFAR detector.

In presence of two (or more) interfering targets, the results are the same as for one interfering target because the second interfering target does not contribute to the computation of α. The study of the effect of α in presence of a number greater than $\frac{3N}{4}$ is not interesting because both the CA-CFAR and the OS-CFAR performances are degraded.

4.3.4 The threshold multiplier

The threshold multiplier of the ALC-CFAR detector is determined using Monte Carlo simulations. The number of experiments is taken to be $\frac{100}{P_{fa}}$ which is sufficient for the probability of false alarm evaluation [9].

Fig. 4.6 presents the variation of the threshold multiplier, T, of the ALC-CFAR detector versus the desired P_{fa}, for different number of the reference range cells. It can be shown that when N increases, T decreases, and when the P_{fa} increases T decreases. For a given P_{fa} and a fixed N, the threshold multiplier can be deduced directly from Fig. 4.6.

4.4 Performance assessment

In this section, the performances of the ALC-CFAR detector are analyzed and compared with the CA-CFAR and the OS-CFAR detectors in different radar situations. The comparison is based on the evaluation of the probability of detection, P_d, versus SNR and the effective P_{fa} using intensive Monte Carlo simulations. The gain in the detection probability of the ALC-CFAR compared with the OS-CFAR is also

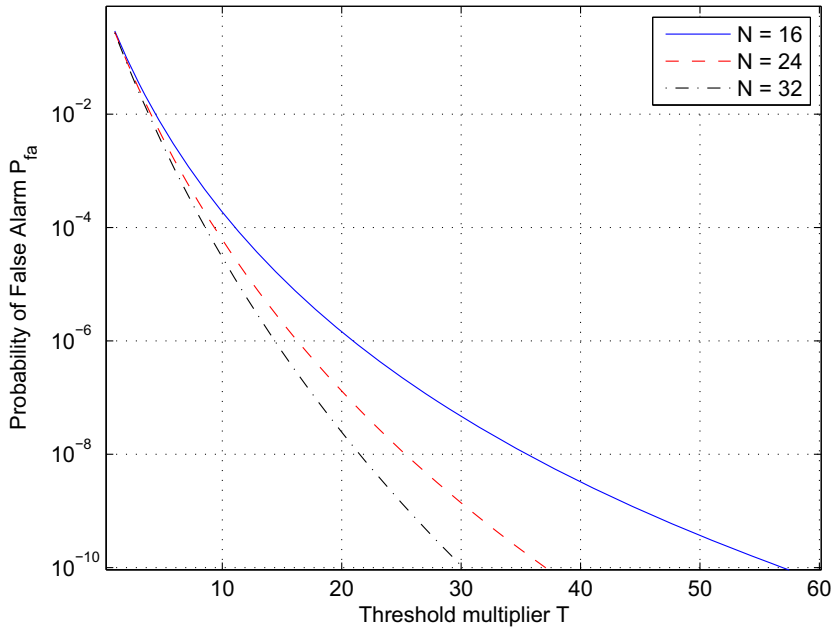

FIGURE 4.6: The threshold multiplier of the ALC-CFAR detector versus P_{fa} for different N.

investigated. The number of experiments is taken equal to 10^4 for P_d and $\frac{100}{P_{fa}}$ for P_{fa} [9].

4.4.1 Probability of detection

The simulations are conducted for different N and P_{fa}. Two environments are considered ; an homogeneous environment and non-homogeneous environment (presence of interfering targets).

The curves plotted in Fig. 4.7, 4.8 and 4.9 show the detection probabilities of the CA-CFAR, the OS-CFAR and the ALC-CFAR detectors for $N = 16$ and different values of $P_{fa} = 10^{-4}, 10^{-5}$ and 10^{-6}, respectively.

It can be seen from the presented curves that the performance of the ALC-CFAR belongs always between the CA-CFAR and the OS-CFAR for different P_{fa}. The difference between the ALC-CFAR and the OS-CFAR detectors increases for lower values of P_{fa}. The ALC-CFAR detector performs better than the OS-CFAR detector in this

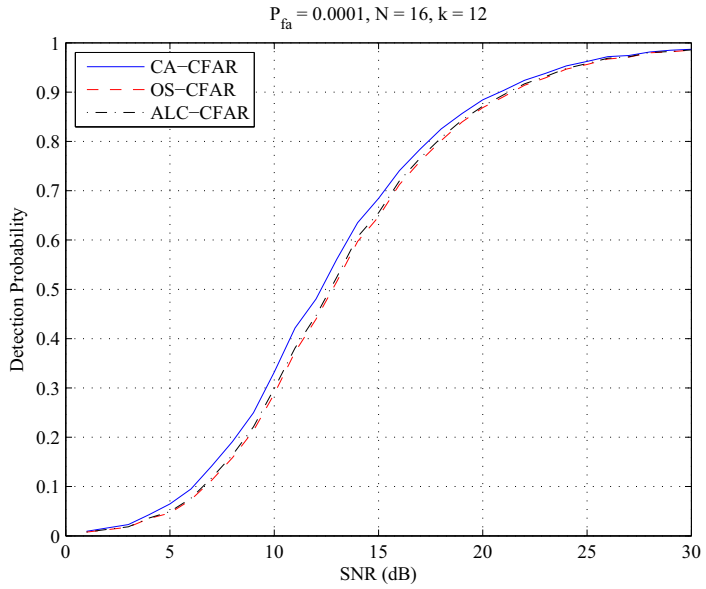

FIGURE 4.7: Detection probabilities of the ALC-CFAR, OS-CFAR and CA-CFAR detectors in homogenous environment, $P_{fa} = 10^{-4}$ and $N = 16$.

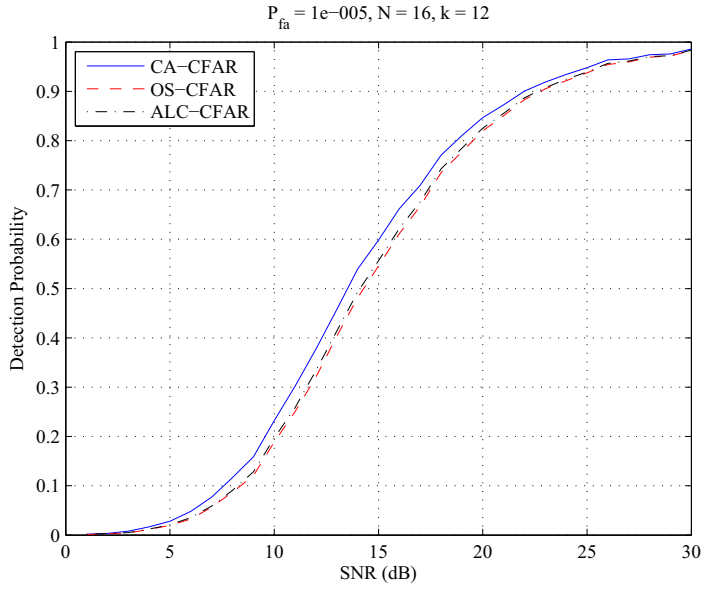

FIGURE 4.8: Detection probabilities of the ALC-CFAR, OS-CFAR and CA-CFAR detectors in homogenous environment, $P_{fa} = 10^{-5}$ and $N = 16$.

kind of environment whatever the P_{fa} value.

Fig. 4.10 and Fig. 4.11 present the detection probabilities of the considered CFAR detectors for $N = 4$ and $N = 32$, respectively.

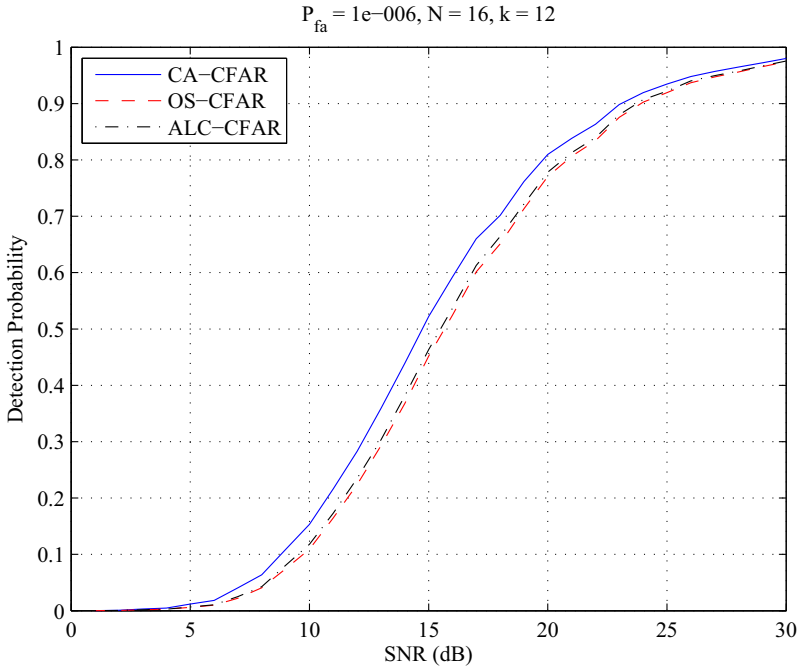

FIGURE 4.9: Detection probabilities of the ALC-CFAR, OS-CFAR and CA-CFAR detectors in homogenous environment, $P_{fa} = 10^{-6}$ and $N = 16$.

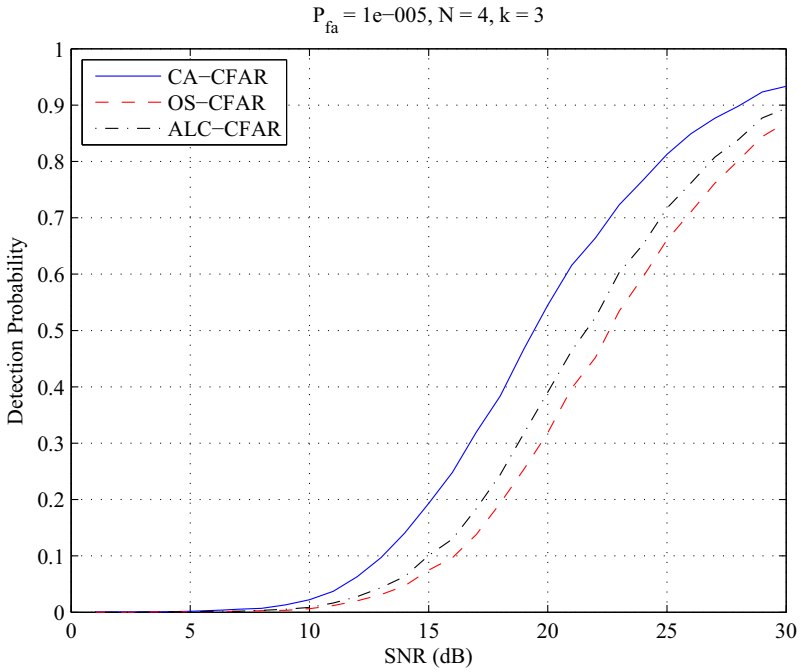

FIGURE 4.10: Detection probabilities of the ALC-CFAR, the OS-CFAR and the CA-CFAR detectors in homogenous environment, $P_{fa} = 10^{-5}$ and $N = 4$.

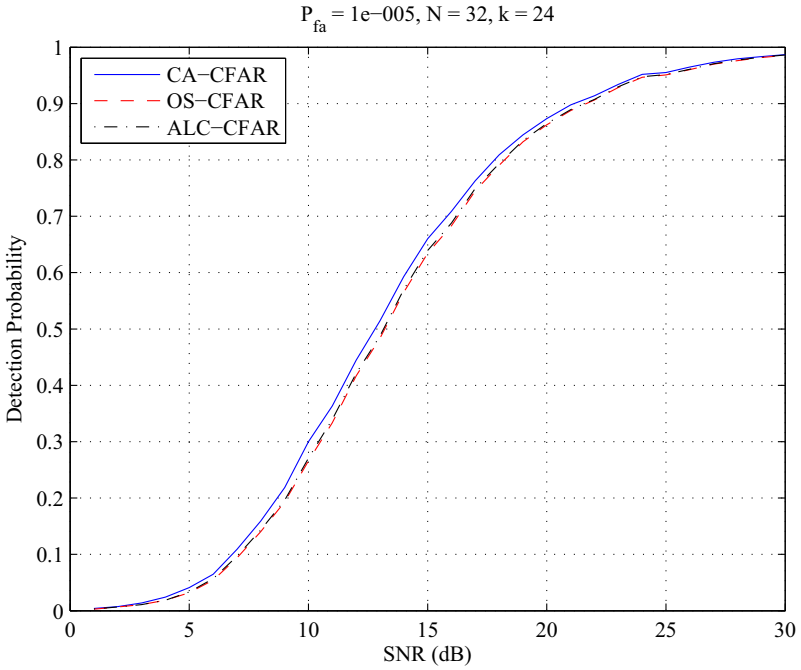

FIGURE 4.11: Detection probabilities of the ALC-CFAR, the OS-CFAR and the CA-CFAR detectors in homogenous environment, $P_{fa} = 10^{-5}$ and $N = 32$.

The desired false alarm rate is fixed to $P_{fa} = 10^{-5}$. It returns out that the gain of the ALC-CFAR detector compared to the OS-CFAR detector is greater for lower values of N. For higher N, the ALC-CFAR converges to the OS-CFAR performances.

It is known that the OS-CFAR detector has an additional detection losses than the CA-CFAR detector in an homogeneous environment, so, the ALC-CFAR reduces these losses in this kind of environment.

In a non-homogeneous environment, Fig. 4.12 depicts the detection probabilities of the ALC-CFAR, the CA-CFAR and the OS-CFAR detectors in presence of one interfering target, for $N = 16$ and $P_{fa} = 10^{-5}$.

The interference to noise ratio, INR, of the interfering target is taken equal to the SNR of the target in the cell under test. It can be seen that the detection probability of the CA-CFAR decreases, while that of the OS-CFAR is maintained and the ALC-CFAR performance remains very close to that of the OS-CFAR detector.

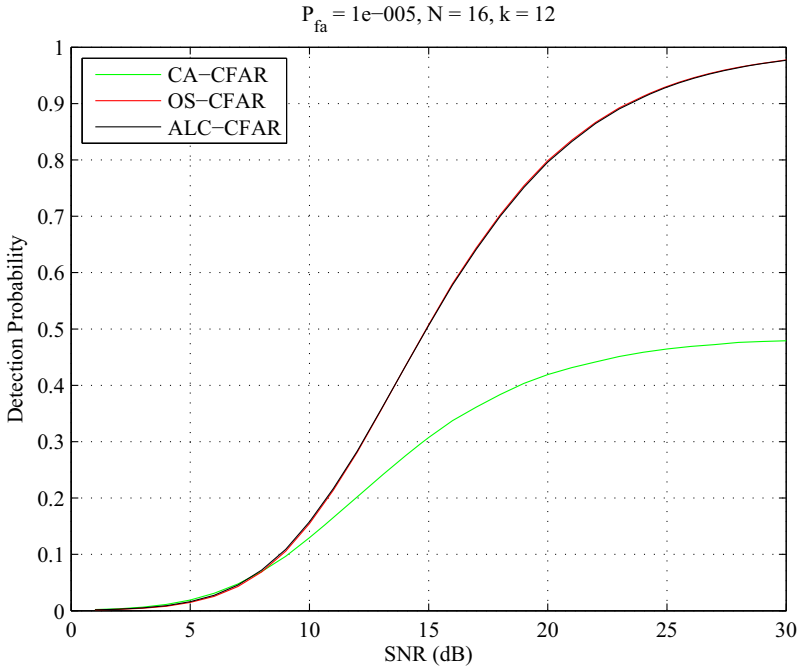

FIGURE 4.12: Detection probabilities of the ALC-CFAR, the OS-CFAR and the CA-CFAR detectors in presence of one interfering target.

When the number of interfering targets increases, and remains less than the tolerable number (four interfering targets are tolerable for $N = 16$), the performance degradation of the CA-CFAR decreases, the OS-CFAR is not affected and the ALC-CFAR remains very close to the OS-CFAR detector.

The curves plotted on Fig. 4.13 show the detection probabilities of the ALC-CFAR, the OS-CFAR and the CA-CFAR detectors in presence of five interfering targets.

It can be seen that when the interfering target number is greater than the tolerable one, the behavior of the ALC-CFAR is similar to the OS-CFAR. As the performance of the OS-CFAR detector is affected in this case, the ALC-CFAR performance is also degraded.

The ALC-CFAR detector offers a tradeoff between the CA-CFAR and the OS-CFAR detectors. In an homogeneous environment, the ALC-CFAR performs better than the OS-CFAR detector by reducing the detection losses.

In presence of interfering targets, the ALC-CFAR is close to the OS-CFAR de-

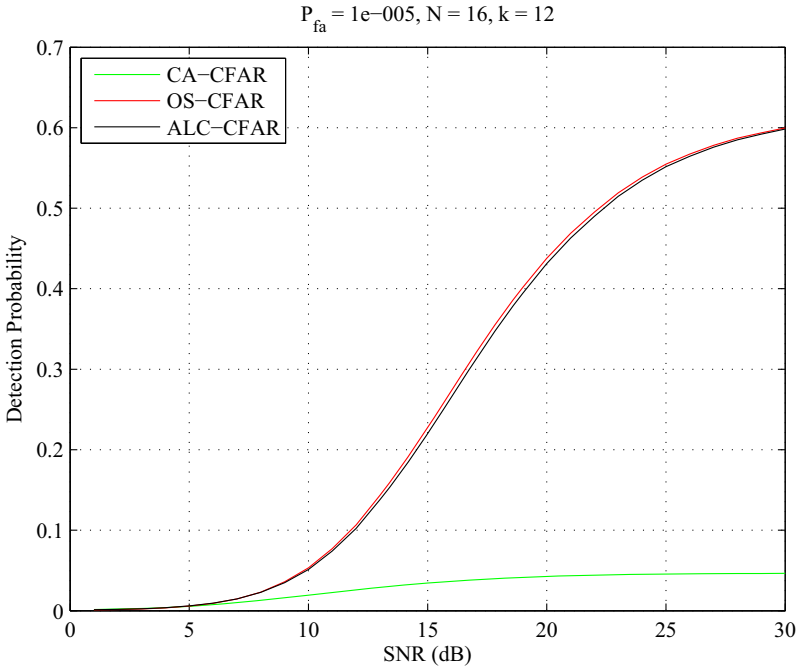

FIGURE 4.13: Detection probabilities of the ALC-CFAR, OS-CFAR and CA-CFAR detectors in presence of five interfering targets.

tector which is designed to support interfering targets and prevents the performance degradation of the CA-CFAR detector in this kind of situation.

The curves plotted in Fig. 4.14 show the detection thresholds of the CA-CFAR, the OS-CFAR and the ALC-CFAR detectors for $N = 16$ and $P_{fa} = 10^{-5}$.

It is clear that the ALC-CFAR threshold is adapted to the environment by means of the parameter, α, to detect targets in clear areas and prevent the target masking effect in presence of interfering targets and consequently it ensures less losses compared with the OS-CFAR detector.

We observe that the CA-CFAR detects only the two targets present in the clear area, while the OS-CFAR detects the six targets. The ALC-CFAR guarantees also the detection of the seven targets with less detection losses compared with the OS-CFAR detector.

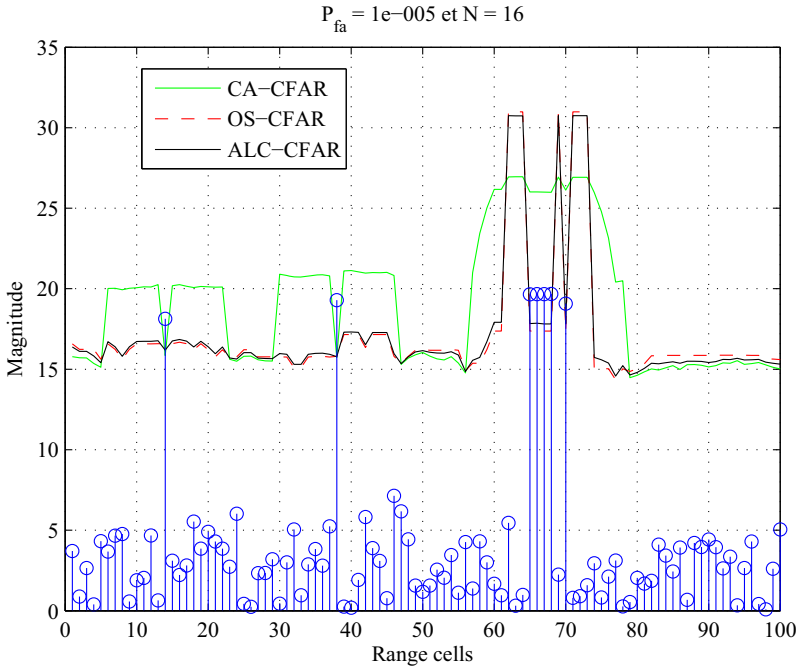

FIGURE 4.14: Detection thresholds for the ALC-CFAR, the CA-CFAR and the OS-CFAR detectors for $N = 16$ and $P_{fa} = 10^{-5}$.

4.4.2 False alarm regulation of the ALC-CFAR detector

The false alarm regulation performance of the proposed detector compared with the CA-CFAR and the OS-CFAR detectors for different N under an homogeneous environment is evaluated.

The obtained results for a desired $P_{fa} = 10^{-4}$, by Monte Carlo experiments using a total of 10^6 independent trials, are presented in Fig. 4.15. It can be seen that the effective P_{fa} of the proposed detector is relatively maintained close to the desired one.

4.4.3 Gain of the ALC-CFAR detector

The obtained gain, defined as the difference between the corresponding SNRs to yield $P_d = 0.5$, of the ALC-CFAR compared with the OS-CFAR detector for different P_{fa} and N is given in Table 4.3.

It can be seen that the gain is higher for lower values of N and P_{fa}. It achieves

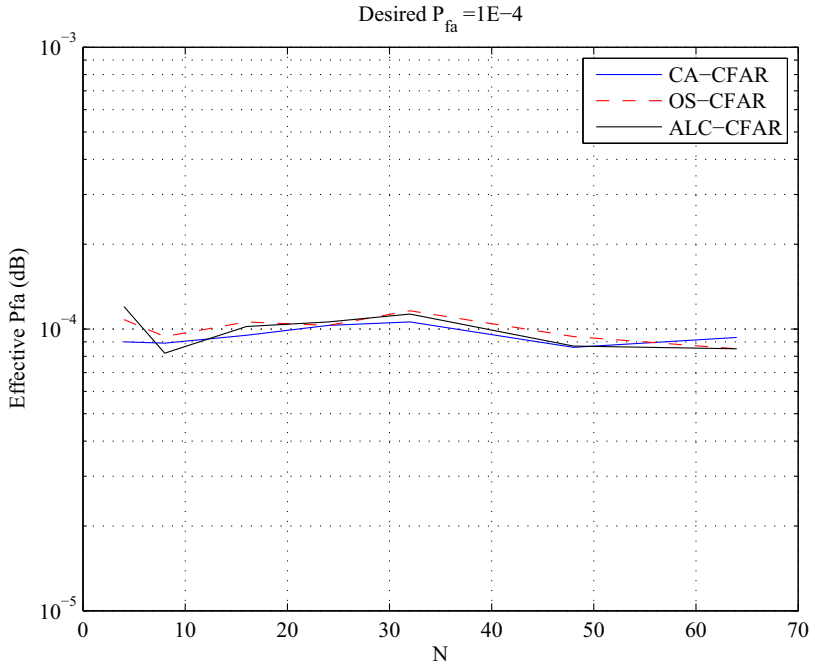

FIGURE 4.15: The false alarm regulation performance for different N. The desired $P_{fa} = 10^{-4}$.

TABLE 4.3: Gain of the ALC-CFAR with respect to the OS-CFAR for different values of P_{fa} and N.

	N	4	8	16	24	32	64
Gain(dB)	$P_{fa} = 10^{-4}$	0.813	0.312	0.145	0.081	0.043	0.024
	$P_{fa} = 10^{-5}$	1.251	0.327	0.214	0.115	0.062	0.031
	$P_{fa} = 10^{-6}$	1.316	0.415	0.223	0.132	0.091	0.035

more than one dB for $N = 4$ and $P_{fa} = 10^{-6}$. For higher N and P_{fa}, the gain is reduced and the ALC-CFAR detector performs like the OS-CFAR detector.

From Table 4.3 it returns out that, by carefully selecting N as well as P_{fa}, it is possible to achieve satisfactory performance in both an homogeneous and non homogeneous environments. According to the obtained results, it is also very interesting to note that the proposed detector is particularly suitable for low resolution radars which use low number of reference cells to ensure the minimum homogeneity range [1].

1. This range is about $1nmi$ for S band radars [1]

4.5 Performance comparison ALC-CFAR vs FAOSOSD

For performance comparison, we have considered the probability of detection of the FAOSOSD and the ALC-CFAR detectors in an homogenous and a non-homogeneous environments.

4.5.1 Homogeneous environment

The curves of Fig. 4.16, Fig. 4.17 and Fig. 4.18 plot the detection probabilities of the ALC-CFAR and the FAOSOSD, in homogeneous environment, for a fixed $P_{fa} = 10^{-5}$ and different reference window size $N = 8$, $N = 16$ and $N = 24$, respectively.

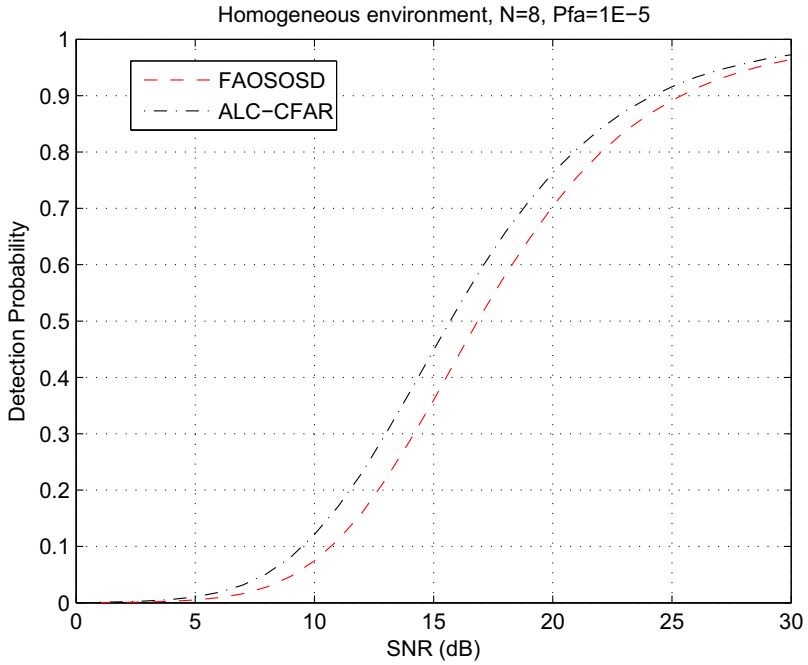

FIGURE 4.16: Probability of detection of the ALC-CFAR and the FAOSOSD for $P_{fa} = 10^{-5}$ and $N = 8$ in homogeneous environment.

It returned out that the ALC-CFAR presents better performance than the FAOSOSD detector. The difference is important for lower reference window sizes.

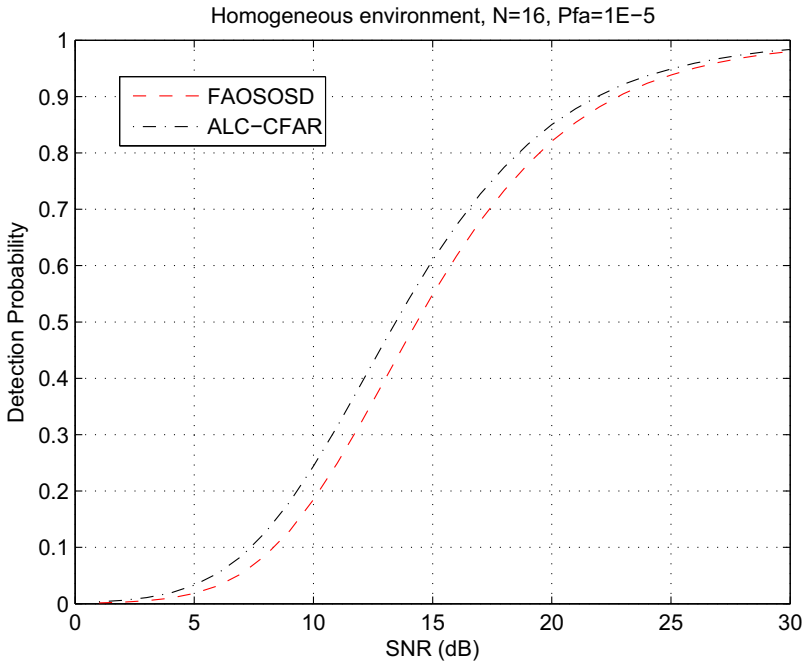

FIGURE 4.17: Probability of detection of the ALC-CFAR and the FAOSOSD for $P_{fa} = 10^{-5}$ and $N = 16$ in homogeneous environment.

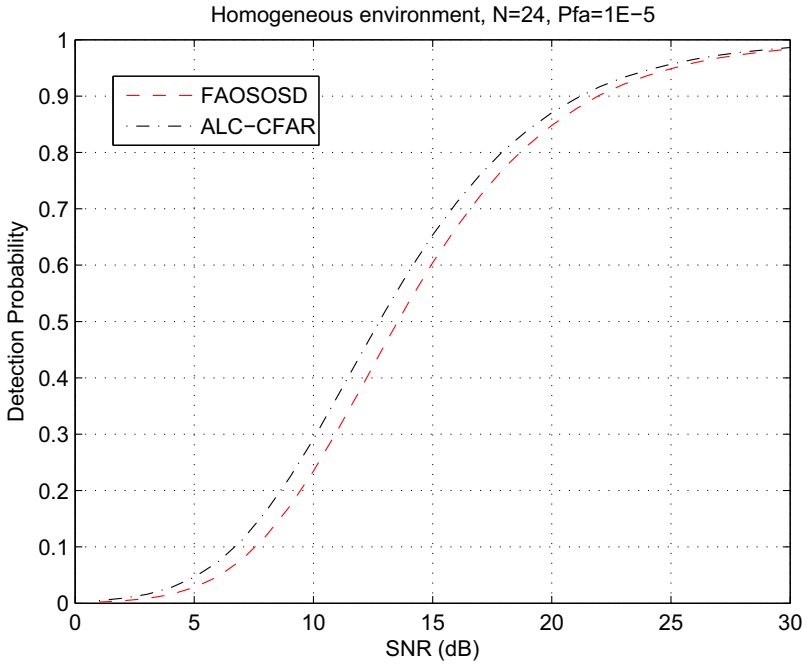

FIGURE 4.18: Probability of detection of the ALC-CFAR and the FAOSOSD for $P_{fa} = 10^{-5}$ and $N = 24$ in homogeneous environment.

4.5.2 Non-homogeneous environment

In presence of interfering targets situation, we consider three cases which correspond to one, three and five interfering targets. The corresponding detection probabilities are shown, respectively, in Fig. 4.19, Fig. 4.20 and Fig. 4.21 for $P_{fa} = 10^{-5}$ and $N = 16$.

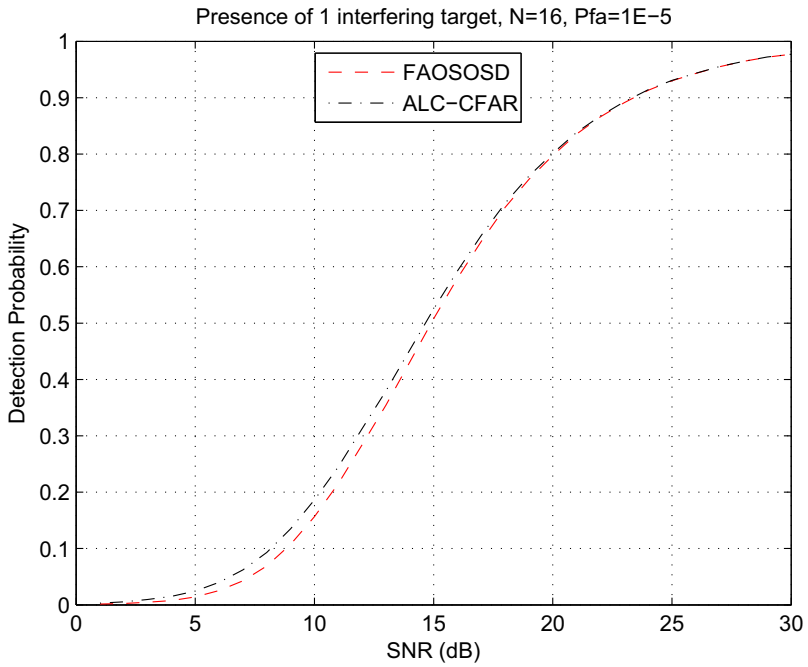

FIGURE 4.19: Probability of detection of the ALC-CFAR and FAOSOSD for $P_{fa} = 10^{-5}$ and $N = 16$ in presence of one interfering targets.

It can be seen that for one interfering target situation, the ALC-CFAR performs better than the FAOSOSD for low signal to noise rations (less than 15 dB, in this case). For higher SNR, they present comparative performances.

For three interfering targets, the probability of detection curves of the considered detectors are superposed and present almost the same performance.

For five interfering targets, the FAOSOSD detector presents the better performance over the ALC-CFAR. For higher number of interfering targets, the difference

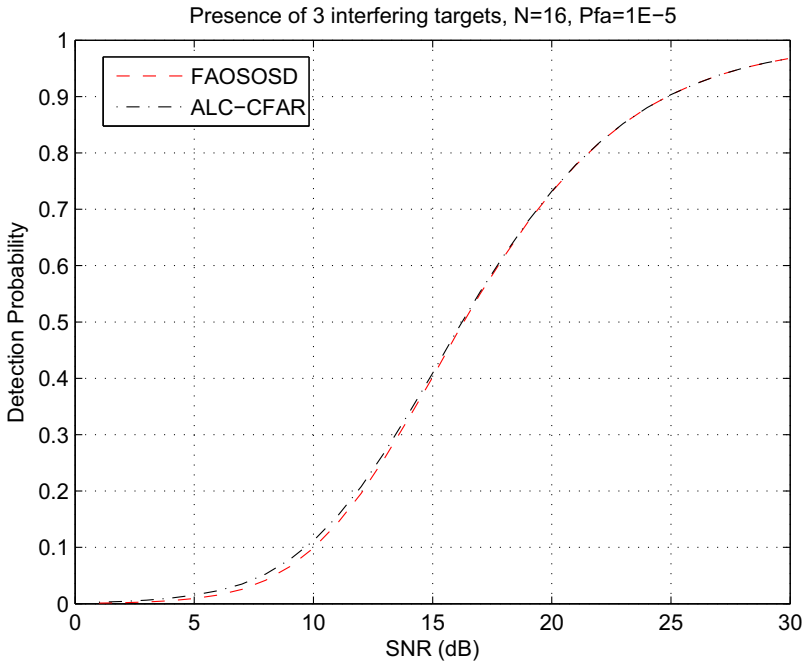

FIGURE 4.20: Probability of detection of the ALC-CFAR and the FAOSOSD for $P_{fa} = 10^{-5}$ and $N = 16$ in presence of three interfering targets.

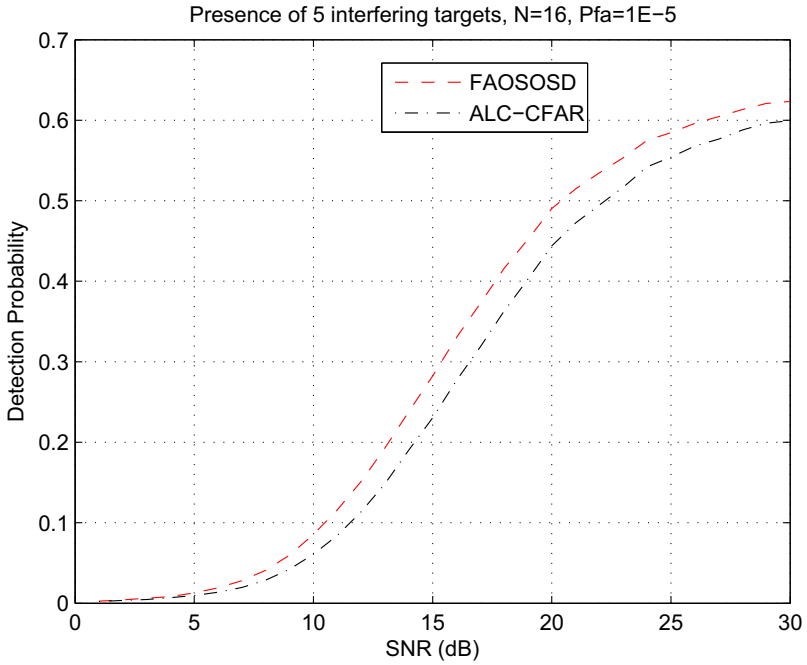

FIGURE 4.21: Probability of detection of the ALC-CFAR and the FAOSOSD for $P_{fa} = 10^{-5}$ and $N = 16$ in presence of five interfering targets.

between the detection probabilities increases.

In Fig. 4.22, we present the threshold level behavior of the ALC-CFAR and the FAOSOSD detectors for $P_{fa} = 10^{-5}$ and $N = 16$.

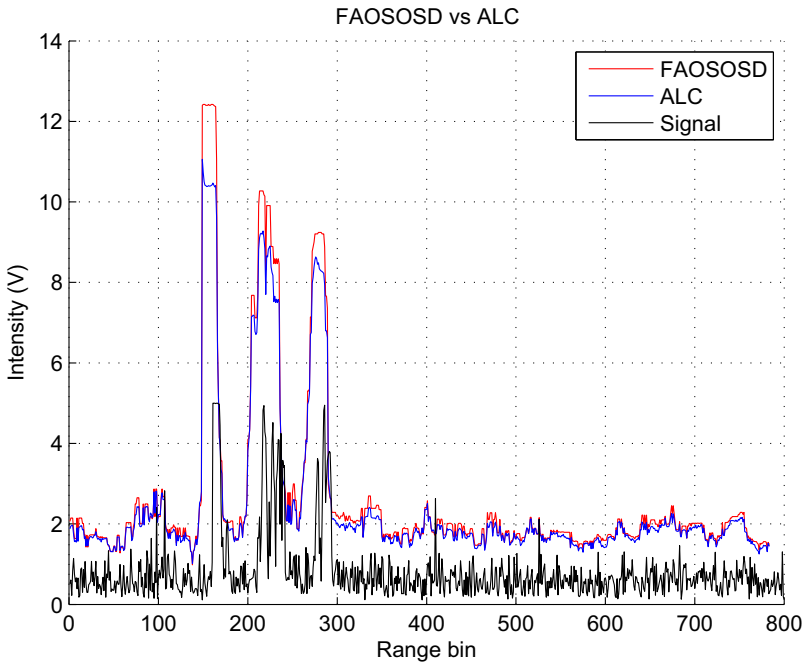

FIGURE 4.22: ALC-CFAR and FAOSOSD thresholds for $P_{fa} = 10^{-6}$ and $N = 16$.

It can be seen in this special situation, that the two considered processors detect the four targets located at range bin number 78, 107, 410 and 527. Nevertheless, the FAOSOSD detector present higher threshold level in the heavy clutter region extended from range bin 160 to 300.

4.6 Conclusion

In this chapter, a new CFAR detector referred to as Adaptive Linear Combined CFAR, ALC-CFAR, is proposed. The proposed detector principle is to wisely combine the threshold estimates of the CA-CFAR and OS-CFAR detectors, based upon the observed characteristics of the environment. This detector requires sensing the CFAR reference window cells, and applying an appropriate adaptive weighting factor in the

fusion scheme to produce an efficient detection decision and ensure a reduced CFAR loss.

The application of the ALC-CFAR detector in presence of interfering targets is demonstrated using an adaptive weighting factor. Simulations based on Monte Carlo experiments show that the ALC-CFAR detector performs much better than the CA-CFAR detector in non-homogenous environment, and has a very close detection performance to the OS-CFAR detector in presence of interfering targets with less CFAR detection loss compared with that of the OS-CFAR detector in homogenous environment.

We notice that the ALC-CFAR performs better than the FAOSOSD in homogeneous environment, and low number of interfering target for reduced values of SNR. In severe interfering target situations, the FAOSOSD is better, especially when the number of interfering target exceeds $(N - K)$.

For practical application in radar detection, it is very interesting to note that the ALC-CFAR detector is particularly suitable for low resolution radars which use low number of reference cells to ensure the minimum homogeneity range.

CHAPTER V

Implementation

In this chapter, we present the second part of our contribution in this thesis. It concerns the real-time DSP implementation of the FAOSOSD and the ALC-CFAR detectors and the experimental results using real-life data. We provide the radar signal processor architecture, the signal digitalization parameters effect on the detection quality, the real-time constraints and the implementation results using a TMS320C6711 processor based development platform.

In addition, we present the generalized automated sliding window, GASW, technique for the CA-CFAR implementation and the direct implementation architecture for ordered statistics based detection. These techniques reduce significantly the computational burden of the proposed detectors. We propose also, a practical relation for an optimal reference window length determination as a function of the radar parameters and the homogeneous range.

5.1 Introduction

The performance of radar systems has improved tremendously within the last years. It is mainly due to the application of digital signal processing and the progress of integrated circuits. The gradual change from small scale integration to very large scale integrated (VLSI) techniques, and the use of microprocessors and spe-

cial purpose digital signal processing elements have led to dramatic improvements in speed, size, cost and power consumption. Furthermore, it means that the real-time implementation of complex algorithms becomes possible [10].

The application of digital signal processing in radar systems began from signal detection in video frequency and is now developing into signal processing in intermediate frequency. It seems possible to process the RF signal directly owing to the development of digital devices. The percentage of digitized parts in radar system becomes larger and larger, since it is a cost-effective way to improve the performance of the hole radar system. Now it is possible to realize the whole radar ranging system in a single chip with LSI technology. Owing to the large bandwidth of radar signals and the requirement of real-time processing, another important specification of the radar signal processor is the speed of processing [9].

While advanced theoretical aspects of radar detection algorithms are being well treated in the literature, the intensive computational requirements, due to the high data rate in radar signal processing, cannot be accomplished only by the technology improvements but also by software architectures based on code optimization models and algorithm-architecture adequation.

5.2 Architecture of the proposed radar signal processor

The purpose of the radar signal processor is to test and evaluate the designed detectors proposed in chapters III and IV, to determine their capability to provide radar data suitable for automated terminal system processing.

The primary area of concern is the ability of the proposed detectors to operate acceptably in a real radar environment.

5.2.1 The proposed radar signal processor scheme

The proposed radar signal processor architecture is depicted in Fig. 5.1. It contains

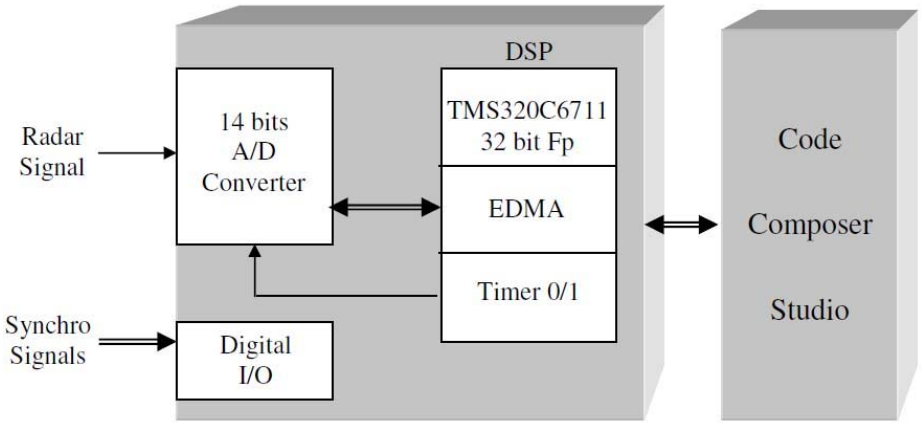

FIGURE 5.1: The proposed radar signal processor architecture.

three fundamental parts.

1. The radar signal digitalization and acquisition using a 14 bits A/D converter synchronized by the DSP timer interrupt and the pulse repetition interval, PRI, signal.

2. The radar synchronization and signal conditioning and acquisition via the digital I/O. The signals of interest are :

- The pulse repetition frequency, PRF ;
- The azimuth resolution pulse, ARP ;

and the north mark (the azimuth reference zero).

3. Finally the processing core based on a TMS320C6711 floating point processor.

The considered DSP board (see Fig. 5.2) is a performance-oriented for PCI-based data acquisition with four analog I/O channels of 14-bit at up to 10MHz input and up to 50MHz output. It uses the TMS320C6711 processor from Texas Instruments as the heart of data management and processing functions. It provides four simultaneous analog inputs, four analog outputs, a logic architecture that supports extremely flexible trigger mechanisms.

It offers 900MFLOPS of processing power at 150MHz. On-chip resources include 8 highly independent parallel execution units, 16 Enhanced Direct Memory Access, EDMA, channels and two 32-bit timers.

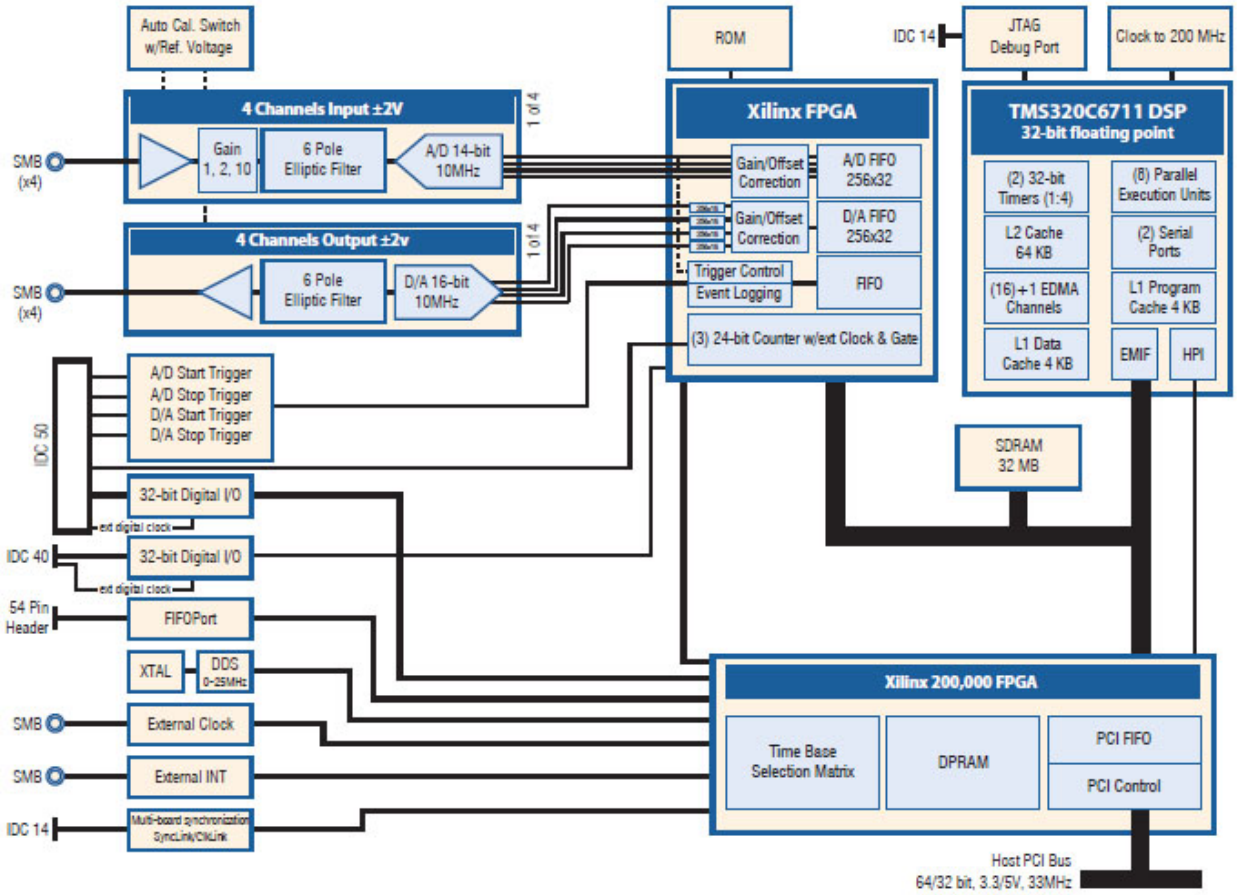

FIGURE 5.2: The development platform architecture.

The sampling frequency is generated by the timer0 interrupt programmed according to the radar video bandwidth which corresponds to 1MHz.

The debugging of the developed codes and the experimental results display is ensured by the Code Composer Studio visualization window.

The code development, debugging and optimization techniques are well detailed in [83-97].

5.3 Real time constraints

The period between two sweeps is the critical time for the implementation of the proposed detectors, in case of one pulse processing. For non-coherent pulse integration,

the critical time corresponds to the angular resolution time. This means that these periods determine the amount of time for acquisition, storage, threshold computation, comparison and storage of the output decision. This critical time depends on the size of the reference window of the CFAR detector.

The real time considerations are managed so as to satisfy the requirements of the air surveillance radar, ASR-12, with a pulse repetition frequency of 1200Hz, an angular resolution of 1.4° and 1 μs pulse width. The minimum critical time corresponds to 125000 cycles, for pulse processing, and 2.9 millions of cycles for non coherent pulse integration processing case for an antenna rotation speed of 12rpm [1].

The corresponding times are illustrated in Fig. 5.3.

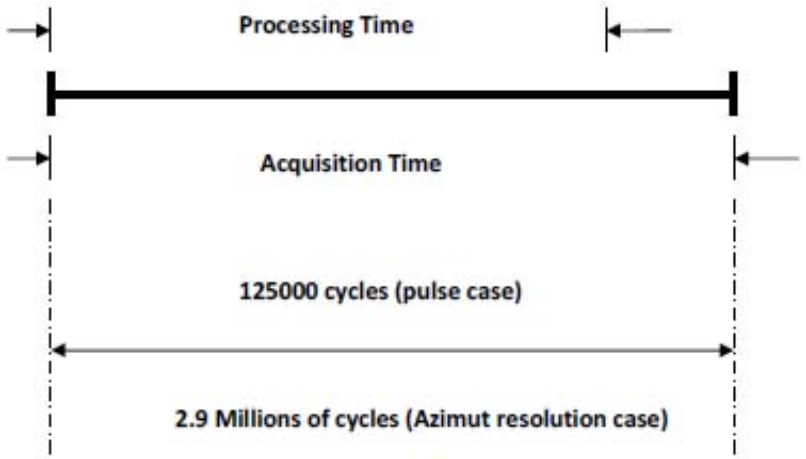

FIGURE 5.3: Real time constraints.

To achieve the desired performance in real time, all the software is written completely in TMS320C6711's assembly language. This enables full optimization of generated code. Due to the limited amount of time, the number of samples per sweep that can be processed is limited.

1. revolutions per minute.

5.4 Digitalization effect on the detection performance

The digitalization parameters of the radar signal effect on the performance of the CA-CFAR, the OS-CFAR, the FAOSOSD and the ALC-CFAR detectors is studied. The considered parameters are :

- The number of the Analog to Digital conversion bits ;
- The presence of an offset ;
- The sampling frequency.

5.4.1 Number of the Analog to Digital conversion bits

The number of bits of the A/D converter affects the performance of many parts in the radar signal processor such as Moving Target Indication, Doppler filtering, adaptive detection, tracking and display.
Herein, we are interested in the adaptive detection performance.

Although the dynamic range of radar signal processor is determined by the A/D converter, it does not mean that the number of bits of the A/D converter is determined by the dynamic range.

It is well known that the A/D converter will introduce quantization noise. This quantization noise will cause, on average, a limit to the improvement factor [2][10] which is given by

$$I_{QN} = 20\log[(2^N - 1)\sqrt{0.75}]dB \tag{5.1}$$

Each bit in a binary converter represents a doubling of the voltage, or $6dB$.

2. The improvement factor is defined as the signal to clutter ratio of the output divided by the signal to clutter ratio at the input.

5.4.1.1 The number of integrated sweeps limitation

The number of A/D conversion bits of radar signal processor is related to the radar performance and the used signal processor.

First, we consider the limitation of the number of integrated sweeps using the 16 bits fixed point 'C24x Texas Instruments processor. The obtained results are presented in Fig. 5.4.

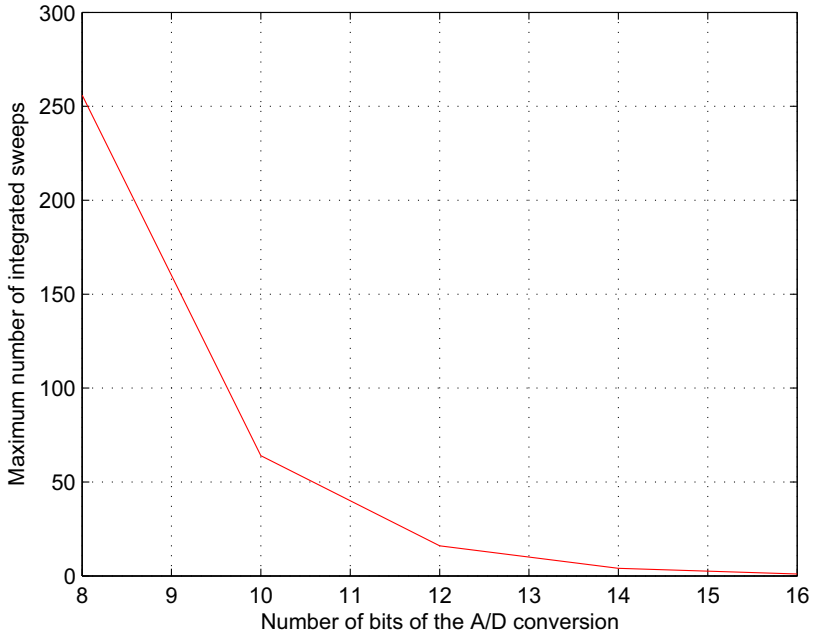

FIGURE 5.4: Effect of the number of A/D conversion bits on the number of integrated sweeps using the 16bits 'C24x fixed point processor.

It can be seen that the number of integrated sweeps decreases when the number of A/D conversion bits increases. To explain these results, lets consider the following example.

We suppose that the A/D conversion is done using 8 bits, the DSP acquisition register is 16 bits and we consider the worst case (overflow) when the signal presents the maximum strength. The signal level corresponding value after the A/D conversion is FF (8 bits).

We can conclude that, the maximum number of integrated sweeps is "FFFF" divided by "FF", which equals to 256 sweeps.

If the maximum number of the A/D conversion bits is increased to 12 bits, the number of integrated sweeps decreases to "16".

In practical radar detection, we look for improving the detection performance which is related to the number of the A/D number of bits and the number of integrated sweeps, so it is necessary to realize a tradeoff between these two parameters.

According to the ASR-12 radar specifications, the number of integrated sweeps is about 20. Consequently, the number of bits of the A/D converter must be less than 12 bits to ensure the integration of the entire number of sweeps using the 16 bits fixed point 'C24x Texas Instruments processor.

For the TMS320C6711 32bit processor, the corresponding number of integrated sweeps is 256 which is widely sufficient for our application.

5.4.1.2 The detection quality

As mentioned in the previous subsection, the choice of the number of the A/D conversion bits is very important in the radar detection system. The number of bits of the A/D conversion affects the detection threshold level.

To show the level of this effect, we consider the CA-CFAR, the FAOSOSD and the ALC-CFAR detectors as shown in Fig. 5.5, Fig. 5.6 and Fig. 5.7, respectively, for $N = 16$ and $Pfa = 10^{-5}$. This study is conducted for 4, 6, 8 and 10 bits.
The OS-CFAR detector is not considered since it uses the same threshold estimation approach as the FAOSOSD.

It can be seen that, the threshold level for 8 and 10 bits are very close to each other. For 4 bits, we obtain the lowest threshold level and consequently this can invokes additional false alarms. For higher number of bits, the threshold levels are superposed for all the detectors.

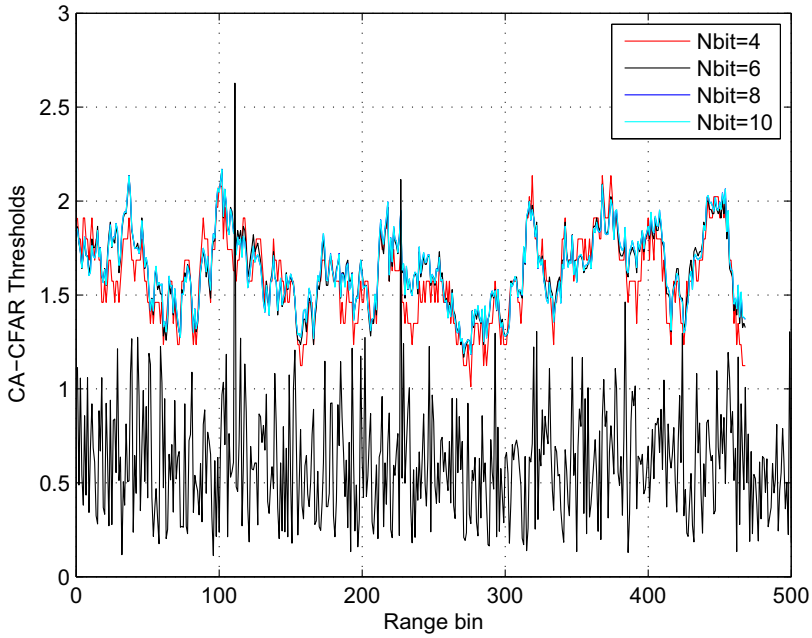

FIGURE 5.5: Effect of the number of the A/D conversion bits on the CA-CFAR threshold level for $N = 16$ and $Pfa = 10^{-5}$.

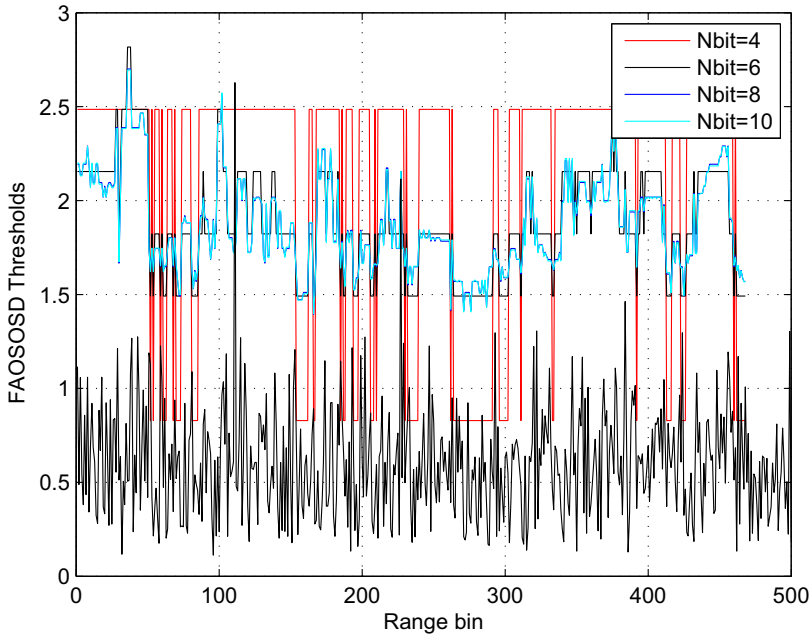

FIGURE 5.6: Effect of the number of the A/D conversion bits on the FAOSOSD threshold level for $N = 16$ and $Pfa = 10^{-5}$.

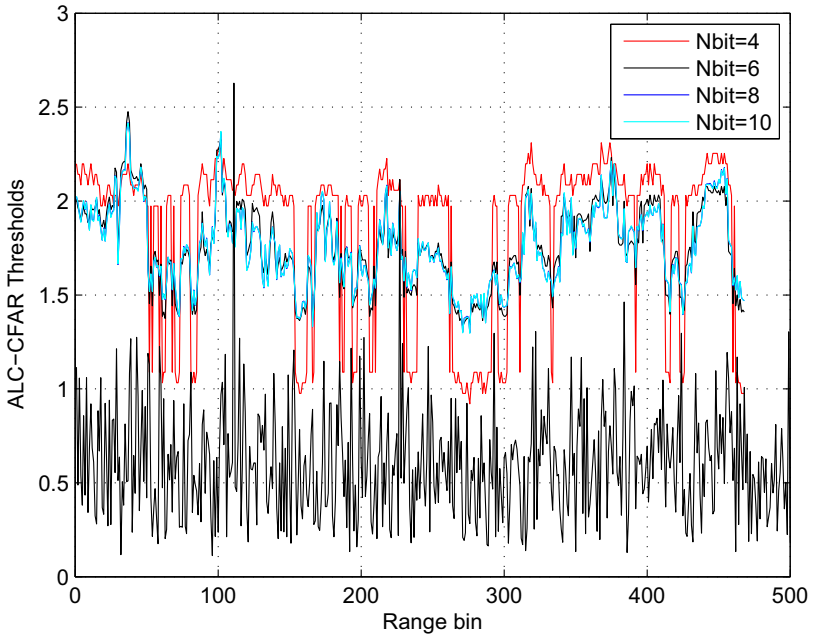

FIGURE 5.7: Effect of the number of the A/D conversion bits on the ALC-CFAR threshold level for $N = 16$ and $Pfa = 10^{-5}$.

It should be noticed that the CA-CFAR detector in the lowest affected, than the ALC-CFAR and finally the FAOSOPSD which is the most affected. The obtained results show that 10 bits is sufficient to ensure a good detection quality.

5.4.2 Presence of an offset

The offset is defined as an additional voltage to the received signal level. In a radar signal receiver, this offset may be caused by [10] :

- Antenna mismatch ;
- Receiver output mismatch ;
- A/D converter of the acquisition and conditioning unit ;

In order to illustrate the offset level effect on the detection performance, we have considered four situations.

The considered signal contains 800 samples with a maximum strength level of 5 Volts. The corresponding offset levels are 0.25V, 1V, and 5V. Negative offset levels are not

considered since they may cause the complete noise samples elimination.

The curves of Fig. 5.8, Fig. 5.9, Fig. 5.10 and Fig. 5.11 plot the offset level effect on the detection thresholds of the ALC-CFAR and the FAOSOSD detectors for 0V, 0.25V, 1V and 5V, respectively.

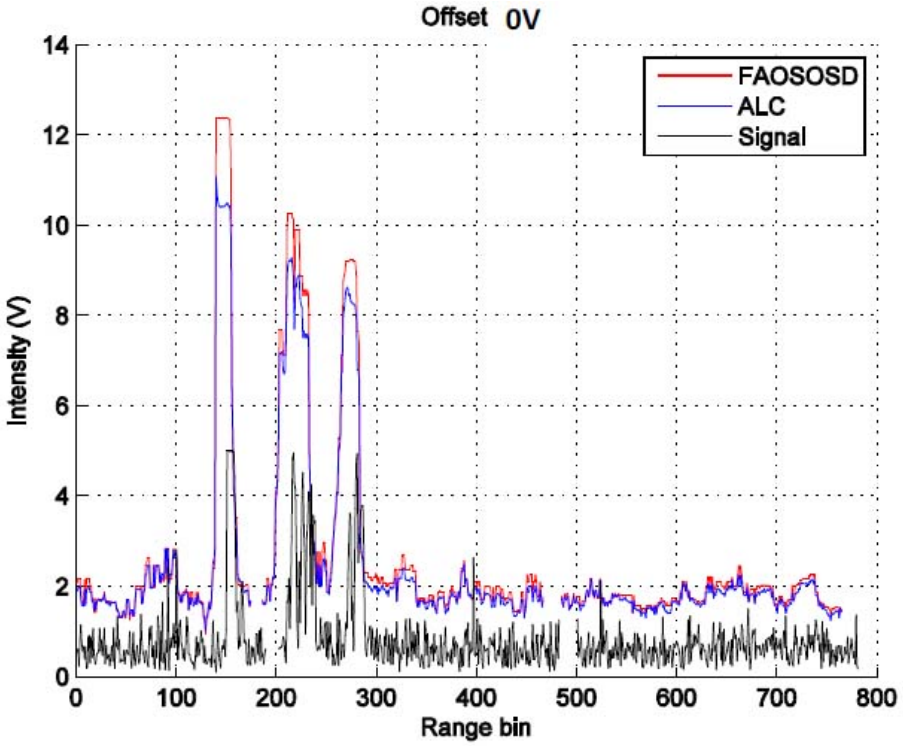

FIGURE 5.8: The FAOSOSD and the ALC-CFAR thresholds, Offset=0V.

It can be seen that the presence of a positive offset invokes a loss in the probability of detection for both detectors and for higher offset level, the loss is important. In this special situation, all the targets are missed for offsets greater than 1.25V.

It should be noticed that the FAOSOSD detector is slightly less affected than the ALC-CFAR detector for higher offset levels. This is due to the important loss induced by the CA-CFAR detector in this case.

In practice, the solution to this problem is the determination of the offset level and the readjustment of the threshold multiplier consequently to detect targets properly.

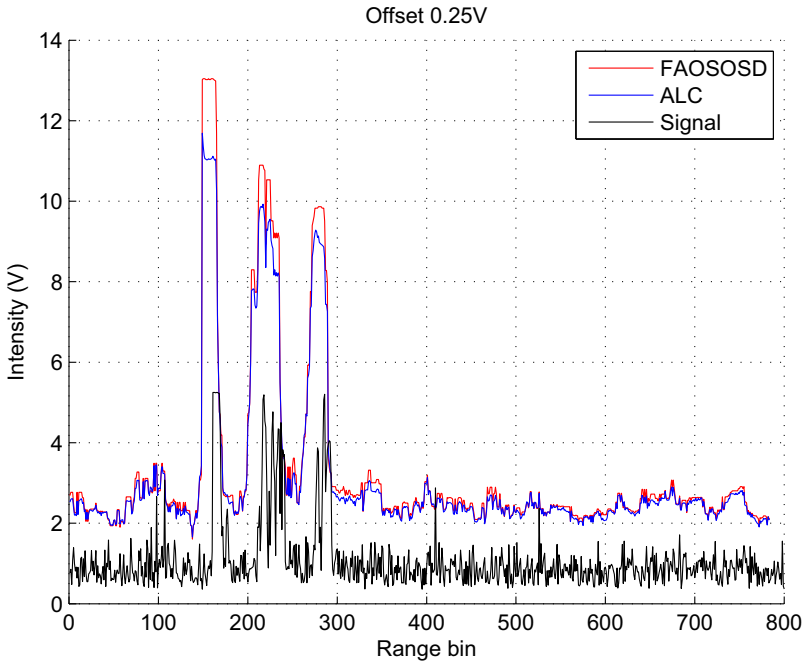

FIGURE 5.9: The FAOSOSD and the ALC-CFAR thresholds, Offset=0.25V.

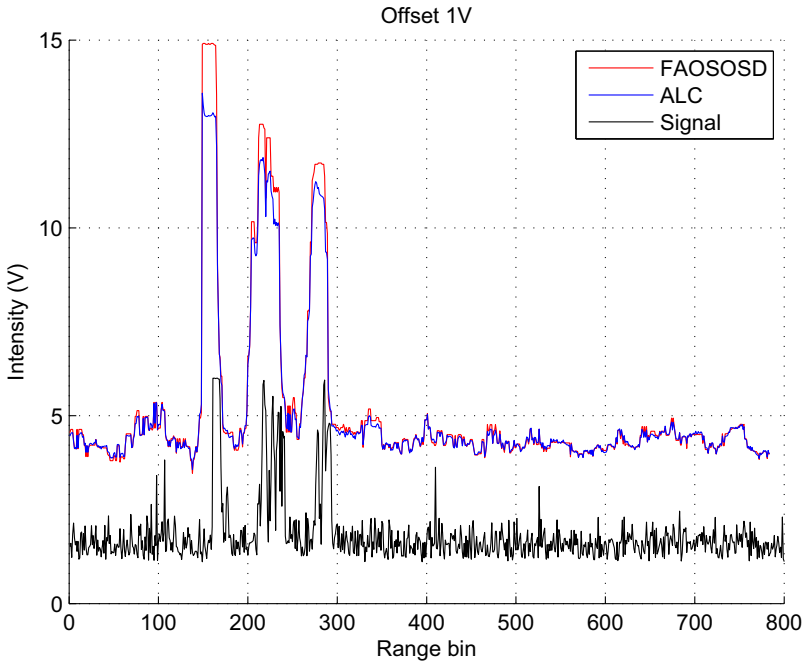

FIGURE 5.10: The FAOSOSD and the ALC-CFAR thresholds, Offset=1.25V.

5.4.3 Sampling frequency

In general, the sampling rate of a digital signal processor can be determined by the Nyquist sampling rate of the signal, which is equal to twice the signal bandwidth.

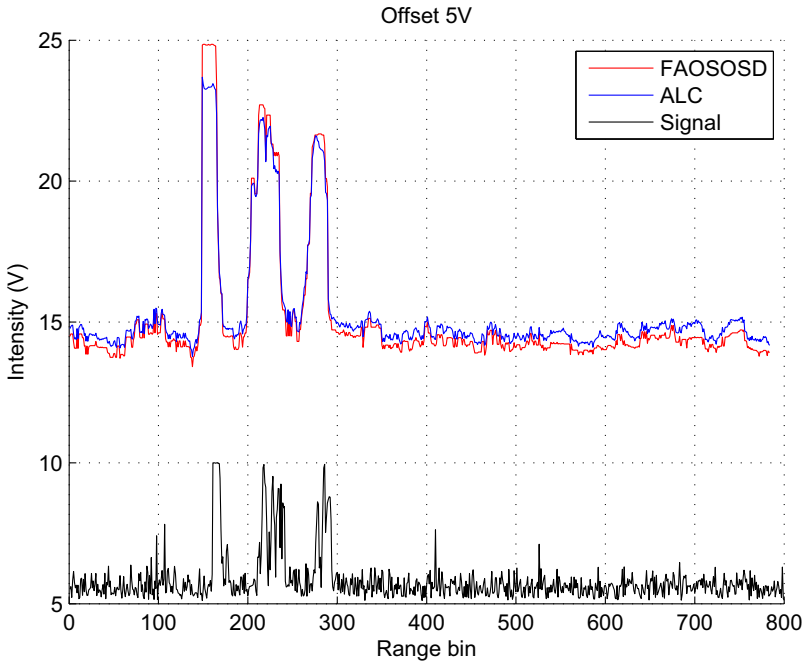

FIGURE 5.11: The FAOSOSD and the ALC-CFAR thresholds, Offset=5V.

In fact, radar signal processing can be divided into two classes. In the first class, the radar signal is processed in the azimuth direction, such as moving target indication, MTI, moving target detection, MTD, and moving window detector, etc. In this class, the radar signal is sampled at an interval equal to pulse width and then rearranged into azimuth sequences for each range bin.

In the second class, the radar signal is processed in the range direction, such as digital pulse compression. In this case, the Nyquist sampling rate must be considered. However, it can be shown that, when quadrature channel is employed, the sampling rate can be one half of the Nyquist rate plus maximum Doppler shift for a linear FM signal.

For a practical point of view, the sampling frequency should be equal to the receiver bandpass.

The conducted experiences show that the sampling frequency increasing is equivalent to the presence of additional interfering targets. The number of interfering

targets equals to the multiplying factor of the sampling frequency minus one.
The obtained results are summarized in Table 5.1 as a function of the radar pulse width τ.

TABLE 5.1: The sampling frequency vs the number of equivalent interfering targets.

The sampling Frequency (Hz)	$\frac{1}{\tau}$	$\frac{2}{\tau}$	$\frac{3}{\tau}$	$\frac{4}{\tau}$	$\frac{m}{\tau}$
The number of interfering targets	0	1	2	3	$m-1$

It should be noticed that for sampling frequencies lower than $\frac{1}{\tau}$ (which is not recommended), the target sample may be missed.

The obtained results of the conducted studies allow an adequate selection of the radar signal digitalization parameters according to the specifications of the ASR-12 radar.
The considered parameters are :

- The sampling frequency, 1MHz ;
- The number of the A/D conversion bits, 10 ;
- The number of integrated sweeps, 20.

5.5 Implementation of the proposed detectors

5.5.1 Introduction

To implement radar detection algorithms in real time, it is necessary to have enough processing power to process an important quantity of radar data.

Digital signal processors such as the TMS320C6x family are dedicated purpose microprocessors with a specialized type of architecture and instruction set appropriate for signal processing and very well suited for numerical intensive calculations [77].

For practical application in radar detection, it is clear, however, that the computation burden is greater for the proposed detectors than the OS-CFAR and the

CA-CFAR. In order to overcome this limitation, a solution to this problem is to take the advantages of the optimized implementation architectures developed for the CA-CFAR and the OS-CFAR detectors.

The combination of these two approaches improves significantly the computational burden of the proposed detectors for real time applications.

Two types of radar signals are used in the processing; video signals and synchronization signals.

Five softwares are realized, the first one is the signal acquisition core, the second one is the CA-CFAR, the third is the OS-CFAR, the fourth is the FAOSOSD and the fifth one is the ALC-CFAR detector.

5.5.2 Radar signal acquisition and data rearrangement

Most radar signal processors process the data sequence in azimuth direction, but the output of the A/D converter is arranged in the range direction. Therefore, a buffer memory for data rearranging is needed. This is shown schematically in Fig. 5.12.

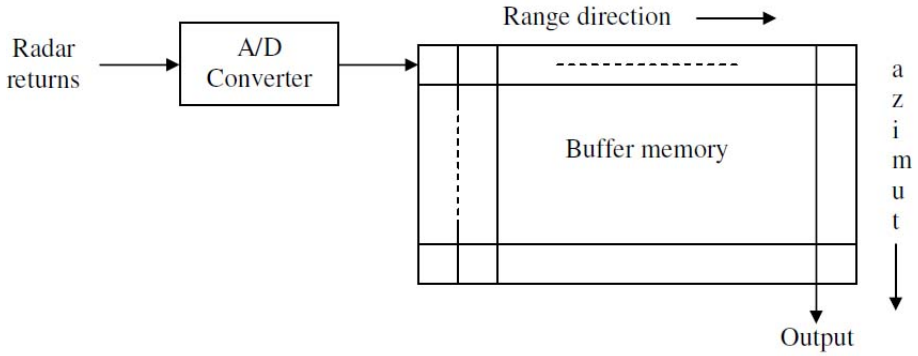

FIGURE 5.12: Buffer memory and data rearrangement.

For the ASR-12 radar, the number of cells in range direction is taken equal to 800, and 256 in azimuth direction.

The acquisition is ensured by the EDMA (Enhanced Direct Memory Access) co-processor which uses the synchronization signal as an interrupt to reset the Timer

(end of sweep data). The beginning of the current sweep is determined by the radar synchronization signal, PRI, which marks also the end of the previous sweep [68].

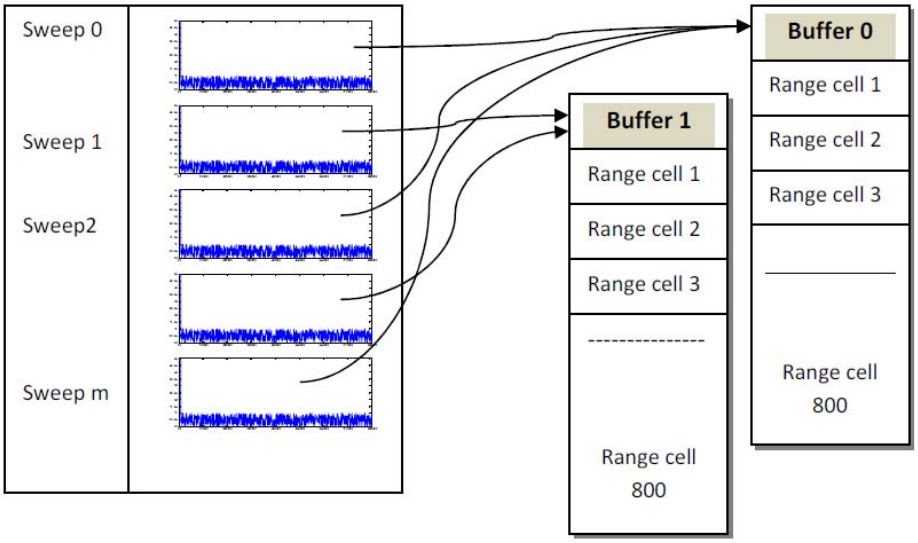

FIGURE 5.13: The double buffering technique principle.

To avoid erasing the samples acquired from two consecutive sweeps, we use the double buffering technique (see Fig. 5.13) which consists of using two buffers with flipping from a sweep to another in an automatic manner controlled by the synchronization signal. The same technique is used for the integration buffers, but controlled by the antenna azimuth data.

By using the synchronization signal, the integration consists of adding the samples of the current sweep to the samples of the previous sweep. After the acquisition completion, an interrupt is asserted to the DSP to start the CFAR processing for each cell of the range.

5.5.3 Radar signal processing

After the acquisition process, four types of processing relative to the CA-CFAR, the OS-CFAR, the FAOSOSD and the ALC-CFAR detectors are performed on a TMS320C6711 based development platform and tested using synthetic and real-life

data. During the acquisition of the current sweep samples, the CFAR processing is performed on the previous sweep samples.

In practice, the observations show that the clutter is homogeneous for about 1.8Km [3]. For a convenable application of CFAR detectors, the reference window size is limited by the radar resolution (pulse width, τ)and the homogeneous range, R_h, as shown in Fig. 5.14. Consequently, the optimal number of reference cells can be expressed by :

$$N_{opt} = \frac{2R_h}{c\tau} - (1 + 2g) \tag{5.2}$$

where c : is the velocity of electromagnetic wave propagation and g : the number of guard cells in a half reference window.

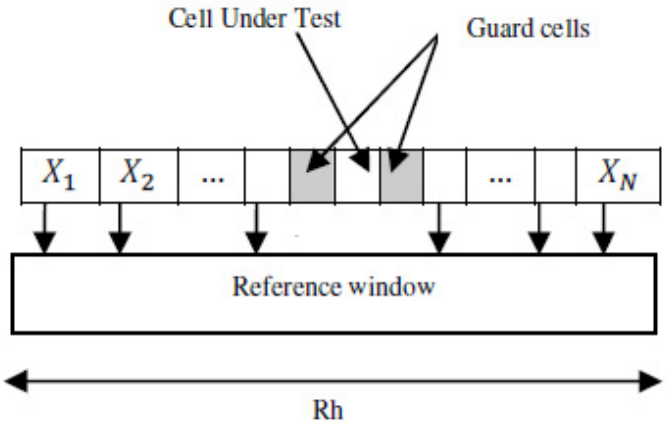

FIGURE 5.14: The homogeneous range and the reference window size limitation.

It should be noticed that it is strongly recommended to choose the number of reference cells according to Eq.5.2.

5.5.3.1 The CA-CFAR detector

The CA-CFAR detection consists of three steps :

1. Computing of the threshold level by adding all the reference window samples multiplied by the scaling factor, T_{CA} ;

2. Comparison of the cell under test to the obtained threshold level ;

3. Save the decision result in the output buffer. It contains the range bin number of the detected target.

The CA-CFAR threshold level computation needs the addition of the N samples of the reference window. The obtained sum is multiplied by the scaling factor to get the decision threshold. So, we need $2N$ additions and one multiplication for each cell under test.

It should be noted that, the increase of the number of reference cells improves the threshold estimation, but the real-time implementation requires the minimum of operations. Thus it will be necessary to make a tradeoff and choose an optimal number of reference cells.

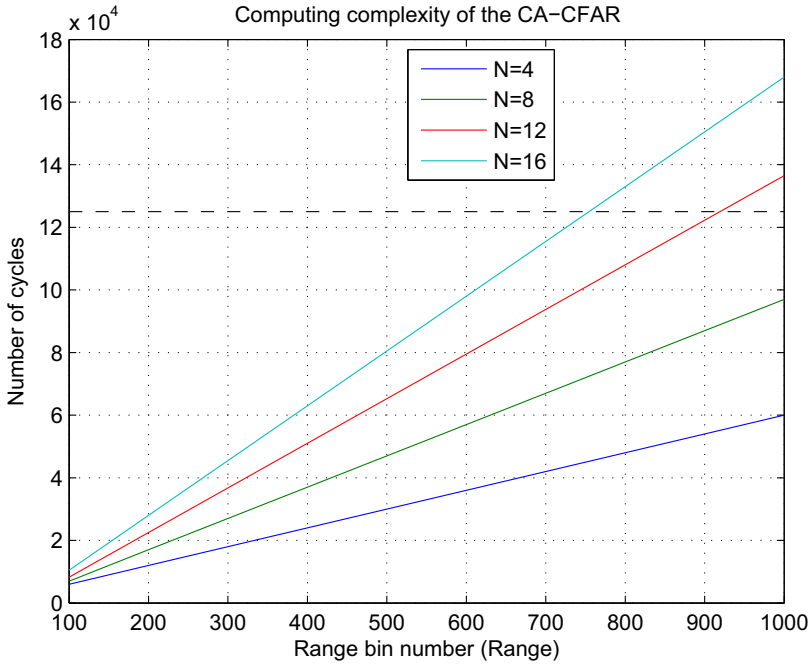

FIGURE 5.15: The execution time for the CA-CFAR detector DSP implementation for different reference window sizes.

The obtained results reported in Fig. 5.15 show the estimation time of the CA-CFAR threshold for different reference window sizes, N=4, N=8, N=12 and N=16 as

a function of the processed radar range.

It can be seen that the execution time is proportional to the number of reference cells, N, and the number of radar range cells. Thus, it represents a limitation for the real-time implementation of the CA-CFAR detector for large reference window size.

We notice that the reference window size is limited between 12 and 16 cells for a real-time processing of the entire radar range.

Theoretically, the increase of the reference window size improves the threshold estimation, but the real-time processing requires the minimum of operations to meet the corresponding constraints.

This situation requires to develop new computing procedures in order to reduce the number of operations and thus ensure the real-time processing.

The Generalized Automatic Sliding Window

Instead of using the classical sliding window for the CA-CFAR implementation, we propose the Generalized Automatic Sliding Window (GASW) technique [68] in order to keep the estimation time constant what ever the number of reference cells is, and the number of guard cells, as shown in Fig. 5.16.

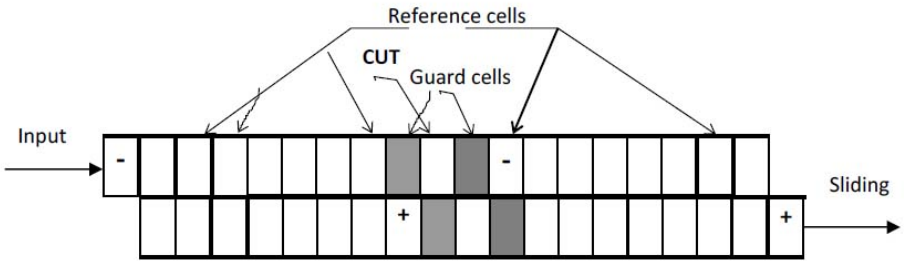

FIGURE 5.16: The GASW technique principle.

The CA-CFAR detector is hence implemented using the GASW technique. The threshold estimate for the k^{th} cell under test is given by :

$$Q(k) = \sum_{i=1}^{m} q(k+i+g) + q(k-i-g) \tag{5.3}$$

where q(.) : is the output of the square law detector, m : the number of cells in left/right reference window ; and g : the number of guard cells.

The estimate for the $(k+1)^{th}$ range cell under test may be updated by Eq. 5.4.

$$Q(k+1) = Q(k) + [q(k+m+g+1) + q(k-g)] - [q(k-m-g) + q(k+g+1)] \quad (5.4)$$

We note that the GASW technique reduces the computing time to four operations only (two additions and two subtractions) whatever the reference window size is, and the number of guard cells.

So, the introduction of this automatic technique makes the computing time almost constant independent of the number of reference and guard cells.

The execution time

Fig. 5.17 shows the GASW technique effect on the processing time of the CA-CFAR detector for the entire range cells.

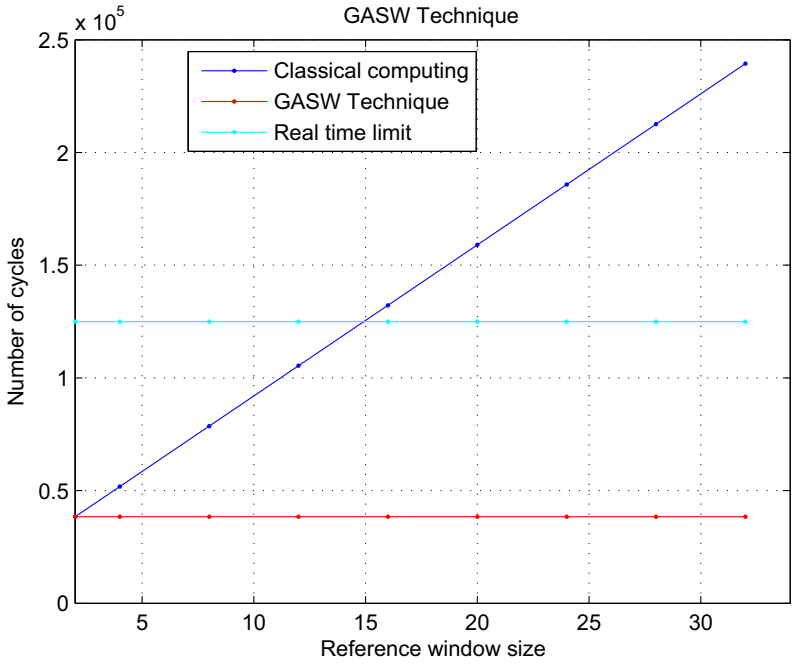

FIGURE 5.17: The GASW technique effect on the processing time.

It can be pointed out that the introduction of this technique guarantees the real-time processing whatever the reference window size is. This technique is suitable for high resolution radar detection systems.

Implementation results

The implementation results of the CA-CFAR detector are presented in Fig. 5.18. Fig. 5.18 (a) shows the received signal samples. It can be seen the presence of six targets, five in the clear area and one in a clutter region.

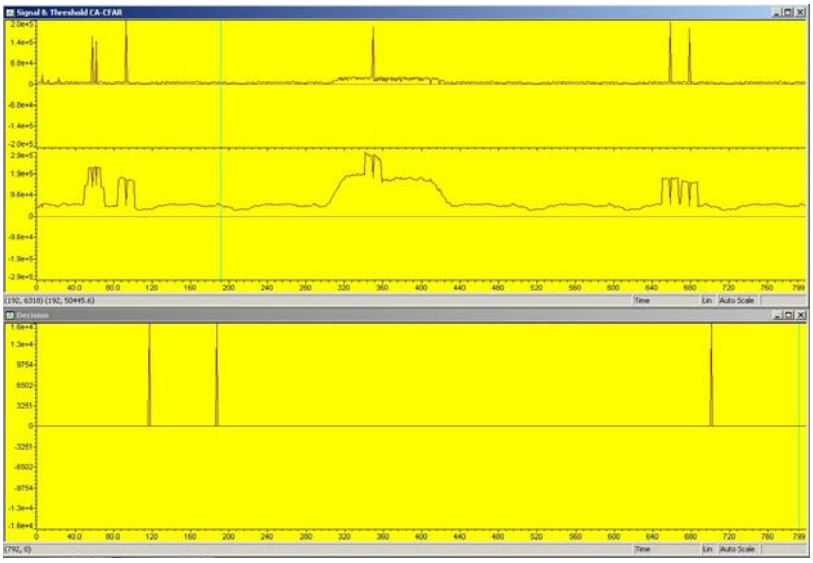

FIGURE 5.18: Implementation results of the CA-CFAR detector, (a) : The input radar signal, (b) : The CA-CFAR threshold, (c) : The decision.

In Fig. 5.18 (b), we present the CA-CFAR threshold level progression. We can observe in Fig. 5.18 (c) the decision at the corresponding range bins. All the targets in the clear area are detected, while the target in the clutter region is missed as shown in the decision window.

5.5.3.2 The OS-CFAR detector

The OS-CFAR processor estimates the noise power simply by selecting the K^{th} largest cell in the reference window ; the threshold is obtained from one of the ordered samples of the reference window. The range samples are first ordered according to

their magnitudes, and the statistic Z is taken to be the K^{th} largest sample.

Ordinary implementation of the OS-CFAR processor

In order to implement the OS-CFAR processor, we have to rank-order all the reference data cells, as shown in Figure 5.19.

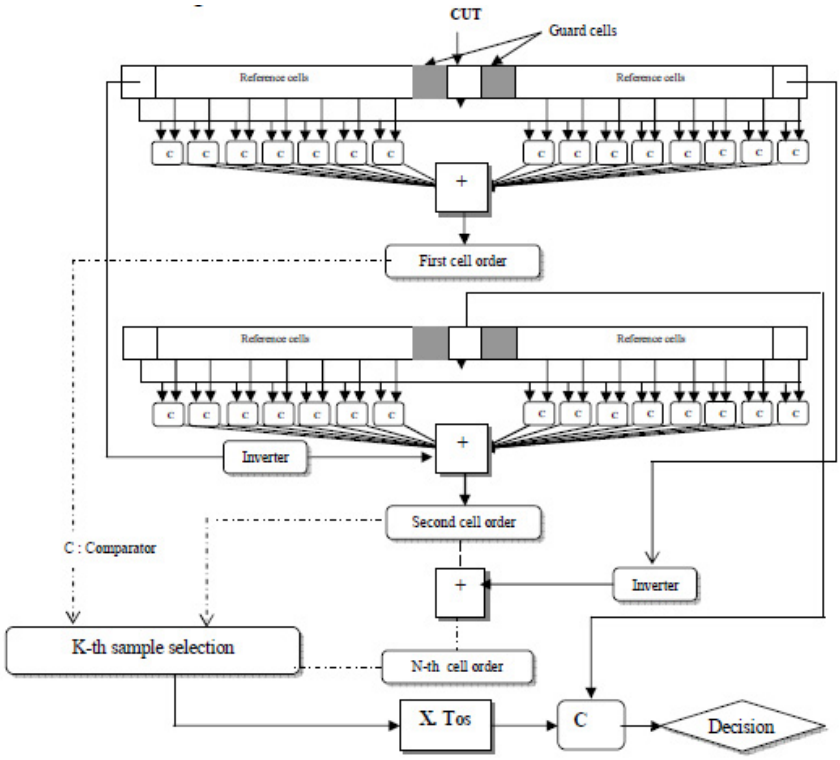

FIGURE 5.19: Direct implementation of the OS-CFAR processor architecture.

However, it is more difficult to realize the OS-CFAR detection in real time with general purpose microprocessors or digital signal processors because of the high throughput rate required in radar systems. Therefore, it is preferred to design a special structure for the OS-CFAR processing. The computational complexity of OS-CFAR is of a different form since other types of operations have to be performed, mainly comparison and move operations.

The threshold is obtained by the comparison of each reference cell with all other reference cells. The implementation of this approach requires $(N-1).(N/2)$ comparators and $(N-1).(N/2)$ inverters for a reference window size, N.

Furthermore, this method makes the required resources depend strongly on N^2. For example, for $N = 16$, we need 120 comparators and 120 inverters.

The proposed structure scheme

The proposed structure for the OS-CFAR processor implementation is shown in Figure 5.20.

The proposed architecture is based on the $(N-K+1)^{th}$ maximum determination [74]. By showing that the determination of the K^{th} order out of N reference cells is equivalent to selecting the $(N+1-K)^{th}$ maximum, the detector that uses N reference cells can be implemented using only $(N-1)$ comparators and $(N-1)$ inverters.

This architecture with a window size, N, consists of $(N-1)$ comparators and $(N-1)$ inverters and one decision bloc (one multiplier and one comparator).

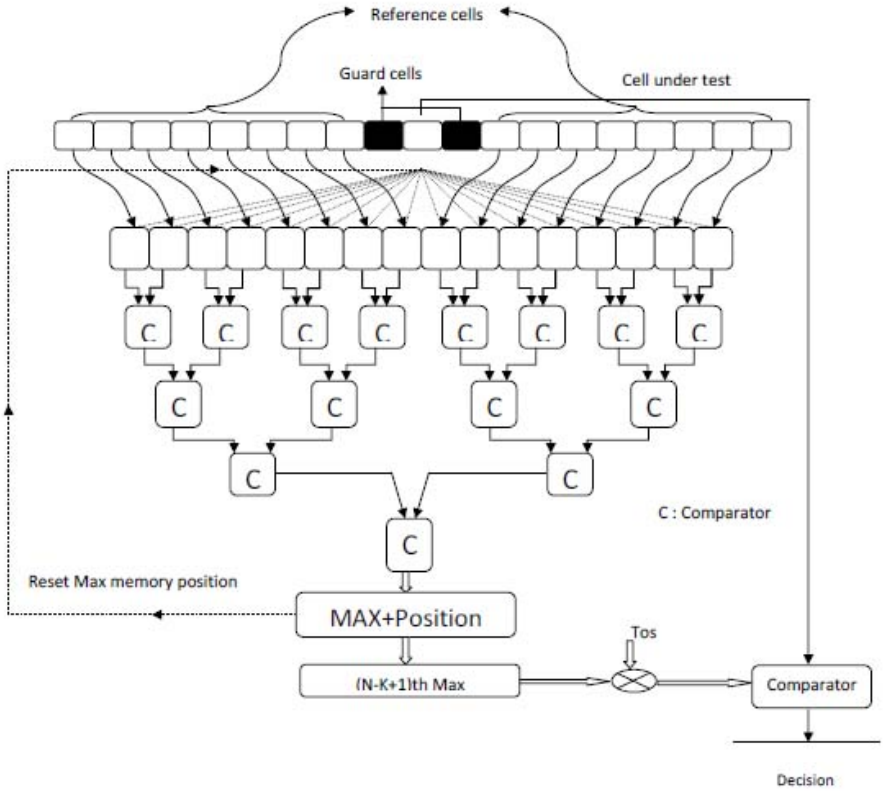

FIGURE 5.20: Block diagram of the OS-CFAR processor DSP optimized implementation

The proposed approach consists of the following steps :

1. Determine the maximum and its position in the reference window by successive comparisons ;

2. Zero setting of the current maximum in the reference window ;

3. Repeat steps 1 and 2 up to $(N - K + 1)$;

4. The $(N - K + 1)$ maximum represents the K^{th} order.

For a number of reference cells N, only $(N - 1)$ comparators are needed to determine the maximum. In practice, K is greater than $N/2$, the proposed structure reduces the number of comparators by (K/N)*100 $^{o}/_{o}$.

This reduction achieves $75^{o}/_{o}$ if $K = 3N/4$.

Implementation results

The implementation results of the OS-CFAR detector, presented in Fig. 5.21, indicate that it declares the presence of all targets presented in the received signal as shown in the decision window.

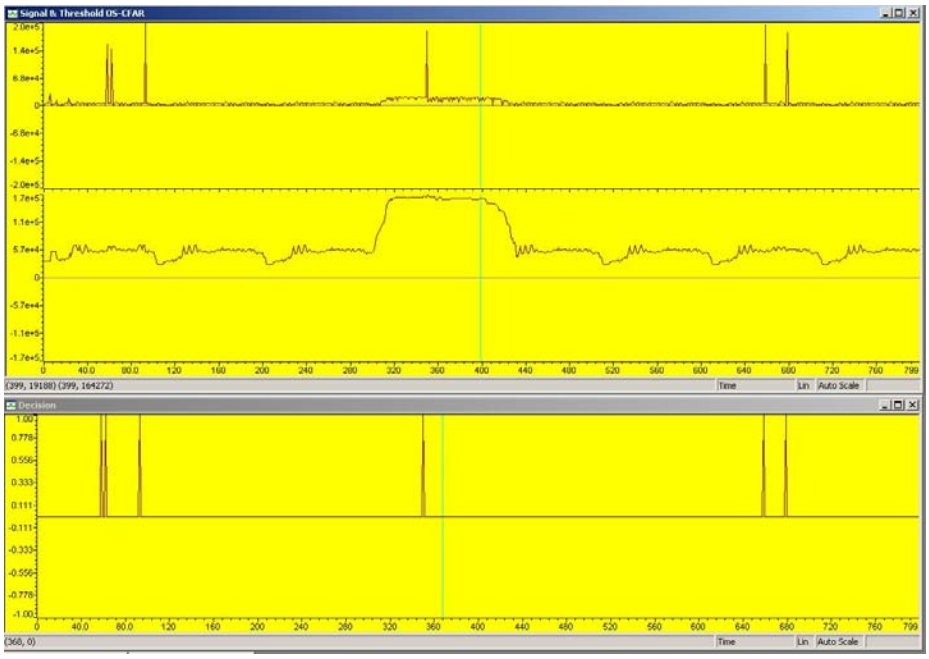

FIGURE 5.21: Implementation results of the OS-CFAR detector, (a) : The input radar signal, (b) : The OS-CFAR threshold, (c) : The decision.

5.5.3.3 The FAOSOSD detector

The FAOSOSD algorithm implementation is subdivided into four fundamental steps :

1. Sorting the reference window samples in ascending order ;
2. Computing the ITC for different samples and determining the order of the minimum ;
3. Determining the optimum order for the OS-CFAR detector ;
4. Computing the corresponding threshold and establish a detection test.

The execution time

The global execution time of the FAOSOSD algorithm has been optimized thanks to the exploitation of the parallel architecture of the considered processor and the use of pre-determined lookup tables to compute the logarithmic function involved in the ITC computation.

The numerical results of the proposed implementation show that the computing time increases for higher values of the number of reference cells.

Table 5.2 shows the maximum range processing in real time for different number of reference cells, N.

TABLE 5.2: Real time maximum processed range by the FAOSOSD detector.

N	4	8	16	24	32	***40***	48
Processed Range (Km)	72.3	65.2	52.7	36.8	25.4	***14.3***	7.1

The obtained execution times of the FAOSOSD processor show that, whatever the reference window size is, the real-time processing of the whole radar coverage cells is not respected for one pulse processing. Consequently, the FAOSOSD detector cannot cover the entire range of the ASR-12 radar coverage for real-time application.

The numerical results presented in Table 5.2 show clearly the real time processing limitation of the FAOSOSD. The increase of the number of the reference cells invokes the reduction of the processed range. For example, for $N = 40$, the processed range is reduced to only $14Km$.

As a final comment, the use of the FAOSOSD detector application is suitable after a non-coherent pulse integration within an azimuth resolution angle and not for pulse to pulse processing.

Implementation results

In Fig. 5.22, we present an example of the obtained implementation results of the FAOSOSD using the graphic interface of the Code Composer Studio.

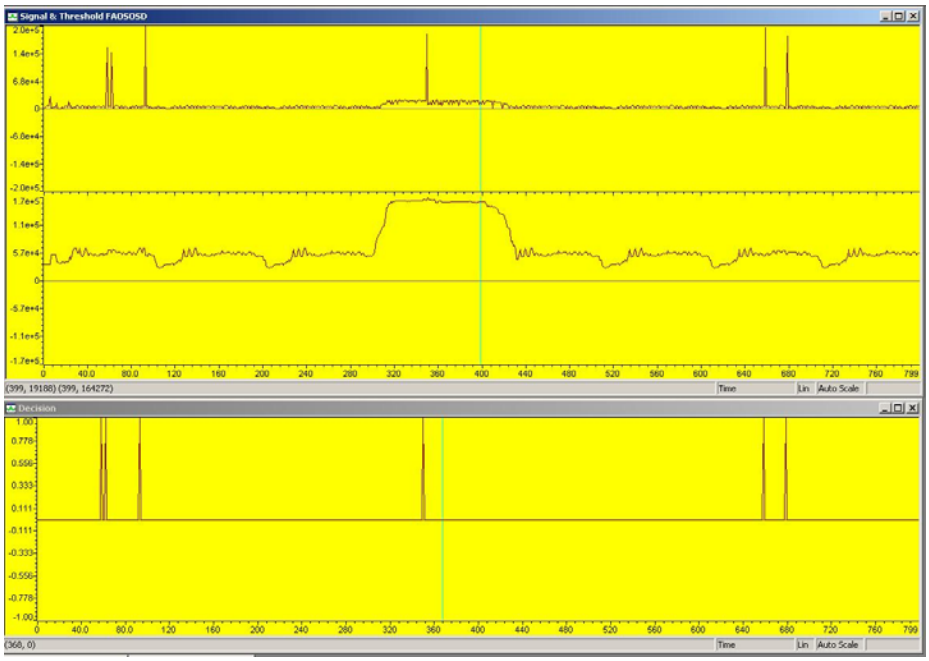

FIGURE 5.22: Implementation results of the FAOSOSD, (a) : The input radar signal, (b) : The FAOSOSD threshold, (c) : The decision.

In Fig. 5.22 (a), we consider six targets. In Fig. 5.22 (b), we show the FAOSOSD threshold level variation. Fig. 5.22 (c) presents the decision. We note that all the targets are detected using the FAOSOSD thresholding.

5.5.3.4 The ALC-CFAR detector

The ALC-CFAR algorithm implementation consists of four operations :

1. Computing the CA-CFAR threshold estimate ;
2. Computing the OS-CFAR threshold estimate ;
3. Computing the adaptive weighing factor ;
4. The ALC-CFAR threshold computing and detection test.

The execution time

In table 5.3, we present the obtained execution time for one range cell for different sizes of the reference window.

TABLE 5.3: Computational load of the ALC-CFAR for one range cell.

N	4	8	16	24	32	40	48
Number of cycles	189	421	1013	1893	3061	4617	6261
Time,(μs)	1.22	2.81	6.75	12.62	20.41	30.11	41.74

It can be seen that the processing time is proportional to the reference window size N. This time is greater than τ in all cases.

For real-time application, we must consider the hole radar coverage range to determine the processing limitation.

Table 5.4 shows the maximum range processing in real time for different number of reference cells, N. The obtained execution times of the ALC-CFAR processor show that the reference window size is limited to 32 range cells to ensure a real time processing of the whole range cells of the considered radar coverage.

We note that the execution time has been optimized by exploiting the techniques developed in [68] and [74] for the CA-CFAR and the OS-CFAR implementation, respectively.

TABLE 5.4: Real-time maximum processed range by the ALC-CFAR detector.

N	4	8	16	24	32	***40***	48
Maximum Processed Range (Km)	120	120	120	120	120	***86.1***	62.1

The numerical results presented in Table 5.4 show the real time processing limitation. We observe that the reference window size is limited between 32 and 40 cells to process the entire range samples.

The increase of the number of reference cells decreases the processed range. For example, for $N = 40$, the processed range is reduced to $86Km$.
For practical application in the ASR-12 radar, the obtained results are widely sufficient for real-time application since the reference window size is 16 according to Eq.5.2.

Implementation results

Fig. 5.23 shows the obtained implementation results of the ALC-CFAR detector. In Fig 5.23 (a), we have considered six targets separated in three groups. In Figure 5.23 (b), we illustrate the evolution of the estimated ALC-CFAR threshold, and in Figure 5.23 (c), we present the decision. We note that all the targets are detected using the ALC-CFAR thresholding.

5.6 Validation with real-life data

In addition to the validation of the implementation of the designed algorithms, using synthetic data, other experiments based on real-life recorded data have been conducted.

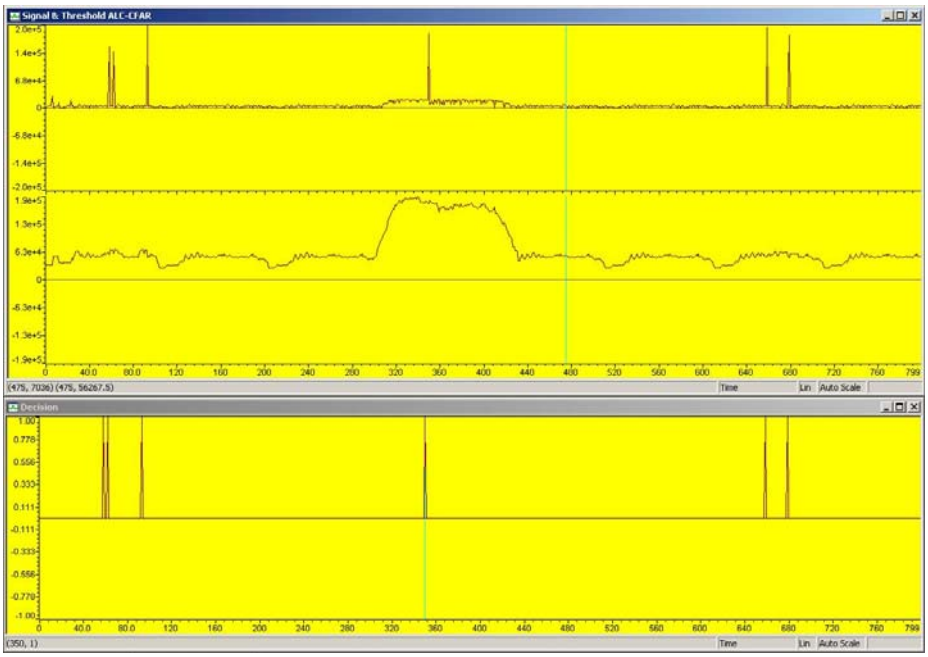

FIGURE 5.23: Implementation results of the ALC-CFAR, (a) : The input radar signal, (b) : The ALC-CFAR threshold, (c) : The decision.

5.6.1 Data description

The radar signal samples are gathered using 10 bits A/D converter and $1MHz$ sampling rate. The range resolution is about $150m$.

The covered range corresponds to 800 range bins (120Km).

Several situations have been considered in the conducted experiences. We present here two situations where two data files are considered.

First situation (datafile1) :

In a more realistic scenario, the radar signal's PDF is not perfectly known. It depends particularly on the clutter type and the radar waveform.

In Fig. 5.24, we plot the intensity of the datafile1 samples. It contains echoes of six targets present at cell range number 113, 181, 183, 187, 300 and 400. We can observe also the presence of clutter samples near the range bin number 400.

Fig. 5.25 plots the datafile1 histogram compared to the exponential PDF. It can be seen that it does not match the considered distribution.

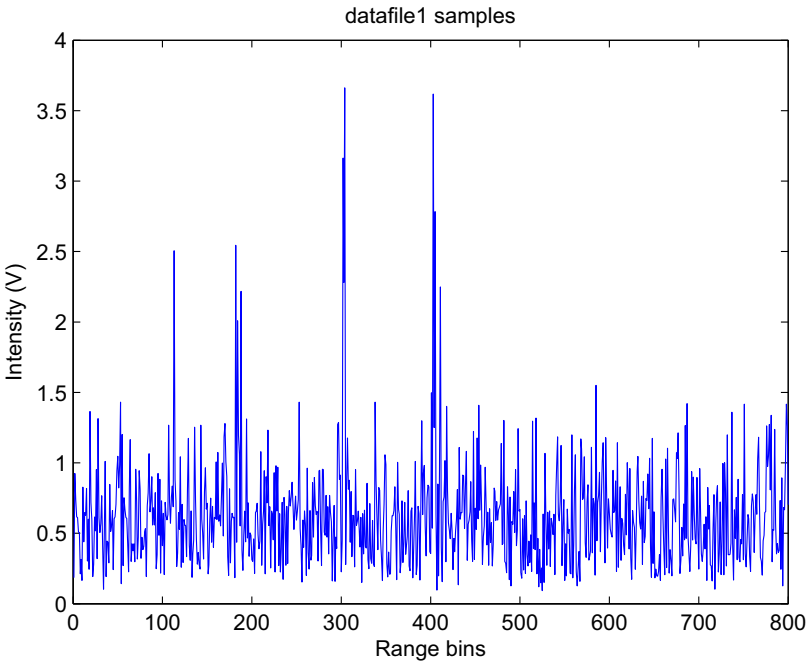

FIGURE 5.24: Radar signal intensity of the datafile1

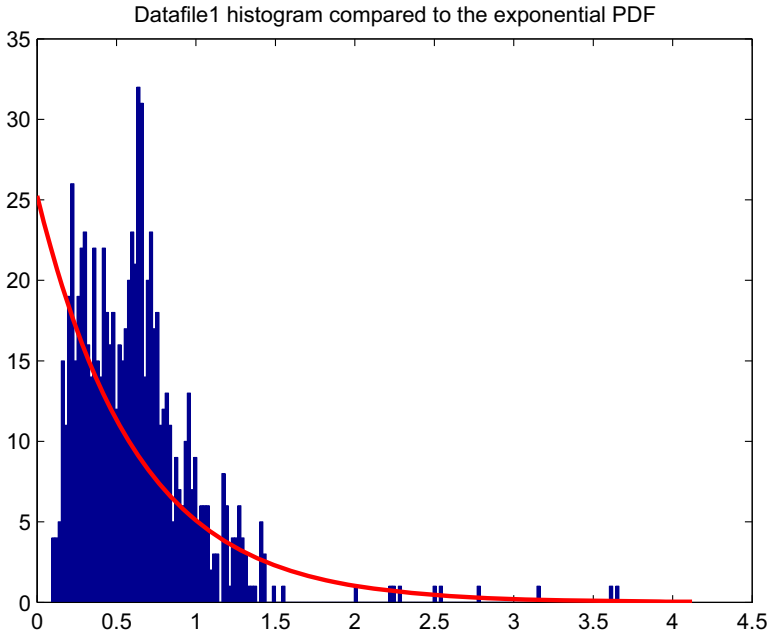

FIGURE 5.25: Datafile1 histogram compared to the exponential PDF.

In Fig. 5.26, we consider the datafile1 histogram compared to the log-normal PDF. It is clear to us that the datafile1 samples histogram is more matched to the

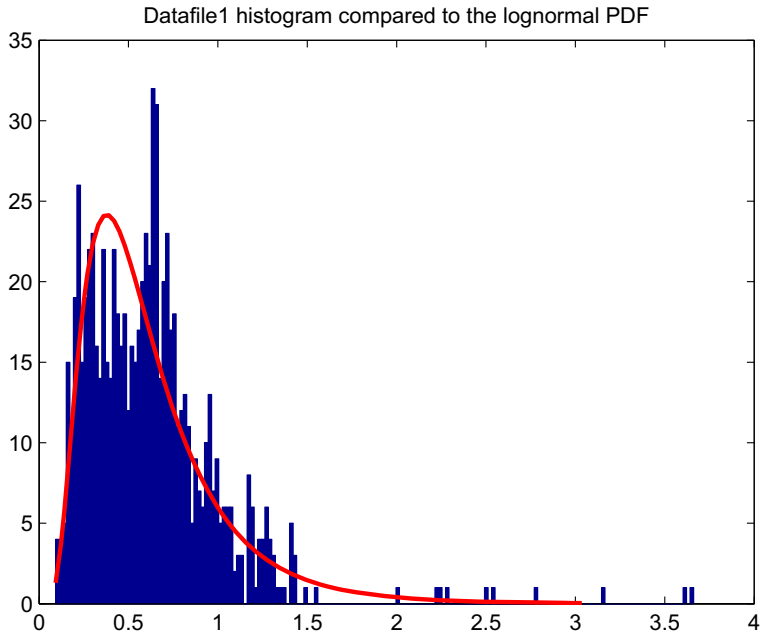

FIGURE 5.26: Datafile1 histogram compared to the log-normal PDF.

log-normal distribution.

Second situation (datafile2) :

In Fig. 5.27, 5.28 and 5.29, we present the datafile2 samples intensity and the corresponding histogram compared to the exponential and the log-normal PDFs, respectively.

It can be seen that the main difference compared with the datafile1, is the presence of a heavy clutter between cell range number 160 and 300. The considered targets in this case are present at range bin number 98, 107, 410 and 527.

5.6.2 Experimental results

In this subsection, we present the experimental results of the FAOSOSD and the ALC-CFAR detectors implementation using the data files presented in the previous subsection.

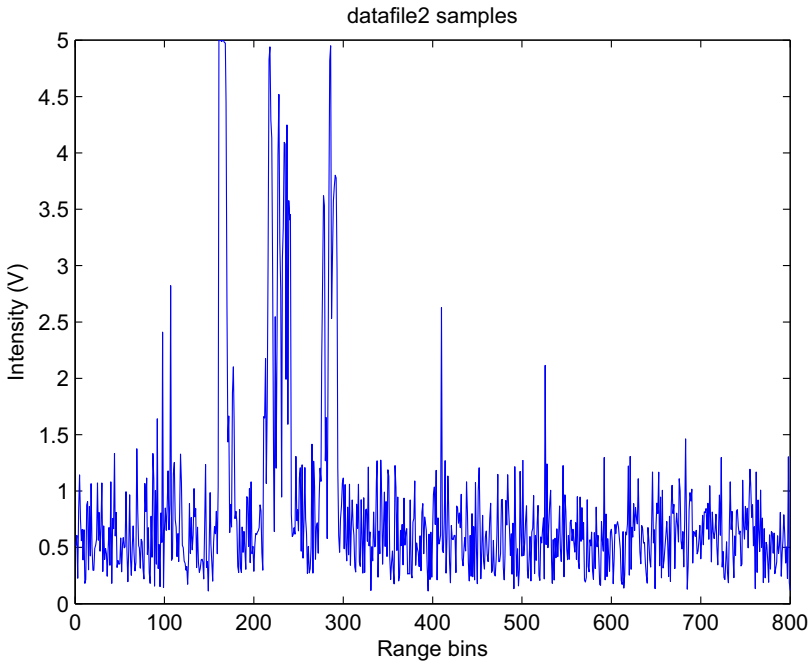

FIGURE 5.27: Radar signal intensity of the recorded datafile2.

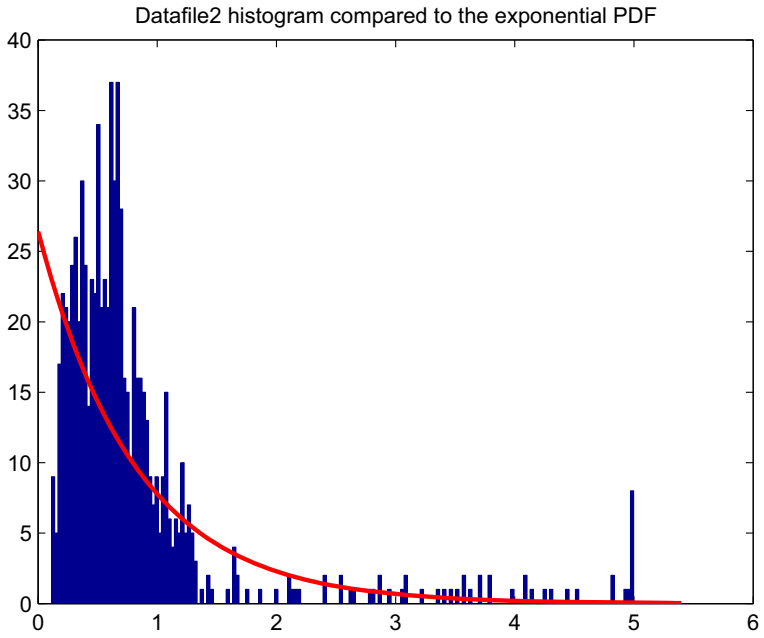

FIGURE 5.28: Datafile2 histogram compared to the exponential PDF.

5.6.2.1 The FAOSOSD detector

Fig. 5.30 and 5.31 show the experimental results of the FAOSOSD detector, for $N = 16$ and $P_{fa} = 10^{-5}$, using the first and the second data files, respectively.

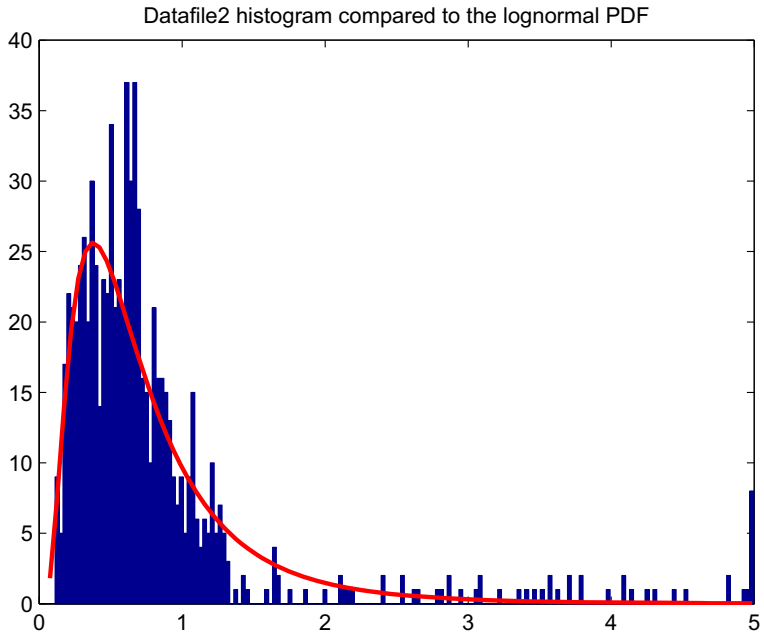

FIGURE 5.29: Datafile2 histogram compared to the log-normal PDF.

It appears that for data file1, the FAOSOSD detector declares the presence of six targets as shown in the decision window. Nevertheless, it generates some additional false alarms in the clutter region of data file 2.

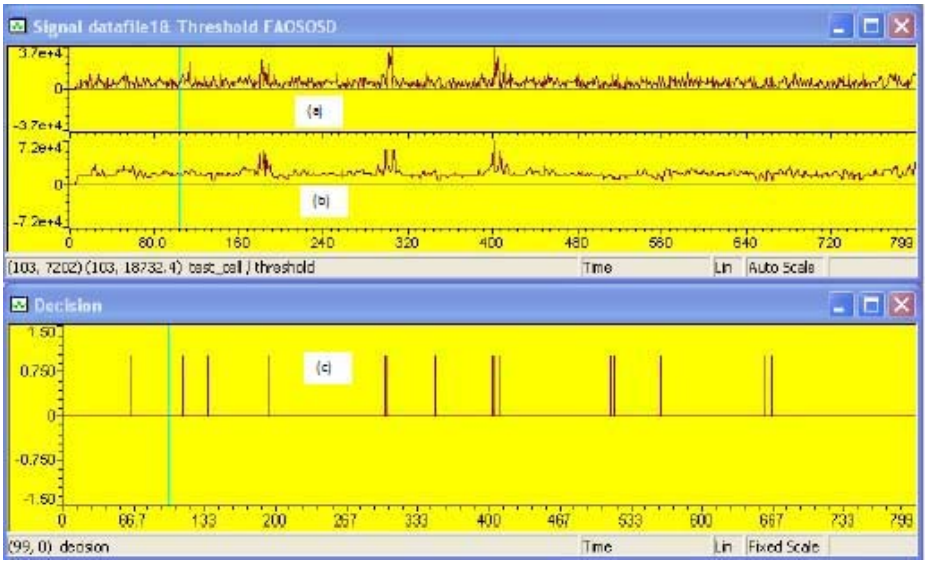

FIGURE 5.30: Results of the FAOSOSD (Datafile1).

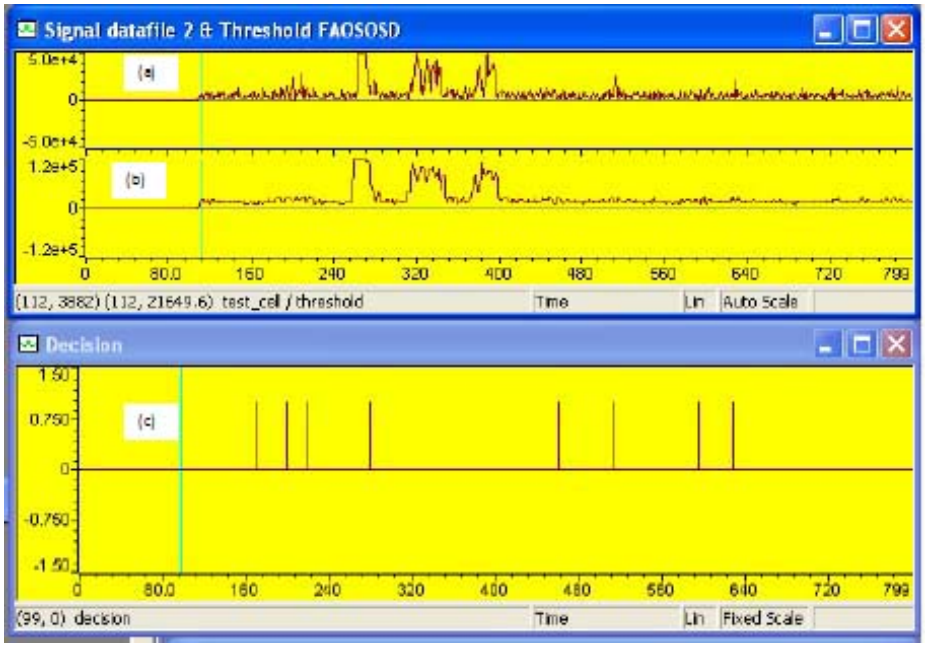

FIGURE 5.31: Results of the FAOSOSD (Datafile2).

5.6.2.2 The ALC-CFAR detector

Fig. 5.32 and 5.33 show the obtained results of the ALC-CFAR detector, for $N = 16$ and $P_{fa} = 10^{-5}$, using the first and the second data files, respectively. It can be seen that for data file1, the ALC-CFAR detector declares the presence of the six targets as shown in the decision window. Nevertheless, it presents a limitation in the heavy clutter region of data file 2. This is due to the performance degradation of the CA-CFAR detector in this kind of situation.

We note that, the detection quality can be improved by the readjustment of the threshold multipliers of the considered detectors accordingly to fit the real PDF of the radar signal.

5.7 Conclusion

In this chapter, we have presented the implementation results of the proposed detectors on a Texas Instruments TMS320C6711 based development platform. The

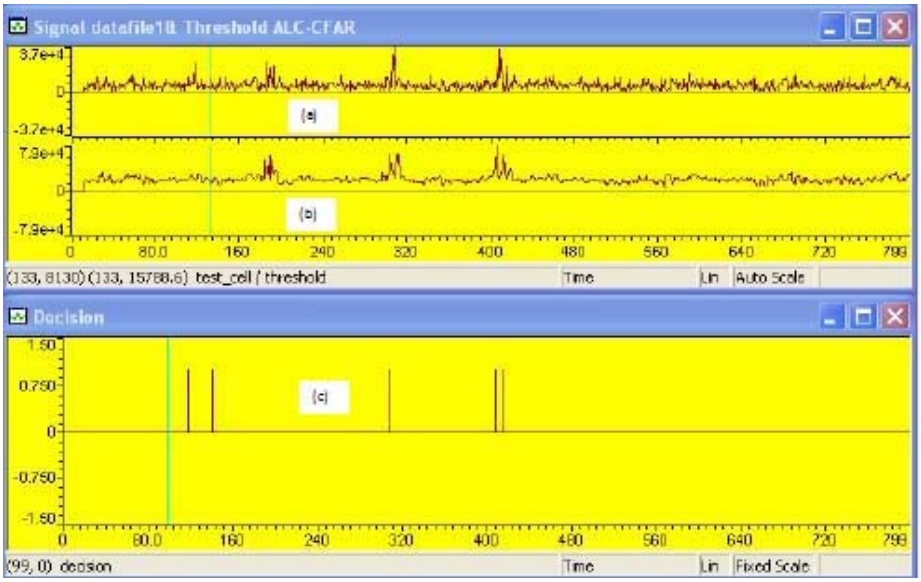

FIGURE 5.32: Results of the ALC-CFAR (Datafile1).

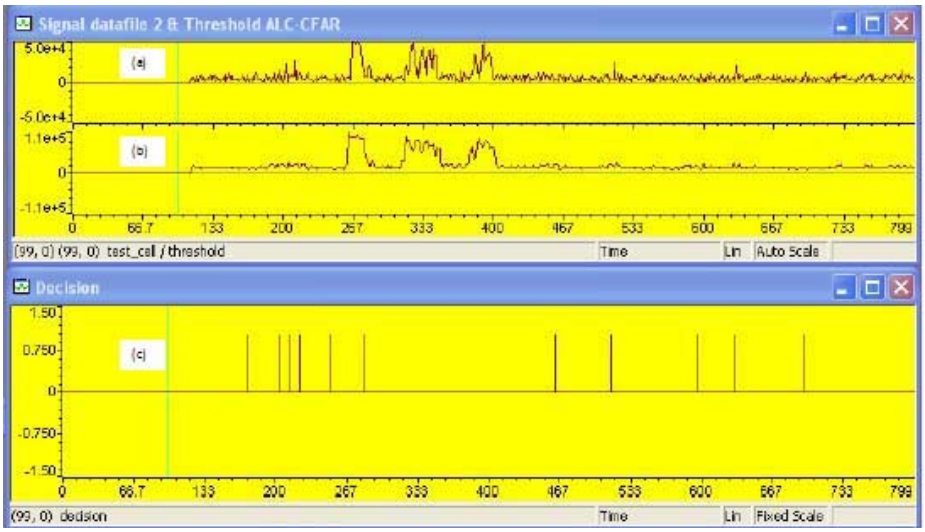

FIGURE 5.33: Results of the ALC-CFAR (Datafile2).

real time constraints are managed and evaluated so as to satisfy the requirements of the ASR-12 air surveillance radar for real-time applications. The obtained results show the application of the developed architectures for reduced reference window sizes after non-coherent pulse integration within the azimuth resolution angle.
The developed DSP implementation architectures are validated using real-life data.

It should be noted that the comparison of the suggested approach with respect to

other configurations in term of performance and execution time is difficult because of the non availability of similar work in the open literature.

Conclusion

This chapter concludes this thesis by summarizing and highlighting the key contributions of this research. We also present some areas of potential future work.

Summary of key contributions

The main contribution of this thesis involves two parts. The first one concerns the proposition of two novel algorithms for radar target detection referred to as, respectively, FAOSOSD, Forward Automatic Order Selection Ordered Statistics Detector, based on the minimization of the information theoretic criteria, and ALC-CFAR, Adaptive Linear Combined CFAR, based on an adaptive linear combination of the CA-CFAR and the OS-CFAR detector thresholds. These algorithms present the ability to sense automatically the environment changes, especially in presence of interfering targets, by adapting their thresholds to ensure better performance compared to ordinary detectors.

The FAOSOSD detector offers the ability to determine the number of interfering targets in the reference window by minimizing the information theoretic criteria and the adjustment of the OS-CFAR threshold consequently.

For the second detector, the ALC-CFAR, the threshold is adapted automatically according to the environment changes thanks to an adaptive weighing factor which measures the homogeneity level of the reference window samples. It presents performances closer to the CA-CFAR detector in homogeneous environment, with less

CFAR losses compared to the OS-CFAR, and performs like the OS-CFAR in presence of interfering targets.

The second part of our contribution deals with the development of new and efficient implementation architectures suitable for the proposed detectors using DSP development platform based on the Texas Instruments TMS320C6711 processor. The real time processing constraints and the radar signal digitalization effect on the detection quality have been evaluated and discussed, considering the satisfaction of the Air Surveillance Radar, ASR-12, technical characteristics.

We note the improvement of the computing burden using the Generalized Automated Sliding Window, GASW, technique for the CA-CFAR threshold estimation and the determination of the $(N - K)$ maximum for the OS-CFAR detector implementation.

The obtained results show the feasibility of real-time processing for the developed detectors for practical applications in radar detection.

The proposed implementation has been validated using real-life radar data presenting different kind of situations.

For practical application in radar detection, it is very interesting to note that the proposed detectors are particularly suitable for low resolution radars which use low number of reference cells to ensure the minimum homogeneity range.

In addition, the implementation architectures are fully parameterizable in terms of the sampling frequency, the reference window size, the number of guard cells and the false alarm probability. The default configuration uses 12 bits for data, 16 reference cells and 2 guard cells which is a common configuration used for most radar based application with a good performance-accuracy tradeoff.

This feature offers the ability to apply these architectures to other kind of radars by a simple readjustment of the corresponding parameters.

It should be noted that the comparison of the suggested approach with respect to

other configurations in term of performance and execution time is difficult because of the non availability of similar work in the open literature, and that the detection issue presented in this thesis presents only a part of more complex radar detection system.

As a conclusion, we would like to highlight that our work has shed new light on the applied radar research, and there are still lots of interesting methodologies to be discovered.

Future works

We can put forward many suggestions for extending the current research work. Some possible future work based on the obtained results is provided in this subsection.

- In this work, we have considered the ALC-CFAR and the FAOSOSD detectors separately. In the future, these two detectors could be merged to form one detection system which incorporates the adaptive combination aspect and the detection of the interfering target number. This combination would improve the detection quality.
- In this thesis, we have only considered the single pulse case. It will be interesting to consider the post integration processing to improve the detection probability.
- We have considered exponential distribution for the radar samples. It will be interesting to consider more general distributions such as Weibull and lognormal. An investigation towards this direction is of primary concern.
- Since the obtained processing times are suitable only for low resolution radars, it would be very important to optimize the implementation using multiprocessors configuration to support the computational burden related to low resolution radars.
- It is also interesting do derive the analytical expressions of the detection and the false alarm probabilities of the ALC-CFAR detector.

"This page is intentionally left blank"

APPENDICES

"This page is intentionally left blank"

APPENDIX A

The ASR-12 Radar specifications

The ASR-12 radar, is a modular, fully solid-state S-Band radar system that incorporates the latest technologies in airport surveillance radar systems. It is a further development of the ASR-9 and also uses the same reflector.
The main specifications of the ASR-12 radar are given in Table A.1.

TABLE A.1: The ASR-12 air traffic control radar specifications

frequency	2.7 to 2.9 GHz
pulse repetition time (PRT)	processor controlled
pulse repetition frequency (PRF)	1200Hz (default)
pulsewidth (PW)	1 Microsecond and 55 Microseconds
peak power	22 kilowatts
displayed range	60 / 80 / 100 NM
range resolution	700 ft
beamwidth	1.4 degrees
hits per scan	20
antenna rotation	10 / 12 / 15 rpm

"This page is intentionally left blank"

APPENDIX B

Résumé

B.1 Context et motivation

Le radar est un système électromagnétique qui détecte, localise, et identifie les cibles. Il émet des ondes électromagnétiques et reçoit les échos d'une cible qui lui permet de la détecter, de déterminer sa position et d'obtenir d'autres informations. Le signal reçu est fréquement accompagné du bruit, du clutter et d'interférences qui causent souvent des problèmes de détection de cibles [1,2,3,4].

Pour réaliser une décision correcte sur la présence ou l'absence d'une cible, le récepteur radar est conçu pour assurer un taux de fausses alarmes constant (CFAR) et une probabilité de détection maximale.

Les radars modernes détectent les cibles par la comparaison des niveaux des signaux correspondants avec des seuils adaptatifs déterminés dynamiquement à partir de la puissance du bruit local et du clutter. Ce seuil est fixé pour chaque cellule sur la base de la puissace du bruit, qui est déterminée par le traitement d'un ensemble de cellules de référence entourant la cellule sous test. Par exemple, le détecteur Cell Averaging, CA-CFAR [18] calcule le seuil automatiquement par l'estimation du niveau moyen des échantillons de la fenêtre de référence.

La performance du détecteur CA-CFAR est optimale dans un environnement homogène lorsque les cellules de référence contiennent des échantillons indépendants et identiquement distribués (i.i.d).

En pratique, l'environnement est souvent non-homogène à cause de la présence de cibles interférentes ou des bords du clutter dans la fenêtre de référence, ce qui peut causer une dégradation significative des performances lorsque la supposition d'environnement homogène n'est pas vérifiée [19, 20, 21, 22, 36, 62, 65].

Des modifications du detecteur CA-CFAR ont été proposées, dans la littérature, pour améliorer les performances dans des régions de transition du clutter ou des situations multi-cibles.

Les détecteurs à statistiques d'ordre sont conçus pour opérer en présence de cibles interférentes [20]. Cependant, ils présentent des pertes de détection additionnelles comparativement au détecteur CA-CFAR dans un environnement homogène.

Pour des environnements complexes comme le cas des radars d'anti-collision où l'environnement change brusquement, ces détecteurs conventionnels ne peuvent pas détecter les cibles proprement.

En l'occurence, plusieurs algorithmes CFAR ont été développés pour s'adapter aux différentes situations notamment en présence de cibles interférentes. Lorsque le nombre de cibles interférentes dépasse le nombre supposé, ces détecteurs présentent une forte dégradation de performances.

C'est dans ce contexte que les travaux de recherche menés dans cette thèse ont été initiés. La contribution principale de cette thèse comporte deux axes. Le premier concerne la proposition de deux nouveaux algorithmes de détection de cibles radar baptisés, respectivement, FAOSOSD, Forward Automatic Order Selection Ordered Statistics Detector, basé sur la minimisation du critère de la théorie de l'information [6, 61], et ALC-CFAR [33,74], Adaptive Linear Combined CFAR, basé sur une combinaison linéaire adaptative des estimés des seuils des détecteurs classiques CA-CFAR

et OS-CFAR.

Ces algorithmes présentent la capacité de s'adapter automatiquement aux changements de l'environnement, notamment en présence de cibles interférentes, par l'ajustement de leurs seuils afin d'assurer de meilleures performances comparativement aux détecteurs classiques.

Le deuxième axe porte sur le développement de nouvelles architectures d'implémentation efficace des détecteurs proposés. Ces derniers sont implémentés sur une plateforme de développement à base du processeur numérique du signal, DSP, type TMS320C6711 de Texas Instruments. Les contraintes de traitement en temps réel et l'effet de numérisation du signal radar sur la qualité de détection ont été considérés, étudiés, évalués et discutés.

En tenant compte des contraintes imposées par les spécifications techniques du radar de surveillance aérienne ASR-12, les résultats d'implémentation, à base des données expérimentales, des détecteurs développés montrent la faisabilité du traitement en temps réel pour des applications pratiques dans une chaine de détection radar.

Cette annexe est dédiée au résumé des travaux réalisés dans cette thèse.

Dans la section B.2, nous introduisons une approche qui permet l'estimation du nombre de cibles interférentes dans la fenêtre de référence par la minimisation du critère de la théorie de l'information. La méthode proposée permet ensuite d'ajuster l'ordre du détecteur OS-CFAR pour éviter l'effet de maskage lorsque le nombre d'interférences dépasse (N-K), N étant le nombre de cellules de référence et K est l'ordre du détecteur OS-CFAR.

Dans la section B.3, nous présentons les améliorations apportées à la qualité de détection de cibles par le détecteur ALC-CFAR dans des milieux homogène et non-homogène comparativement aux détecteurs classiques CA-CFAR et OS-CFAR.

Dans la section B.4, nous décrivons les architectures d'implémentation et les résultats expérimentaux des détecteurs proposés sur une plateforme de développement

à base du processeur de traitement numérique du signal, DSP, type TMS320C6711 de Texas Instruments. Nous présenterons enfin une conclusion.

B.2 Application des critères de la théorie de l'information à la détection radar

B.2.1 Le détecteur FAOSOSD

Le schéma du détecteur FAOSOSD est illustré dans la Figure B.1.

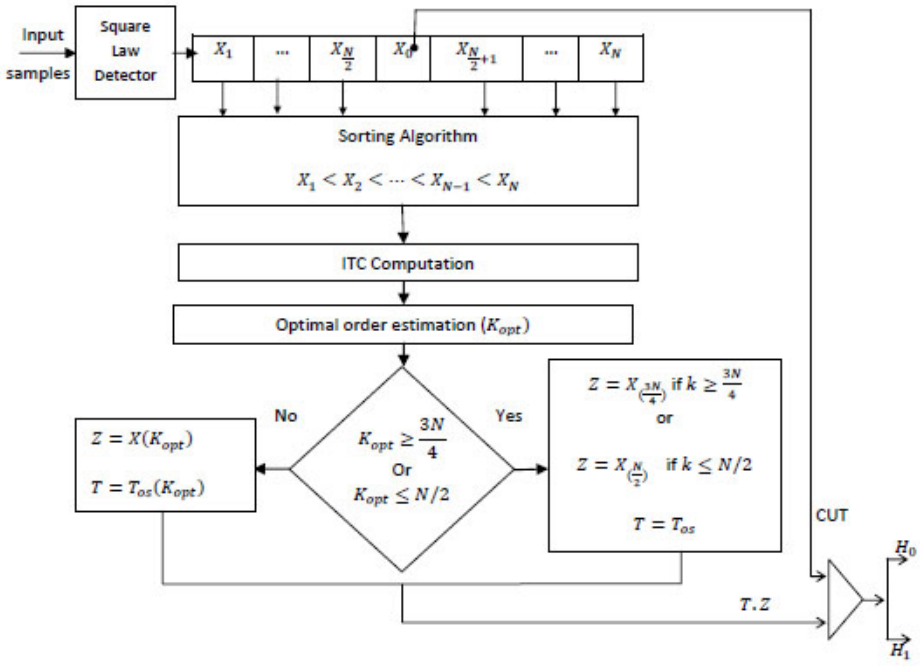

FIGURE B.1: Schéma bloc du détecteur FAOSOSD.

Le détecteur FAOSOSD (Forward Automatic Order Selection Ordered Statistics Detector), est basé sur cinq étapes fondamentales.

Etape1 : Ordonner les échantillons de la fenêtre de référence ;

$$X(1) \leq X(2) \leq \cdots \leq X(k) \leq \cdots \leq X(N) \tag{B.1}$$

Etape2 : Calculer le critère théorique de l'information.

Etape3 : Estimer l'ordre optimal pour le détecteur OS-CFAR, K_{opt}.

On note que dans le cas où ce nombre dépasse $\frac{3N}{4}$ ou inférieur à $\frac{N}{2}$, on maintient le seuil du détecteur OS-CFAR classique pour un ordre $k = \frac{3N}{4}$ ou $k = \frac{N}{2}$, respectivement.

Etape4 : Choisir le facteur d'échelle correspondant et calculer le niveau de seuil.

$$TZ = TX(K_{opt}) \tag{B.2}$$

Etape5 : La cellule sous test est comparée avec le seuil calculé et une décision est prise selon les tests :

$$H_1 : X_0 \geq TX(K_{opt}) \tag{B.3}$$

$$H_0 : X_0 < TX(K_{opt}) \tag{B.4}$$

L'hypothèse H_1 représente l'existence de la cible dans la cellule de test, et H_0 représente l'absence de cible.

Pour le détecteur FAOSOSD, le facteur d'échelle T est défini selon le nombre de cibles interférentes estimé.

Ces étapes sont exécutées dynamiquement en utilisant un ordre adapté pour estimer le niveau du clutter et calculer le seuil adaptatif en conséquence. Ce détecteur n'exige aucune information a priori sur les paramètres du clutter et le nombre de cibles interférentes.

B.2.2 Principe d'estimation du nombre de cibles interférentes

L'approche proposée procède, premièrement, par ordonner les échantillons de la fenêtre de référence selon un ordre croissant, ensuite appliquer le critère de la théorie de l'information, $ITC(k)$, pour chaque échantillon. On détermine le ITC minimal et l'ordre de l'échantillon correspondant. L'ordre obtenu représente l'estimé du nombre

de cibles interférentes dans la fenêtre de référence.

Le ITC est défini par [6] :

$$AIC(k) = -2(N-k)N\ln(\frac{G(\lambda_{k+1},\cdots,\lambda_N)}{A(\lambda_{k+1},\cdots,\lambda_N)}) + 2k(2N-k) \tag{B.5}$$

pour le critère Akaike, AIC, et

$$MDL(k) = -(N-k)N\ln(\frac{G(\lambda_{k+1},\cdots,\lambda_N)}{A(\lambda_{k+1},\cdots,\lambda_N)}) + \frac{1}{2}k(2N-k)\ln(N) \tag{B.6}$$

pour le critère MDL (Minimum Description Lenght).
avec $\lambda_1, \lambda_2 \cdot\cdot, \lambda_N$ représentent, dans notre cas, les amplitudes des échantillons de la fenêtre de référence [1], N est le nombre d'échantillons, et G et A représentent respectivement, les moyennes géométrique et arithmétique de leurs arguments.

L'ordre k du détecteur OS-CFAR est pris égal à la valeur de k pour laquelle le $ITC(k)$ est minimisé, avec $k \in \{0, 1, ..., N-1\}$.

Pour montrer l'efficacité de l'approche proposée, plusieurs sénarios ont été réalisés. Nous présentons ici un exemple illustratif.

Dans la Figure B.2 (a), on considère une fenêtre de référence de 32 cellules en présence de cinq cibles interférentes dans les cellules 17, 18, 19, 20 et 24 avec des rapports interférence à bruit égaux, $INR = 15dB$. En observant la décroissance graduelle des amplitudes des échantillons dans la Figure B.2 (b), il est clair que la séparation des cinq plus grands échantillons des faibles échantillons est une opération facile pour les grandes valeurs de INR.

Le nombre estimé de cibles interférentes est déterminé à partir de l'ordre pour lequel le critère ITC est minimisé. La position du minimum indique l'ordre du premier échantillon du bruit dans la fenêtre de référence ordonnée. Les plus grandes amplitudes

1. On note que ces échantillons sont positifs à la sortie du détecteur quadratique.

correspondent aux échantillons des cibles interférentes.

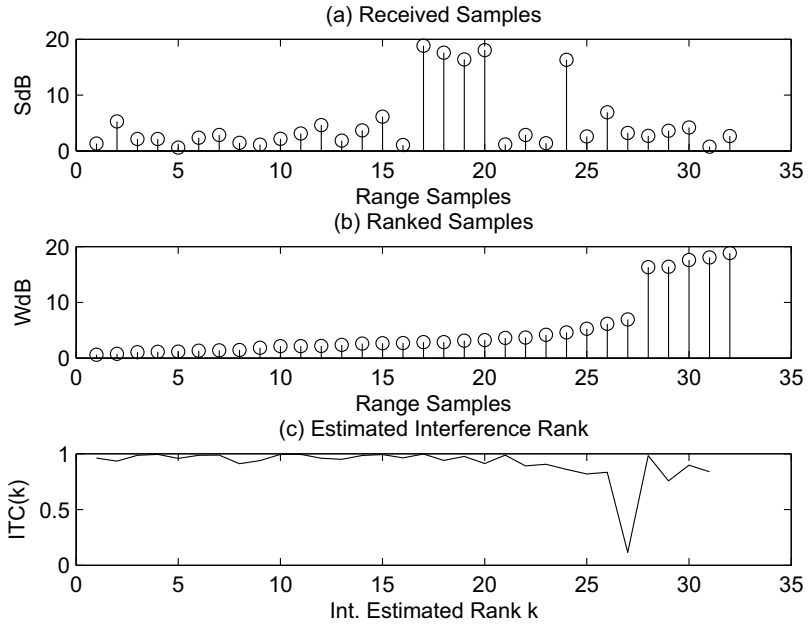

FIGURE B.2: Estimation du nombre de cibles interférentes présentes dans la fenêtre de référence, $INR = 15dB$.

Pour le choix de l'ordre du détecteur OS-CFAR, on utilise le $(K_{opt})^{eme}$ échantillon ordonné pour éviter l'utilisation d'un échantillon correspondant à une cible interférente pour calculer le seuil. Cette approche réduit l'effet de maskage des cibles lorsque le nombre de cibles interférentes dépasse la limite tolérée.

B.2.3 Résultats de simulation

Le détecteur FAOSOSD a été évalué dans différentes situations radar en présence de cibles interférentes. Nous examinons dans ce qui suit, l'évolution des seuils de détection, l'amélioration apportée à la probabilité de détection et la régulation de la fausse alarme effective.

B.2.3.1 Seuils de détection

La Figure B.3 illustre l'évolution des seuils de détection des détecteurs OS-CFAR et FAOSOSD en présence de cibles interférentes. On remarque que le groupe de huit cibles (centré à la cellule 50) n'est pas détecté par le détecteur OS-CFAR du fait que le nombre de cibles interférentes dépasse quatre, pour $K = 12$ et $N = 16$, bien que le détecteur FAOSOSD détecte les huit cibles présentes dans le groupe par l'ajustement de l'ordre de l'échantillon formant le seuil en fonction du nombre estimé de cibles interférentes.

D'une manière similaire, le détecteur FAOSOSD détecte toutes les cinq cibles présentes entre la cellule distance 10 et 20, cependant, le détecteur OS-CFAR rate la cible avec le plus faible rapport signal à bruit présente dans la cellule 11. La cible ratée est masquée par les signaux d'interférence présents dans la fenêtre de référence correspondante.

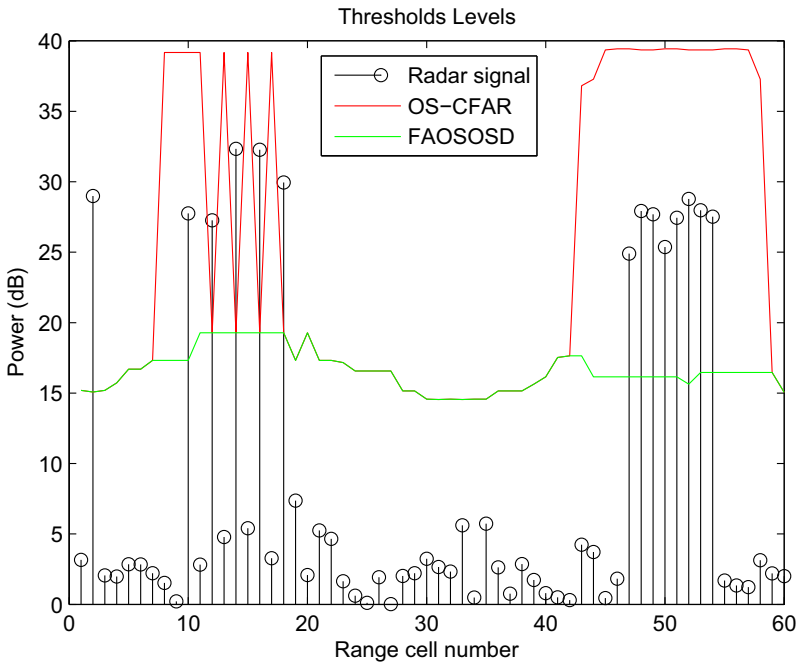

FIGURE B.3: Seuils CFAR en présence d'un groupe de huit cibles interférentes, et cinq signaux d'interférence, $Pfa = 10^{-5}$, $N = 16$ et $K = 12$.

B.2.3.2 Probabilités de détection

Les performances du détecteur FAOSOSD dans des situations d'interférences sévères sont comparées avec les détecteurs OS-CFAR, AND-CFAR et OR-CFAR.

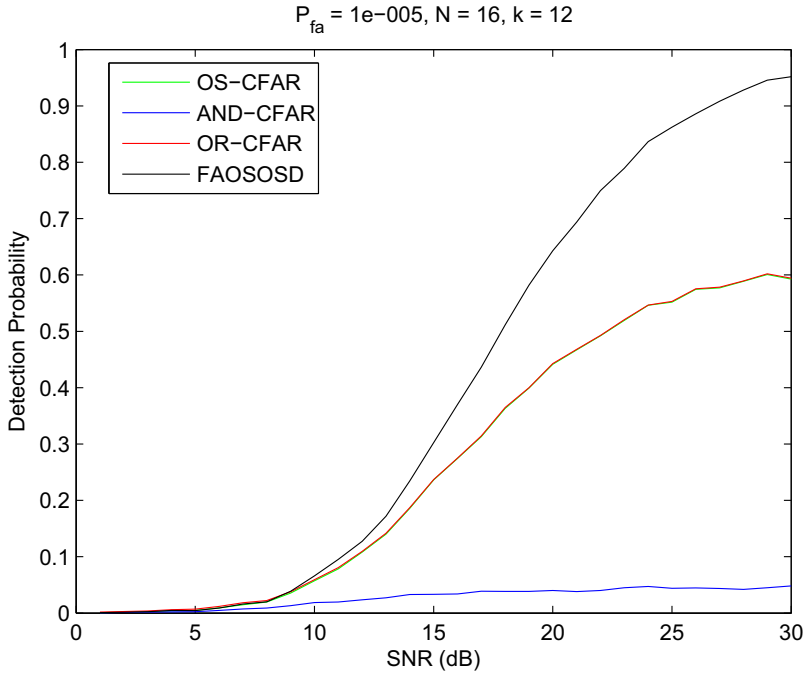

FIGURE B.4: Probabilités de détection pour $N = 16$, $K = 12$ et $Pfa = 10^{-5}$.

Les probabilités de détection correspondantes, en présence de cinq cibles interférentes, sont illustrées dans la Figure B.4. Il est remarquable que le détecteur FAOSOSD présente les meilleures performances parmi les quatre détecteurs. La performance du détecteur AND-CFAR est la plus dégradée.

Cette limitation est liée à la dégradation des performances du détecteur OS-CFAR lorsque le nombre de cibles interférentes dépasse la limite tolérable d'une part, et les mauvaises performances du détecteur CA-CFAR en présence de cibles interférentes, d'autre part. Le détecteur OR-CFAR demeure sujet aux performances des détecteurs CA-CFAR et OS-CFAR.

Pour généraliser les résultats obtenus, d'autres simulations ont été conduites pour différentes valeurs de la probabilité de fausses alarmes, P_{fa}, et de la taille de la fenêtre

de référence, N.

Les résultats obtenus montrent que lorsque la probabilité de fausses alarmes augmente, la probabilité de détection s'améliore et le détecteur FAOSOSD présente les meilleures performances. On note que les détecteurs OS-CFAR et OR-CFAR présentent les mêmes performances à cause des grandes pertes du détecteur CA-CFAR en présence d'interférences sévères, donc, dans ces conditions d'environnement, le détecteur OR-CFAR tend vers le détecteur OS-CFAR .

Il est à noter aussi que les grandes valeurs de N entraînent de meilleures probabilités de détection et le détecteur FAOSOSD présente toujours les meilleures performances.

B.2.3.3 Evaluation de la probabilité de fausses alarmes effective

Une quantification de l'effet de la présence des cibles interférentes, dans la fenêtre de référence, sur le contrôle du taux de fausses alarmes du détecteur FAOSOSD a été effectuée pour différentes valeurs de N en fonction du rapport interférence sur bruit, INR. Le nombre de cibles interférentes utilisées dans ces simulations, N_i, est pris égal à $(N - K + 1)$. Les résultats ont été obtenus par des réalisations de Monte Carlo en utilisant un total de 10^7 réalisations indépendantes.

La Figure B.5 montre les performances en terme du maintien du taux de fausses alarmes effectif du détecteur FAOSOSD pour différentes valeurs de INR. On remarque que la P_{fa} effective présente une faible fluctuation relativement à celle désirée ($P_{fa} = 10^{-5}$) pour les grandes valeurs de N et de faibles INR.

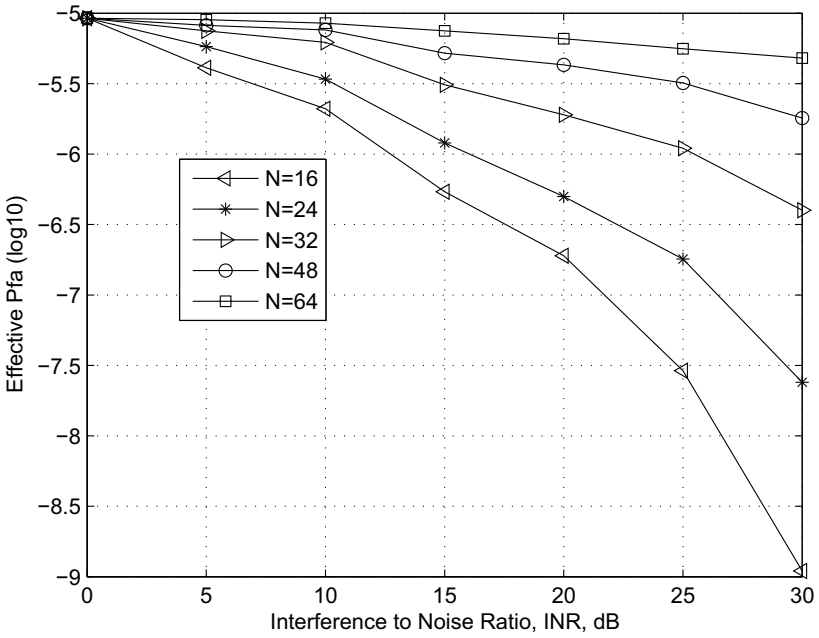

FIGURE B.5: Effet du INR sur la P_{fa} effecftive du détecteur FAOSOSD en présence de $(N-K+1)$ cibles interférentes, P_{fa} désirée $P_{fa}=10^{-5}$, $N=16,24,32,48$ et 64.

B.3 Détection CA/OS combinée en présence d'interférences

B.3.1 Le détecteur ALC-CFAR

Nous proposons un nouveau détecteur, baptisé ALC-CFAR (Adaptive Linear Combined CFAR). Il possède la capacité de présenter des performances de détection proches au détecteur CA-CFAR avec moins de pertes CFAR comparativement au détecteur OS-CFAR dans un environnement homogène, et très proches au détecteur OS-CFAR en présence de cibles interférentes.

B.3.1.1 Principe du détecteur ALC-CFAR

L'architecture du détecteur ALC-CFAR est présentée dans la Figure B.6.

Le détecteur ALC-CFAR est une combinaison linéaire adaptative des estimés des seuils des détecteurs CA-CFAR et OS-CFAR en utilisant un facteur de pondération

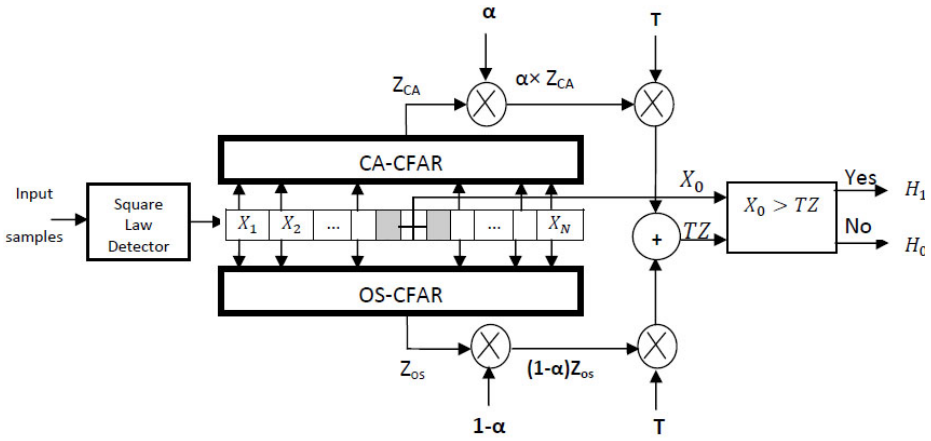

FIGURE B.6: Architecture du détecteur ALC-CFAR.

adaptatif aux changements de l'environnement [74].

Le détecteur ALC-CFAR estime le niveau du bruit, Z, dans la fenêtre de référence suivant l'équation B.7.

$$Z = \alpha Z_{CA} + (1 - \alpha) Z_{OS} \tag{B.7}$$

avec Z_{CA} et Z_{OS} sont les estimés du niveau du bruit des détecteurs CA-CFAR et OS-CFAR respectivement et α est une mesure d'homogéniété des échantillons de la fenêtre de référence et appartient à l'interval [0,1].

L'estimé Z est multiplié par le facteur d'échelle T pour former le seuil. Après comparaison, si la cellule sous test est supérieure au niveau du seuil, l'hypothèse H_1 (présence de cible) est déclarée vraie ; si non l'hypothèse H_0 (absence de cible) est déclarée vraie.

B.3.1.2 Facteur de pondération adaptatif

Le paramètre α est calculé selon les étapes suivantes :

Etape1 : les échantillons de la fenêtre de référence sont ordonnés pour former une nouvelle fenêtre W qui sera subdivisée en deux sous-fenêtres W_0 et W_1 selon la règle :

$$k_{\leq W_0}^{\geq W_1} \beta \tag{B.8}$$

où β est un seuil entier. La cellule de référence $Z_k \in W$, $k = 1, 2, ..., N$, appartient à W_1 si $k > \beta$ et appartient à W_0 si $k \leq \beta$.

Etape2 : les deux sous-fenêtres W_0 et W_1 sont utilisées pour calculer α selon l'équation (B.9).

$$\alpha = \frac{1}{\beta Z_N} \sum_{k=1}^{\beta} Z_k \tag{B.9}$$

où Z_N est l'échantillon le plus grand dans la fenêtre de référence, donc dans W_1, et Z_k est le k^{eme} grand échantillon dans W_0.

Les expressions de Z_{CA} et Z_{OS} sont données par les équations (B.10) et (B.11), respectivement :

$$Z_{CA} = \frac{1}{N} \sum_{k=1}^{N} Z_k \tag{B.10}$$

$$Z_{OS} = Z_{K_{OS}} \tag{B.11}$$

Nous considérons $K_{OS} = \frac{3}{4}N$, qui est connu comme étant la valeur optimale, pour se protéger contre les cibles interférentes. Le seuil entier β défini dans l'équation (B.8) est aussi pris égal à K_{OS}. L'objectif de cette préférence est pour avoir uniquement les échantillons du bruit dans W_0 avec un grand nombre de cellules possible.

De l'équation (B.9), on observe que α est la moyenne arithmétique des échantillons de W_0 dévisée par le plus grand échantillon dans la fenêtre de référence. Selon la valeur du paramètre α, le détecteur ALC-CFAR utilise le seuil du CA-CFAR ($\alpha = 1$) ou le seuil de l'OS-CFAR (pour $\alpha = 0$) dans ces cas limites.

B.3.2 Evaluation des performances

Les performances du détecteur ALC-CFAR ont été analysées et comparées avec celles des détecteurs CA-CFAR et OS-CFAR dans différentes situations radar. La

comparaison est basée sur l'évaluation de la probabilité de détection, P_d, en fonction du SNR et la P_{fa} effective par des simulations Monte Carlo. Le gain en probabilité de détection du détecteur ALC-CFAR par rapport au détecteur OS-CFAR est aussi quantifié.

B.3.2.1 Probabilité de détection

Les simulations sont réalisées pour différentes valeurs de N et P_{fa}.

Dans ***un environnement homogène***, les résultats obtenus des probabilités de détection des détecteurs CA-CFAR, OS-CFAR et ALC-CFAR pour $N = 16$ et différentes valeurs de P_{fa}, montrent que la probabilité de détection du détecteur ALC-CFAR reste toujours entre celles des détecteurs CA-CFAR et OS-CFAR pour les différentes valeurs de P_{fa}. La différence entre les probabilités de détection des détecteurs ALC-CFAR et OS-CFAR augmente pour les faibles valeurs de P_{fa}.

Les résultats obtenus pour les différentes valeurs de N montrent que le gain du détecteur ALC-CFAR comparé au détecteur OS-CFAR est important pour les faibles valeurs de N. Pour les grandes valeurs de N, les performances du détecteur ALC-CFAR convergent vers celles du détecteur OS-CFAR.

Il est connu que le détecteur OS-CFAR présente des pertes de détection additionnelles par rapport au détecteur CA-CFAR dans un environnement homogène, donc, le détecteur ALC-CFAR minimise ces pertes dans ce type d'environnement.

Dans ***un environnement non-homogène***, la probabilité de détection du CA-CFAR diminue, par contre celle du détecteur OS-CFAR est maintenue et les performances du ALC-CFAR sont proches de celles du détecteur OS-CFAR.

Lorsque le nombre de cibles interférentes augmente, et reste inférieur au nombre tolérable par le détecteur OS-CFAR (quatre pour $N = 16$), les performances du détecteur CA-CFAR se dégradent considérablement, le détecteur OS-CFAR n'est pas affecté et le détecteur ALC-CFAR reste très proche du détecteur OS-CFAR.

La Figure B.7 montre les probabilités de détection des détecteurs ALC-CFAR, OS-CFAR et CA-CFAR en présence de cinq cibles interférentes.

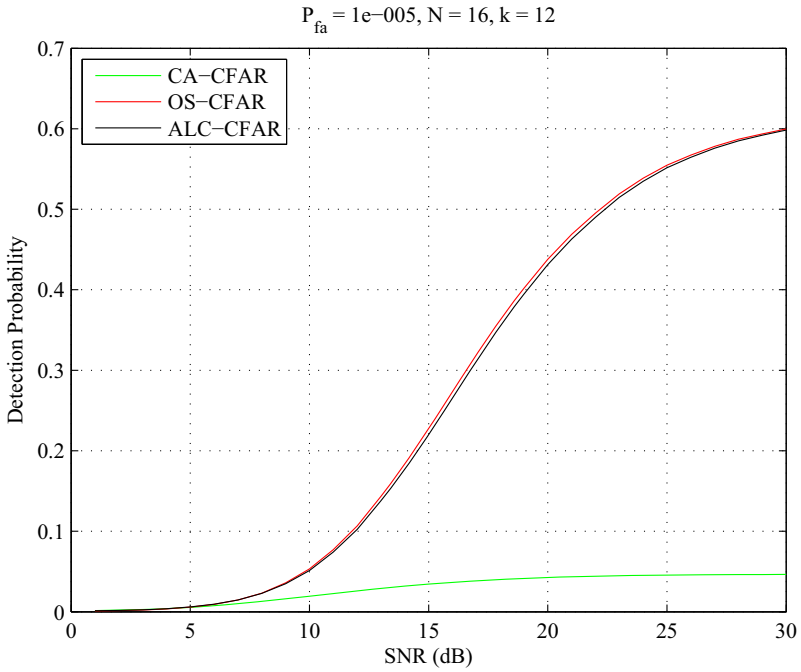

FIGURE B.7: Probabilités de détection des détecteurs ALC-CFAR, OS-CFAR et CA-CFAR en présence de cinq cibles interférentes.

On constate que lorsque le nombre de cibles interférentes dépasse la limite tolérable, le comportement du détecteur ALC-CFAR est similaire au détecteur OS-CFAR. Comme les performances du détecteur OS-CFAR sont affectées dans ce cas, les performances de l'ALC-CFAR sont aussi dégradées.

Le détecteur ALC-CFAR offre donc, un compromis entre les détecteurs CA-CFAR et OS-CFAR. Dans un environnement homogène, le détecteur ALC-CFAR est meilleur que le détecteur OS-CFAR par la réduction des pertes de détection.

En présence de cibles interférentes, le détecteur ALC-CFAR est très proche du détecteur OS-CFAR qui est conçu pour supporter les situations de présence de cibles interférentes et compense la dégradation du CA-CFAR dans ce type d'environnement.

La Figure B.8 montre les seuils des détecteurs CFAR pour $N = 16$ et $P_{fa} = 10^{-5}$.

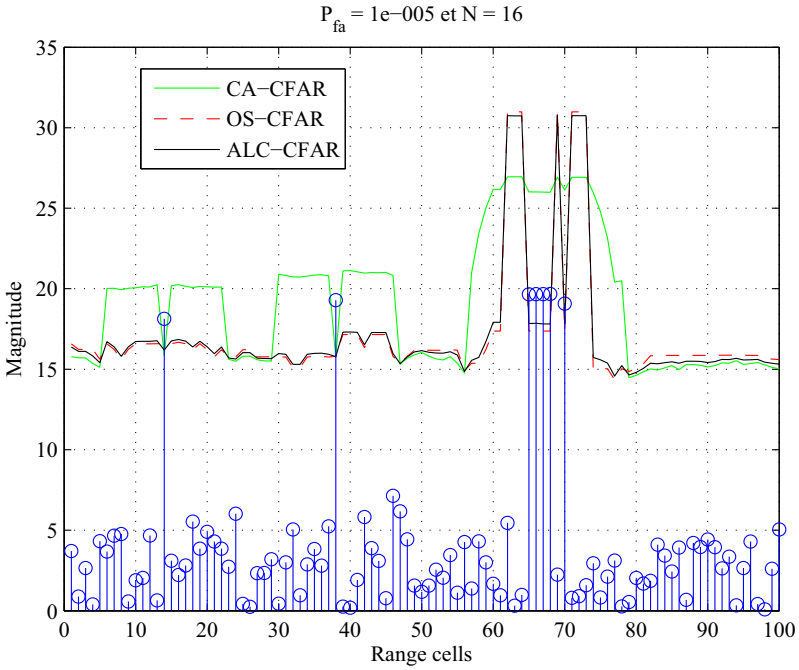

FIGURE B.8: Seuils de détection des détecteurs ALC-CFAR, CA-CFAR et OS-CFAR pour $N = 16$ et $P_{fa} = 10^{-5}$.

Il est clair que le seuil du détecteur ALC-CFAR s'adapte à l'environnement à l'aide du facteur α pour détecter les cibles dans les zones claires et évite l'effet de maskage en présence de cibles interférentes et par conséquent, il assure moins de pertes comparativement au détecteur OS-CFAR. On observe que le détecteur CA-CFAR détecte uniquement les deux cibles dans le clair, tandis que l'OS-CFAR détecte les sept cibles. Le détecteur ALC-CFAR garantit aussi la détection des six cibles avec moins de pertes CFAR.

B.3.2.2 Régulation du taux de fausses alarmes

La performance de régulation de la fausse alarme effective des différents détecteurs considérés pour différents N dans un environnement homogène a été évaluée. Les résultats obtenus pour une $P_{fa} = 10^{-4}$, par des simulations Monte Carlo en utilisant 10^6 expériences indépendantes, sont présentés dans la Figure B.9.

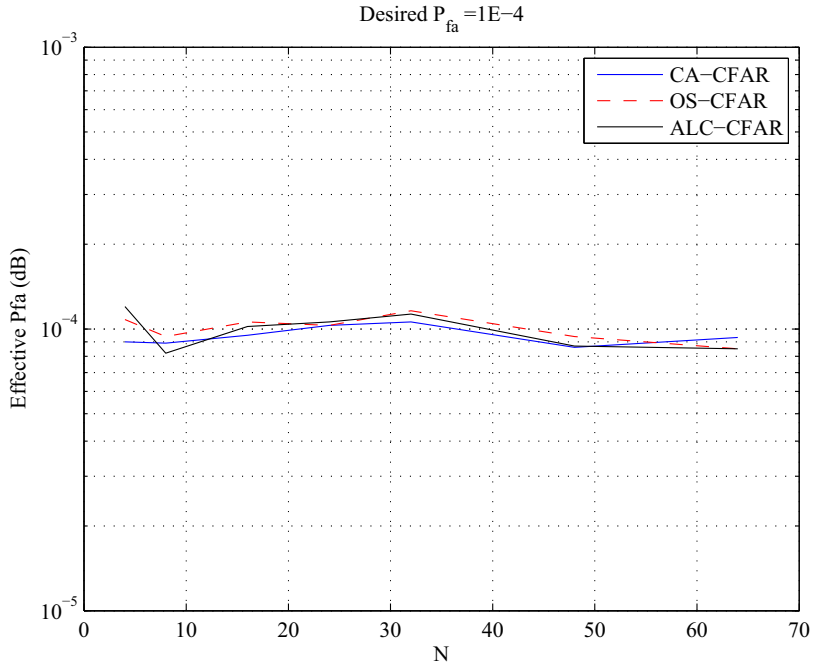

FIGURE B.9: Régulation de la probabilité de fausses alarmes pour différentes valeurs de N. $P_{fa} = 10^{-4}$.

On constate que la P_{fa} effective du détecteur ALC-CFAR est relativement maintenue proche à la P_{fa} désirée.

B.3.2.3 Gain du détecteur ALC-CFAR

Le gain obtenu, défini comme étant la différence entre les SNRs, correspondants aux détecteurs ALC-CFAR et OS-CFAR, pour atteindre une probabilité de détection $P_d = 0.5$, pour différentes valeurs de P_{fa} et N est donné dans le Tableau B.1.

TABLE B.1: Gain du détecteur ALC-CFAR par rapport au détecteur OS-CFAR pour différentes valeurs de Pfa et N.

	N	4	8	16	24	32	64
Gain(dB)	$P_{fa} = 10^{-4}$	0.813	0.312	0.145	0.081	0.043	0.024
	$P_{fa} = 10^{-5}$	1.251	0.327	0.214	0.115	0.062	0.031
	$P_{fa} = 10^{-6}$	1.316	0.415	0.223	0.132	0.091	0.035

On constate que le gain est important pour des faibles valeurs de N et P_{fa}. Il

atteint plus de $1dB$ pour $N = 4$ et $P_{fa} = 10^{-6}$. Pour des valeurs de N et P_{fa} plus grandes, le gain est réduit et le détecteur ALC-CFAR se comporte d'une manière similaire au déteteur OS-CFAR.

D'après ces résultats, on peut conclure qu'avec un choix judicieux de N et de P_{fa}, il est possible d'atteindre des performances satisfaisantes dans des situations d'environnements homogène et non-homogène et minimiser les pertes du détecteur OS-CFAR.

Il est intéréssant de noter que le détecteur proposé est particulièrement recommandé pour les radars à faibles résolutions en distance.

B.4 Implémentation

B.4.1 Contraintes de traitement en temps réel

Les contraintes de traitement en temps réel sont gérées de façon à satisfaire les exigences du radar de surveillance aérienne, ASR-12, qui est un radar de surveillance à portée moyenne (120Km). Il fonctionne dans la bande S (2.7-2.9 GHz) avec une largeur d'impulsion de 1μs, une ouverture du faisceau de 1.4°, une vitesse de rotation de 12 tours/min et une fréquence de répétition de 1200Hz.

Comme la durée d'un balayage du ASR-12 est de 5s, donc le temps d'une cellule azimutale sera $19.53ms$ qui correspond à 2.9 millions de cycles sur un DSP TMS320C6711 dont le temps de cycle est de $6.7ns$. Cet intervalle correspond au temps maximal tolérable pour effectuer le traitement en temps réel d'une cellule azimutale. Pour le traitement d'une seule impulsion, ce temps se réduit à 125000 cycles.

B.4.2 Effet de numérisation du signal radar sur les performances de détection

L'effet de numérisation du signal radar sur les performances des détecteurs CA-CFAR, OS-CFAR, FAOSOSD et ALC-CFAR a été édudié. Les paramètres considérés sont :

- Le nombre de bits de conversion Analogique/Numérique ;
- La fréquence d'échantillonnage ;
- La présence d'offset.

Les résultats obtenus ont permis de faire un choix optimal des paramètres de numérisation du signal radar selon les spécifications techniques du radar ASR-12.

B.4.3 Acquisition des signaux radar

L'acquisition des échantillons du signal radar est assurée par le EDMA (Enhanced Direct Memory Access) qui les transfère et les organise dans deux buffers d'acquisition logés dans la mémoire du DSP.

Le nombre d'échantillons est choisi de façon à couvrir toute la portée radar, soit 800 cellules distance pour le radar ASR-12 avec une fréquence d'échantillonnage de 1MHz.

Afin d'éviter l'écrasement des échantillons de deux récurrences consécutives, nous avons opté pour la technique dite "Double Buffering" qui consiste à utiliser deux buffers avec un basculement d'une récurrence à la suivante de manière automatique. Pendant l'opération d'acquisition des échantillons de la récurrence courante, on effectue le traitement CFAR de la récurrence précédente.

B.4.4 Implémentation des algorithmes de détection proposés

Pour des applications pratiques dans la détection radar, il est clair que la charge de calcul est plus importante pour les détecteurs proposés que pour les détecteurs

classiques CA-CFAR et OS-CFAR.

Pour palier à cette contrainte, une solution consiste à exploiter les avantages des architectures d'implémentation des détecteurs CA-CFAR et OS-CFAR développées dans [68] et [74] respectivement.

Pour le détecteur CA-CFAR, le nombre d'opérations est réduit à seulement deux additions et deux soustractions, quelque soient la taille de la fenêtre de référence et le nombre de cellules de garde, grâce à l'utilisation de la technique de la fenêtre glissante automatisée et généralisée (GASW : Genaralized Automatic Sliding Window) [68].

Pour le détecteur OS-CFAR, la charge de calcul est améliorée d'environ 75 $^{o}/_{o}$ comparativement à la configuration d'implémentation classique. L'architecture proposée est basée sur une procédure efficace pour une implémentation en temps réel du détecteur OS-CFAR par la détermination directe du $(N-K+1)^{eme}$ maximum.

Par analogie, la détermination du K^{eme} maximum des N cellules de référence, est équivalent à choisir le $(N+1-K)^{eme}$ maximum, le détecteur qui utilise N cellules de référence peut être implémenté en utilisant seulement $(N-1)$ comparaisons et $(N-1)$ inversions.

La combinaison de ces deux approches a amélioré considérablement le temps de traitement des détecteurs FAOSOSD et ALC-CFAR.

– **A. Implémentation du détecteur FAOSOSD**

L'implémentation du détecteur FAOSOSD est répartie en quatre opérations :

1. Classement des cellules de la fenêtre de référence ;
2. Calcul de ITC et détermination de l'ordre du minimum ;
3. Détermination de l'ordre optimal du détecteur OS-CFAR ;
4. Calcul du seuil du détecteur FAOSOSD et test de détection.

Le temps global pour l'exécution de la détection FAOSOSD a été optimisé grâce à l'exploitation du parallélisme de l'architecture du processeur utilisé et l'utilisation des

tables pour le calcul du logarithme. L'évaluation du temps d'estimation du seuil du détecteur FAOSOSD de toute la portée a montré que le temps d'estimation devient important lorsque le nombre de cellules de référence augmente.

Il est à noter que le temps de traitement est supérieur au temps tolérable maximal dans le cas de traitement d'une seule impulsion quelque soit la taille de la fenêtre de référence. Par conséquent, le détecteur FAOSOSD ne peut pas couvrir toute la portée du radar ASR-12.

Donc, la faisabilité de l'implémentation du détecteur FAOSOSD est recommandée après une opération d'intégration des implusions dans une résolution azimutale.

La Figure B.10 présente les résultats expérimentaux d'implémentation du détecteur FAOSOSD. La Figure B.10 (a) présente le signal radar, la Figure B.10 (b) montre

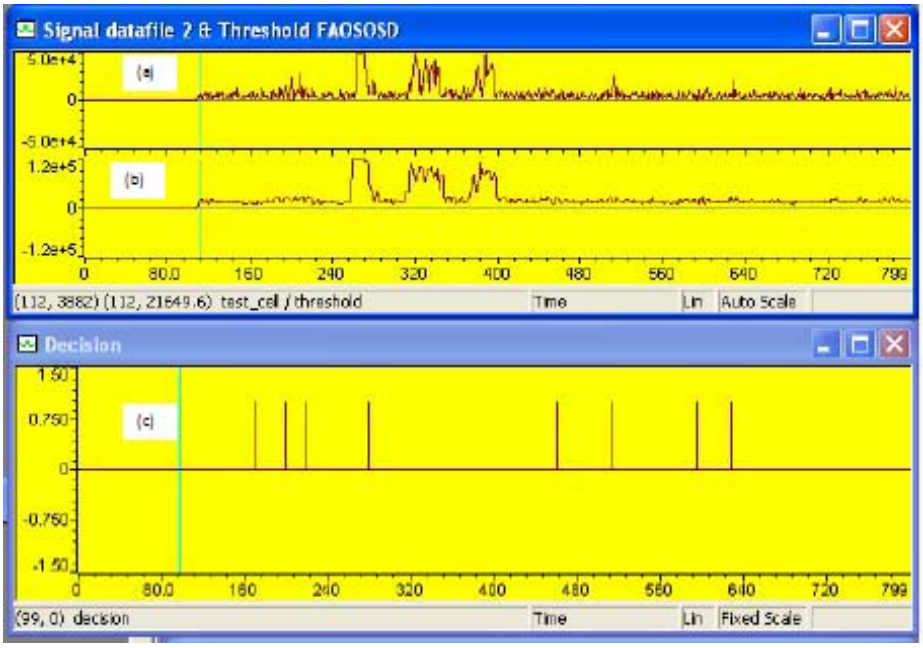

FIGURE B.10: Résultats d'implémentation du détecteur FAOSOSD avec des données expérimentales.)

l'évolution du seuil de détection et la Figure B.10 (c) illustre les positions des cibles détectées.

– **B. Implémentation du détecteur ALC-CFAR**

L'implémentation du détecteur ALC-CFAR est répartie en quatre opérations :

1. Calcul de l'estimé du seuil du détecteur CA-CFAR ;
2. Calcul de l'estimé du seuil du détecteur OS-CFAR ;
3. Calcul du coefficient α ;
4. Calcul du seuil ALC-CFAR et test de détection.

Le temps global pour l'exécution de l'architecture ALC-CFAR a été optimisé grâce à l'utilisation de la technique d'implémentation du détecteur OS-CFAR développée dans [74] et de la technique GASW [68] pour l'automatisation du calcul du seuil du détecteur CA-CFAR. L'évaluation du temps d'estimation du seuil de détecteur ALC-CFAR de toute la portée pour différents nombres de cellules de référence N est présenté dans le Tableau B.2.

TABLE B.2: Portée traitable en temps réel par le détecteur ALC-CFAR.

N	4	8	16	24	32	**40**	48
$Portee(Km)$	120	120	120	120	120	**86.1**	62.1

Nous remarquons que le temps d'estimation devient important lorsque le nombre de cellules de référence augmente, ce qui présente une limitation pour l'implémentation du détecteur ALC-CFAR.

Les données du Tableau B.2 montrent la limitation du traitement en temps réel, où on constate que la taille de la fenêtre d'estimation est limitée à N (compris entre 32 et 48) cellules pour pouvoir effectuer le traitement des échantillons de toute la portée radar en temps réel.

L'augmentation du nombre de cellules conduit à une réduction de la portée pour pouvoir assurer le traitement en temps réel. Au-delà de N = 32, le traitement en temps réel induit la réduction de la portée d'autant plus que le nombre de cellules de

référence est grand. À titre d'exemple, pour N = 40, la portée traitable se réduit à 86.1Km.

La Figure B.11 présente les résultats expérimentaux d'implémentation du détecteur ALC-CFAR.

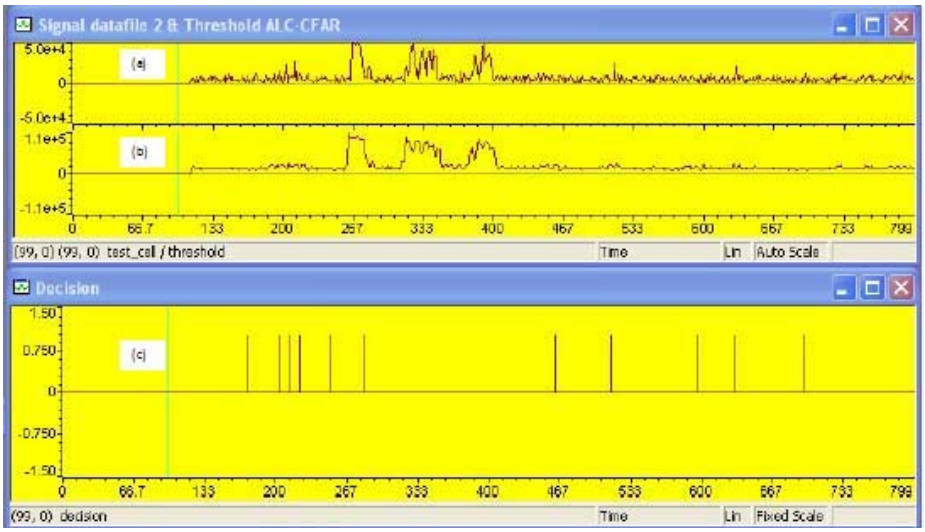

FIGURE B.11: Résultats d'implémentation du détecteur ALC-CFAR avec des données expérimentales.

La Figure B.11 (a) présente le signal radar, la Figure B.11 (b) montre l'évolution du seuil de détection et la Figure B.11 (c) illustre les positions des cibles détectées.

B.5 Conclusion

Les contributions principales de cette thèse couvrent deux axes. Le premier concerne la proposition de deux nouveaux algorithmes de détection de cibles radar baptisés, respectivement, FAOSOSD, Forward Automatic Order Selection Ordered Statistics Detector et ALC-CFAR, Adaptive Linear Combined CFAR.

Ces détecteurs présentent la capacité de s'adapter automatiquement aux changements de l'environnement, notamment en présence de cibles interférentes, par l'ajustement de leurs seuils en conséquence pour assurer de meilleures performances comparativement aux détecteurs classiques.

Le détecteur FAOSOSD est basé sur l'introduction d'une nouvelle approche pour la détermination du nombre de cibles interférentes dans la fenêtre de référence CFAR. Cette approche basée sur le test d'hypothèses de la détection classique, le détecteur FAOSOSD n'exige aucune information a priori sur le nombre de cibles interférentes.

Le nombre d'échantillons des cibles interférentes est estimé par la minimisation d'un critère de la théorie de l'information, ITC. Le nombre obtenu est exploité pour déterminer l'ordre optimal du détecteur OS-CFAR afin d'établir le niveau du seuil de détection en conséquence.

Les résultats de simulation montrent que le détecteur FAOSOSD présente des performances meilleures comparativement aux détecteurs OS-CFAR, AND-CFAR et OR-CFAR en présence d'interférences sévères.

Le deuxième détecteur proposé ALC-CFAR consiste à combiner intelligemment les estimés des seuils des détecteurs CA-CFAR et OS-CFAR. Cette combinaison est basée sur le niveau de changement de l'environnement. Ce détecteur exige un prétraitement des cellules de la fenêtre de référence et applique par la suite un facteur de pondération adaptatif à la procédure de fusion pour produire une décision efficace avec des pertes CFAR réduites.

Les résultats obtenus montrent que cette combinaison permet d'avoir un meilleur compromis entre les performances des détecteurs CA-CFAR et OS-CFAR. Il est montré que cette approche permet de remédier au problème de dégradation des performance du détecteur CA-CFAR en présence d'interférences et de minimiser les pertes du détecteur OS-CFAR dans un milieu homogène.

Le deuxième axe concerne le développement de nouvelles architectures d'implémentation efficace des détecteurs proposés sur une plateforme de développement à base du processeur de traitement du signal, DSP type TMS320C6711 de Texas Instruments. Les contraintes de traitement en temps réel et l'effet de numérisation du signal radar sur la qualité de détection ont été considérés, étudiés, évalués et discutés.

BIBLIOGRAPHY

"This page is intentionally left blank"

Bibliography

1. Skolnik, M. I., *Introduction to Radar Systems*, McGraw-Hill Book Company Wiley-Interscience, 3rd edition,USA, 2001.
2. Gini, F, Farina, A. and Greco, M., Selected list of references on radar signal processing, *IEEE Trans. Aerospace and electronic Systems,* Vol. 29, No. 1, pp. 329-360, Jan. 2001.
3. Skolnik, M. I., *Radar HandBook*, McGraw-Hill, 3rd edition, USA, 2008.
4. Barkat, M., *Signal Detection and Estimation*, 2nd edition, Norwood, MA :Artech House, 2005.
5. G. Minkler and J. Minkler, *CFAR*, Magellan Book Company, 1990.
6. Grunwald, P. D., Myung,I. J. and M. A., Pitt, *Advances in Minimum Description Length Theory and Applications*, The MIT Press, Cambridge, Massachusetts, London, England, 2005.
7. Curtis Schleher D., *MTI and Pulsed Doppler Radar*, Artech House, 1990.
8. Henry W. Cole, *Understanding radar*, Second Edition, Blackwell Scientific Publication, 1992.
9. Farina, A., *Optimized Radar Processors*, Peter Peregrinus Ltd., London, United Kingdom, 1987.
10. G. Galati, *Advanced radar techniques*, Peter Prenium Ltd, 1993.
11. D. K. Barton, *Radar System Analysis and Modeling*, Norwood, MA : Artech House, 2005.
12. I. S. Gradshteym and I. M. Ryzhik, *Table of Integrals, Series, and Products*, Orlando, Florida. Academic Press, Inc. 1980.
13. M. Abramowitz and I. A. Stegun, *Handbook of mathematical Functions, Dover Publications*, INC, New York, 1972.
14. H. A. David, *Order Statistics*, John Wiley and sons, New York. 1981.
15. B. Edde, Radar Principles, Technology, Application, Prentice Hall, New York, 1993.
16. N. Levanon, On radar principles, John Wiley and Sons, New York, 1988.
17. H. L. Van Trees, Detection, estimation and modulation theory, John Wiley and Sons, Part 1, New York, 1968.
18. Finn, H. M., and Johnson, R. S., Adaptive detection mode with threshold control as a function of spatially sampled clutter level estimates, *RCA Review,* Vol. 29, pp. 414-464, Sep. 1968.
19. Hansen, V. G. and Sawyers, J. H., Detectability loss due to greatest of selection in a cell-averaging CFAR, *IEEE Trans. Aerospace and electronic Systems,* Vol. AES-16, pp. 115-118, Jan. 1980.
20. Rohling, H., Radar CFAR thresholding in clutter and multiple target situations, *IEEE Transactions on Aerospace and Electronic Systems*, 19 : pp 608-621, July, 1983.

21. Rickard, J. T. and Dillard, M., Adaptive detection algorithms for multiple target situations, *IEEE Transactions on Aerospace and Electronic Systems*, 13(4) :338-343, July, 1977.
22. Barkat, M., Himonas, S. D. and Varshney, P. K., CFAR detection for multiple target situations, *IEE Proceedings*, Vol : 136, Issue 5, 1989.
23. C. J. Kim, D. J. Han and H. S. Lee, Generalized OS-CFAR Detector with non coherent integration, Signal Processing, Vol. 31. PP. 43-56, 1993.
24. A. R. Elias, M. G. Mercado and E.R. Davo, Analysis of some modified Order Statistics CFAR : OSGO and OSSO CFAR, IEEE Transactions on Aerospace and Electronic Systems, Vol. 26, PP. 608-621, January 1990.
25. M. B. Elmashade, Performance analysis of the OS family of CFAR schemes with incoherent integration of M-pulses in the presence of interferers ; IEE Proceedings on Radar Sonar and Navigation, Vol. 145, PP. 181-190, June 1998.
26. P. P. Ghandi and S. A. Kassam, Analysis of CFAR processors in non-homogenous background, IEEE Transactions on Aerospace and Electronic Systems, Vol. 24, PP. 427-445, July 1988
27. S. D. Himonas and M. Barkat, A robust radar CFAR detector for multiple target situations, Proceedings of the IEEE National Radar conference, Dallas, Texas, PP. 85-90, 1989
28. S. D. Himonas and M. Barkat, Automatic censored CFAR detection for non-homogenous environments, IEEE Transactions on Aerospace and Electronic Systems, Vol. 28, PP. 286-304, January 1992.
29. M. Barkat and F. Soltani, Cell averaging detection in compound clutter with spatially correlated texture and speckle, IEE Proceedings on Radar Sonar, Vol. 146, PP. 279-284, December 1999.
30. S. D. Himonas, On Adaptive and Distributed CFAR Detection with Data Fusion, Ph.D. Thesis, Department of Electrical Engineering, at Stony Brook, New York, December 1989.
31. B. Magaz, B. Ferrah, S. Atta, M. Hamadouche and A. Belouchrani, Conception et Implémentation d'une Nouvelle Architecture de Détection Radar, DAT'2011, Février 2011, Alger.
32. N. Levanon and M. Shor, Order statistics CFAR for Weibull background, IEE Proceedings, Part F, Vol. 137, PP. 63-72, June 1990.
33. B. Magaz, Belouchrani, A. and Hamadouche, M., A New Adaptive Linear Combined CFAR Detection in Presence of Interfering Targets, Progress in Electromagnetics Research B, Vol. 34, 367-387, 2011.
34. D. Moore and N. B. Lawrence, Comparison of Two CFAR Methods used with Square Law Detection of Swerling I Target, Proceedings of IEE International Radar Conference, Arlington, VA, PP. 403-409, April 1980.
35. M. Weiss, Analysis of some modified cell averaging CFAR processors in multiple target situations, IEEE Transaction on Aerospace and Electronic Systems. Vol. 18, pp. 112 - 114, January 1982.

36. G. V. Trunk, Range Resolution of Target Using Automatic Detectors, IEEE Transaction on Aerospace and Electronic Systems. Vol. 14, pp. 750 - 755, September 1978.

37. M. Barkat and P. K. Varshney, A Weighted Cell Averaging - CFAR Detector for Multiple Target Situations, Proceedings of the 21st Annual Conference on Information Sciences and Systems, Baltimore, Maryland, pp. 118 - 123, March 1987.

38. P. Swerling, Probability of detection for fluctuating targets, IEE Transaction on Information Theory, Vol.6 April 1960

39. B. Magaz and M.L. Bencheikh, An Efficient FPGA Implementation of The OS-CFAR Processor, International Radar Symposium, pp. 1-4, May 2008.

40. M. Torres, Contribution à l'étude de l'implantation d'algorithmes de traitement de signal sur plateformes DSP-DSP et DSP-FPGA, Thèse de doctorat, Université de Limoge, France, Décembre 2003.

41. El Mashade, M. B, Analysis of CFAR detection of fluctuating targets, Progress In Electromagnetics Research, Vol. 2, 65-94, 2008.

42. A. Farrouki and M. Barkat, Automatic censoring CFAR detector based on ordered data variability for nonhomogeneous environments, IEE Proc. Radar, Sonar, Navig., Vol. 152, No. 1, Feb. 2005.

43. Saeed Erfanian and Vahid Tabataba Vakili, Introducing Switching Ordered Statistic CFAR Type I in Different Radar Environments, EURASIP Journal on Advances in Signal Processing, Volume 2009, Article ID 525704, 11 pages.

44. Behar V., C. Kabakchiev, L. Dukovska, Adaptive CFAR Processor for Radar Target Detection in Pulse Jamming, Journal of VLSI Signal Processing ", Vol. 26, N°11/12, 2000, pp. 383-386.

45. C. Kabakchiev, L. Dukovska and I. Garvanov, Comparative Analysis of Losses of CA-CFAR Processors in Pulse Jamming, CIT, N° 1, 2001, pp.21-35.

46. T. Laroussi and M. Barkat, Performance analysis of order statistic CFAR detectors in time diversity systems for partially correlated chi-square targets and multiple target situations : A comparaison, Signal Processing 86 (2006) 1617-1631.

47. C. J Kim, H. S. Lee, Detection analysis of a generalized order statistics CFAR detector for a correlated Rayleigh target, Signal Processing 47 (1995) 227-233.

48. V. Anastassopoulos, G. Lampropoulos, A new and robust CFAR algorithm, IEEE Transactions on aerospace and electronic systems, Vol. 28, N°2 April 1992.

49. M. Smith and P. Varsheny, Intelligent CFAR processor based on data variability, IEEE Transactions on aerospace and electronic systems, Vol. 36, July 2000, pp 837-847.

50. L. Zhao, W. Liu, X. Wu and S. Jeffrey, A novel approach for CFAR processor design, IEEE Radar conference, 2001, pp. 284-288.

51. Z. Hammoudi and F. Soltani, Distributed CA-CFAR and OS-CFAR detection using fuzzy spaces and fuzzy fusion rules, Radar, Sonar and Navigation, IEE Proceedings, Volume 151, Issue 3, p135, July 2004.
52. J. S. Fu and W. Lei Zhao, A novel approach for CFAR detector design in Weibull background, Proceedings of the CIE International Radar Conference, 2001.
53. W. Liu and X. Liu, And-CFAR and OR-CFAR detectors design in Weibull background, Proceedings of IEEE 37th Annual International Carnahan Conference on Security Technology, 2003.
54. Qu, Y. and Nemai, C. K., Novel CFAR detection, *Third International conference on Electrical and Computer Engineering, ICECE 2004* , 28-30 Dec. 2004, Daka, Bangladash.
55. F. Soltani, Détection Adaptative CFAR dans un Clutter Non Homogène Gaussien et K-Distribué avec Corrélation Partielle, PhD thesis, University of Constantine, Algeria, March 1999.
56. A. Farrouki, Applications de Censures Automatiques aux Détecteurs Adaptatifs CFAR Basés sue les Statistiques d'Ordre, PhD thesis, University of Constantine, Algeria, June 2005.
57. T. Laroussi, Applications de la Détection Adaptative CFAR aux Cibles Chideux et Partiellement Corrélées, PhD thesis, University of Constantine, Algeria, December 2005.
58. Z. Hammoudi and F. Soltani, Distributed IVI-CFAR detection in non-homogeneous environments, Signal Processing, Volume 84, Issue 7, July 2004.
59. M. Hamadouche, Détection Adaptative CA-CFAR et CMAP-CFAR de cibles Radar dans des Clutters Gaussien et Weibull distribués, PhD thesis, 2001 (Université de Constantine).
60. B. Nadler, Non-parametric detection of signals by information theoretic criteria : Performance analysis and an improved estimator, IEEE Transactions on signal processing, Vol. 58, N°5, May 2010.
61. Wax, M. and Kailath, T., Detection of Signals by Information Theoretic Criteria, *IEEE Transactions on Acoustics, Speech, and Signal Processing* , Vol. ASSP-33, No. 2, Avril 1985.
62. Magaz, B., Belouchrani,A. and Hamadouche, M., Automatic Threshold Selection in OS-CFAR Radar Detection Using Information Theoretic Criteria, Progress in Electromagnetics Research B, Vol.30, 157-175, 2011.
63. S. H. Mousavinezhad and M.Ikhlas, Digital Signal Processing in Theory and practice, 31st ASEE/IEEE Frontiers in Education Conference, Reno, NV, October 2001.
64. R. Chassing, DSP Applications Using C and the TMS320C6x DSK, Wiley, 2002.
65. Magaz, B., Belouchrani, A. and Hamadouche, M., Automatic Order Selection for OS-CFAR Detection Improvement Under Severe Interference Situations Using Information Theoretic Criteria, *Proc. International Radar Conference,* Bordeaux, France, October 2009.

66. N. Dahnoun, *Digital Signal Processing implementation using the TMS320C6000TMDSP Platform*, Prentice Hall, 2000.
67. René Cumplido, césar Torres and santos Lopez, On the implementation of an efficient FPGA based CFAR Processor for target detection, ICEEE and CIE2004, Acapulco, Guerrero ; Mexico, September 2004.
68. B. Magaz, M.L. Bencheikh, M. Hamadouche and A. Belouchrani, Design and real time implementation of a novel combined CA-CFAR/SLB system on TMS320C67x processor, IRS 2006, May 2006, Krakow, Poland.
69. R. Cumplido, C. Torresand and S. Lopez, A configurable FPGA-based Hardware Architecture for Adaptive Processing of Noisy Signals for Target Detection Based on Constant False Alarm Rate (CFAR) Algorithms, Global Signal Processing Conference, GSPX2004, Santa Clara CA. September 2004.
70. N. El-Faramawy, E. El-Badawyand A. Salem, Hardware Implementation of CA-CFAR processor, Proceedings of the Int. Conf. On Computer and Communication Engineering ICCCE06. Vol.1, 9-11May 2006, KualaLumpur, Malaysia. pp. 573-578.
71. B. Magaz, M.L. Bencheikh, M. Hamadouche and A. Belouchrani, Optimized Implementation of a Parallel DSP Architecture for Real-Time Stacked Beam Radar Signal Processing, IET Conference on Radar systems, Oct. 2007, Edinburgh, UK.
72. S.Bhaktavatsala, DSP applications in Radar, M. Tech Credit Seminar Report, Electronic Systems Group, EE Dept, IIT Bombay, Nov2002.
73. P. Ramesh Babu and R. Prasanthi, Analysis of CFAR techniques and FPGA realisation for radar detection, Proceedings of International Conference on intelligent Knowledge Systems (IKS-2004), August 2004.
74. B. Magaz, M. Hamadouche and A. Belouchrani, Design and DSP Implementation of an Adaptive Linear Combined CFAR Processor, International Radar Symposium, IRS'2009, September 2009, Hamburg, Germany.
75. B. Magaz, A. Abbadi, T. Mabed, M. Hamadouche and A. Belouchrani, Using D.S.P in Radar Domain Application : Optimal Implementation of CFAR Detection Algorithms on TMS320C6711 DSP, International Journal on Programmable Devices, Circuits and Systems, PDCS, Volume 9, Issue I, P47-51, October 2009.
76. Uwe Meyer-Meyer, *Digital Signal Processing with Field Programmable Gate Array*, Springer Verlag Berlin Heidelberg, 2001.
77. R. Chassaing, *Digital Signal Processing and Applications with the C6713 and C6416*, John Wiley Sons, 2005.
78. Michael O. Kolawole, Radar systems, peak detection and tracking, Newnes, Oxfoprd, 2002.
79. C. Torres-Huitzil, R. Cumplido-Parra and S. Lopez-Estrada, Design and implementation of a CFAR Processor for target detection, LNCS, August, Vol. 30203/2004 pp. 943-947.

80. T. Saed, J. Ali and Z. Yassen, An FPGA Based Implementation of CA-CFAR Processor, Asian Journal of Information Technology, 2007, pp. 511-514.
81. B. Magaz, A. Abbadi, T. Mabed, M. Hamadouche and A. Belouchrani, Design and Implementation of a Real Time FPGA Based CFAR Processor for Radar Target Detection Using ML403 FPGA Development Board, International Journal on Programmable Devices, Circuits and Systems, PDCS, Volume 9, Issue I, P29-34, October 2009.
82. A. Younsi, Robust Adaptive CFAR detection, PHD thesis, E.M.P, September 2009.
83. Texas Instruments, "TMS320C62x/C67x Technical Brief", 1998.
84. Texas Instruments, TMS320C62x/C67x CPU and Instruction Set Reference Guide, 1998
85. Texas Instruments, TMS320C6x User's Guide, "Digital Signal Processing Solution", 1999.
86. How to Begin Development with the TMS320C6711 DSP, Application Report SPRA522, Digital Signal Processing Solutions, March 1999.
87. Texas Instruments, TMS320C6000 CPU and Instruction Set Reference Guide, SPRU189f.
88. Texas Instruments, TMS320C6000 Optimizing Compiler User's Guide, SPRU187I
89. TMS320C6000 Programmer's guide, SPRU198D, Texas Instruments, Dallas, 2000.
90. TMS320C6000 Assembly language tools user's guide, SPRU186I, Texas Instruments, Dallas, 2001.
91. TMS320C6x C source debugger user's guide, SPRU188D, Texas Instruments, Dallas, 1998.
92. TMS320C6000DSK Board Support Library API User's guide, SPRU432A, Texas Instruments, Dallas, 2001.
93. TMS320C6000 Chip Support Library API User's guide, SPRU401D, Texas Instruments, Dallas, 2002.
94. TMS320C6000 Instruction Set Simulator User's guide, SPRU546, Texas Instruments, Dallas, 2001.
95. TMS320C6000 Peripherals reference guide, SPRU190D, Texas Instruments, Dallas, 2001.
96. Code Composer Studio User's Guide, SPRU509, Texas Instruments, Dallas, 2001.
97. Code Composer Tutorial, SPRU301C, Texas Instruments, Dallas, 2000.

ملـخـص

المساهمة الأساسية في هذه الأطروحة تضم جزئين. يتمثل الأول في إقتراح خوارزميتين جديدتين لكشف الأهداف الرادارية، والمسماة على التوالي، FAOSOSD ، المبنية على أساس تخفيض المعيار النظري للمعلومة، و ALC-CFAR المبنية على أساس تنسيق خطي موافق لعتبات الكواشف CA-CFAR و OS-CFAR. أظهرت هذه الخوارزميات قدرة على التأقلم مع متغيرات المحيط، خاصة في حال وجود أهداف متداخلة، بتكييف العتبات لضمان نوعية كشف عالية مقارنة بالكواشف العادية.

يخص الجزء الثاني تطوير مخططات زرع جديدة و فعالة خاصة بالكواشف المقترحة و زرعها على المعالج الرقمي للإشارة من نوع TMS320C6711. تم تقييم حد المعالجة في الوقت الحقيقي و مدى تأثير رقمنة إشارة الرادار على نوعية الكشف.

تبين النتائج المتحصل عليها كفاءة الكواشف المقترحة في تطبيقات حقيقية في مجال الكشف الراداري.

كلمات مفتاحية: الكاشف ALC-CFAR، الكشف، معالج الإشارة، الكاشف FAOSOSD، الزرع، المعيار النظري للمعلومة، الرادار.

RESUME

La contribution principale de cette thèse comporte deux parties. La première concerne la proposition de deux nouveaux algorithmes de détection de cibles radar baptisés, respectivement, FAOSOSD, Forward Automatic Order Selection Ordered Statistics Detector, basé sur la minimisation du critère de la théorie de l'information, et ALC-CFAR, Adaptive Linear Combined CFAR, basé sur une combinaison linéaire des seuils des détecteurs CA-CFAR et OS-CFAR. Ces algorithmes présentent la capacité de s'adapter automatiquement aux changements de l'environnement, notamment en présence de cibles interférentes, par l'ajustement de leurs seuils pour assurer de meilleures performances comparativement aux détecteurs classiques.

La deuxième partie propose de nouvelles architectures efficaces pour l'implémentation des détecteurs proposés sur processeur DSP type TMS320C6711. Les contraintes de traitement en temps réel et l'effet de numérisation du signal radar sur la qualité de détection ont été évalués et discutés. Les résultats obtenus montrent l'aptitude des détecteurs développés pour des applications pratiques dans une chaine de détection radar.

Mots Clés: ALC-CFAR, Détection, DSP, FAOSOSD, Implémentation, ITC, Radar.

SUMMARY

The main contribution of this thesis involves two parts. The first one concerns the proposition of two novel algorithms for radar target detection referred to as, respectively, FAOSOSD, Forward Automatic Order Selection Ordered Statistics Detector, based on the minimization of the information theoretic criteria, and ALC-CFAR, Adaptive Linear Combined CFAR, based on an adaptive linear combination of the CA-CFAR and the OS-CFAR detectors thresholds. These algorithms present the ability to sense automatically the environment changes, especially in presence of interfering targets, by adapting their thresholds to ensure better performance compared to classical detectors.

The second part deals with the proposition of new and efficient architectures suitable for the implementation of the proposed detectors on the TMS320C6711 DSP processor. The real time processing constraints and the radar signal digitalization effect on the detection quality have been evaluated and discussed. The obtained results show that the developed detectors are suitable for practical applications in radar detection.

Key words: ALC-CFAR, Detection, DSP, FAOSOSD, Implementation, ITC, Radar.